Voltage Dependent Ion Transport by Bolaamphilphilic Oligoester Ion Channels

by

Ye Zong
BSc, The University of Victoria, 2008

A Master Thesis Submitted in Partial Fulfillment
of the Requirements for the Degree of

Master of Science

in the Department of Chemistry

Ye Zong, 2013
University of Victoria

Voltage Dependent Ion Transport by Bolaamphilphilic Oligoester Ion Channels

by

Ye Zong
BSc, The University of Victoria, 2008

Supervisory Committee

Dr. T. M. Fyles, Department of Chemistry
Supervisor

Dr. Peter Wan, Departmental Member
Departmental Member

Supervisory Committee

Dr. Tom M. Fyles, Department of Chemistry
Supervisor

Dr. Peter Wan, Departmental Member
Departmental Member

Abstract

Based on preliminary reports, an extended series of bolamphiphilic oligoester compounds with structural symmetry were synthesized and then tested using a planar bilayer experiment with the voltage-clamp technique. The main structures of these compounds are identical, consisting of a mono or tri-aromatic core, two octamethylene chains and two benzoyl headgroups which are all connected through ester linkages. The structural variance was provided by the four differently functionalized benzoyl headgroups. The synthetic methods of three to five steps were mainly adapted from the previously reported method.[1] The methods successfully produced eight compounds with overall yields of 20 to 30%.

The voltage-clamp data suggested voltage-dependent behaviors occur at low concentrations while Ohmic behaviors require at high concentrations. The activity at low potentials showed relatively erratic behavior but the channels frequently switched between opening and closing states. The activity at high potential lasted longer as the channel maintained a longer state of opening.

The exponential voltage-dependent behaviors were observed at higher potential while the voltage-independent Ohmic behaviors occur at low potential. These channel behaviors are highly time-dependent as there is no control over the stability and the aggregation level for the compounds forming active channels in the membrane. In some cases the current-voltage responses appear to be asymmetrical between the positive and the negative potentials. Mechanisms consistent with the observations are proposed.

Table of Contents

List of Tables

List of Figures

List of Schemes

List of Abbreviations

DCM: dichloromethane

DMF: dimethylformamide

ESI-MS: electrospray ionization mass spectrometry

Et_2O: diethylether

EtOAc: ethylacetate

g: conductance

HPTS: 8-hydroxy-l,3,6-pyrene trisulfonate

MeOH: methanol

mV: miliVolt

NMR: nuclear magnetic resonance

nS: nanoSiemen

PA: phosphatidic acidic

pA: picoAmpere

PC: phosphatidylcholine

pS: picoSiemen

TBDMS-Cl: *tert*-butyl chlorodimethylsilane

TBAF: *tetra*-n-butylammonium fluoride

THF: tetrahydrofuran

List of Numbered Compounds

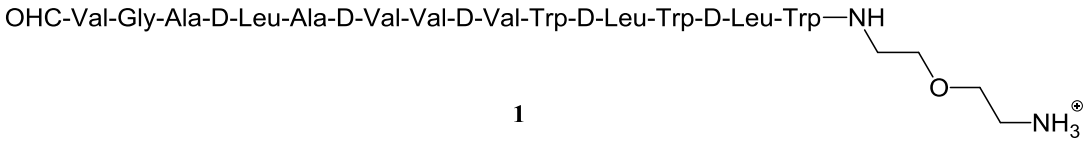

1

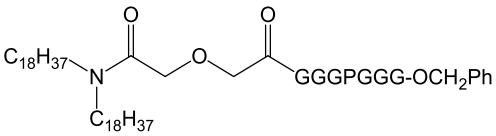

2

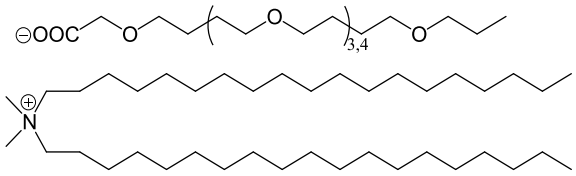

3

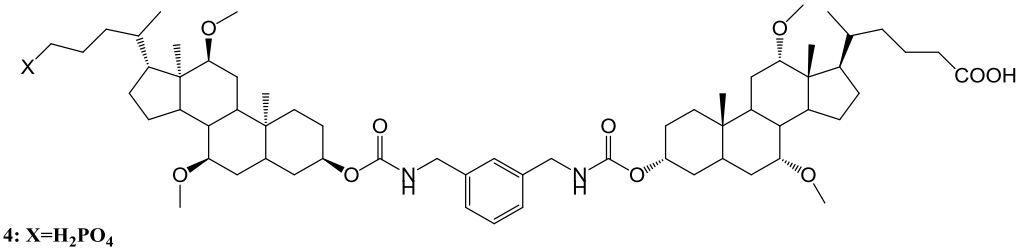

4: X=H_2PO_4
5: X=OH

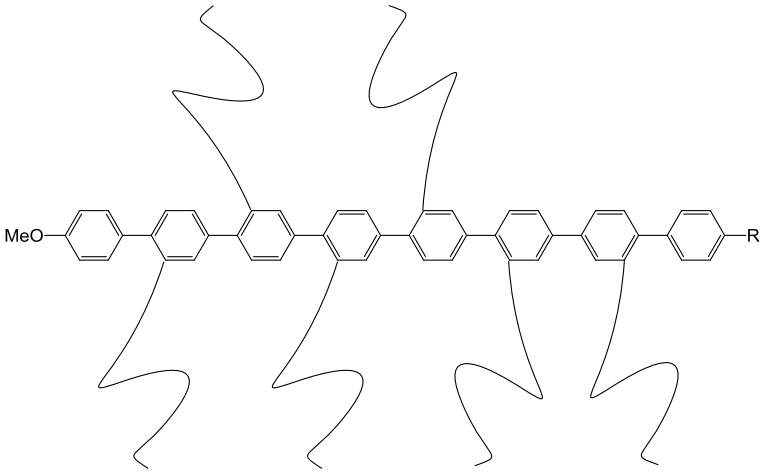

6: R=SO_2Me
7: R=OMe

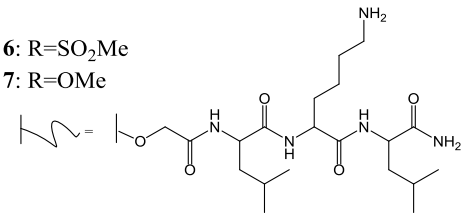

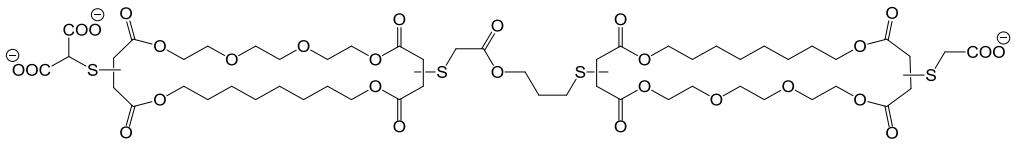

8

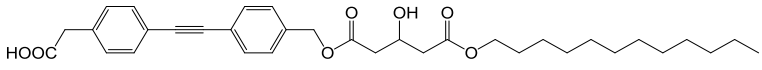

9

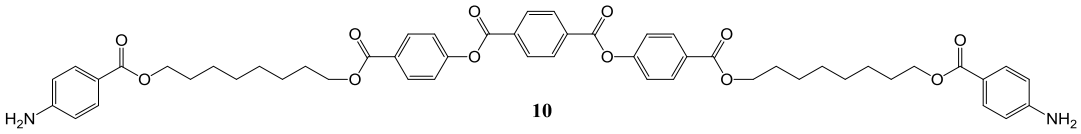

10

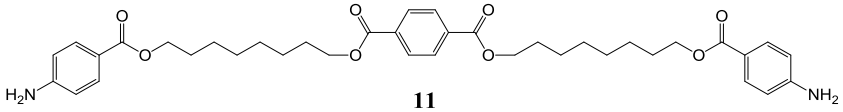

11

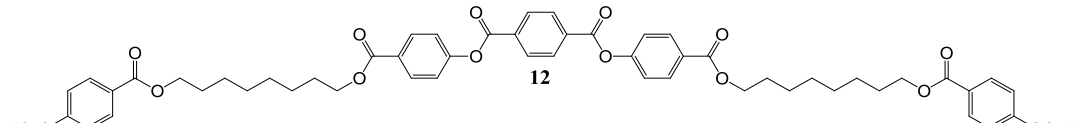

12

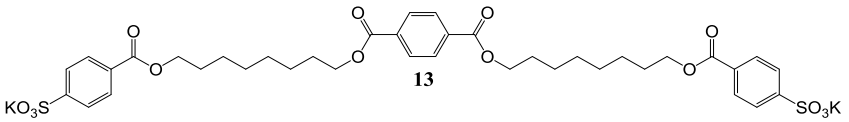

13

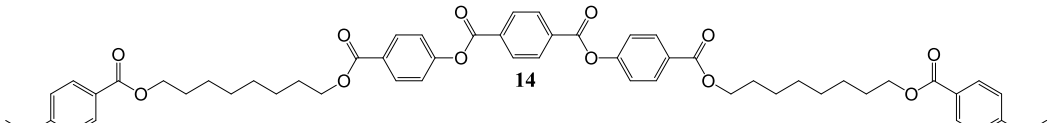

14

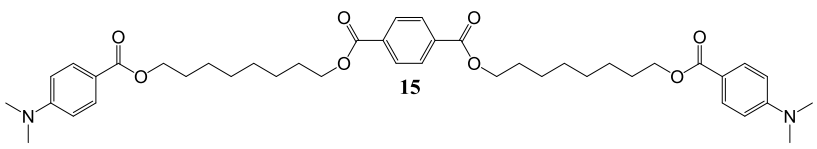

15

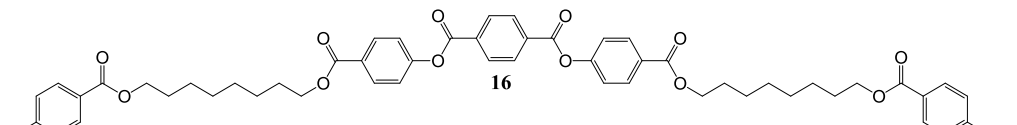

16

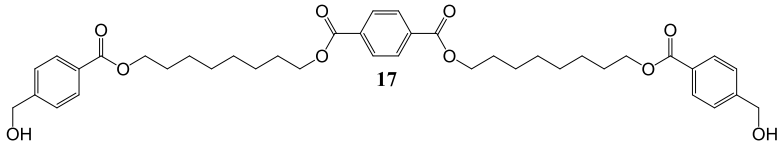

17

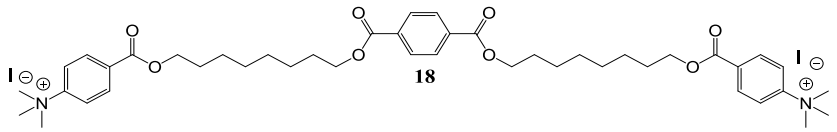

18

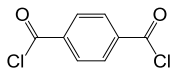

19

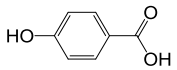

20

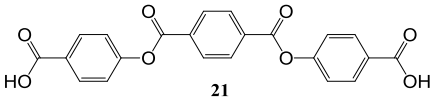

21

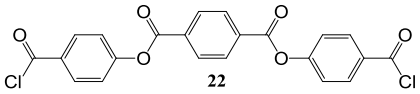

22

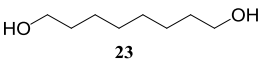

23

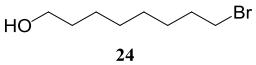

24

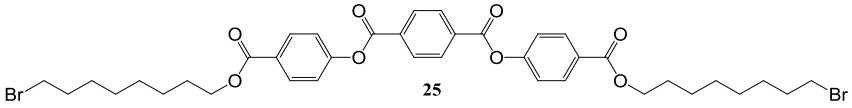

25

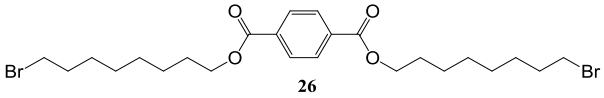

26

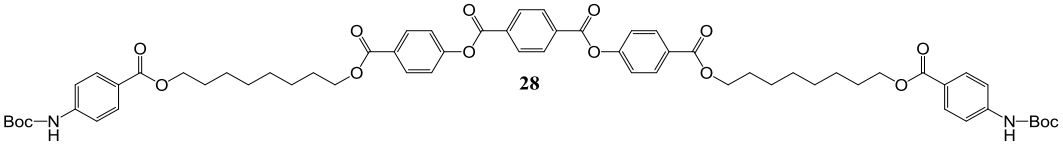

28

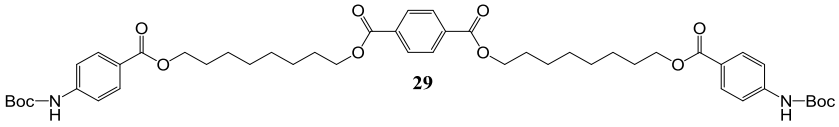

29

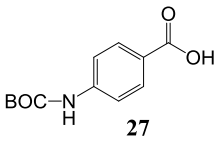

27

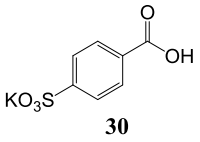

30

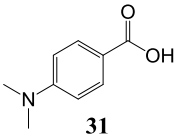

31

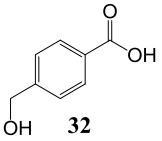

32

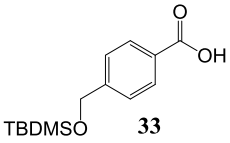

33

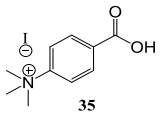

35

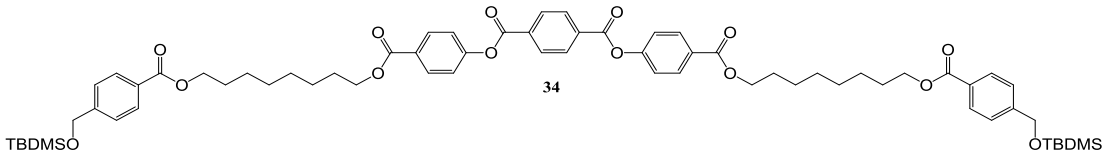

34

1 Introduction

All living cells require a closed environment for processing and regulating the essential biological functions apart from the harsh outside environment. A closed bilayer membrane serves the role of a barrier that encloses and compartmentalizes cells. The bilayer membrane is semi-permeable. Some solutes such as small nonpolar molecules can pass through easily, on the other hand, polar solutes such as amino acids and ions cannot pass through a bilayer membrane on their own, even though they are essential for cellular functions.[2] Nature's solution to transport polar solutes across a membrane is provided by ion channels and pumps.[2]

1.1 Definitions

Natural ion channels are large protein complexes embedded in lipid membrane of living cells that regulate ion passage across the membrane. Together with ion pumps, they are the essential components for control and manipulation of transmembrane potential which enables many biological functions.[3] Their ion transport activity can be regulated through a number of ways such as voltage,[4-12] light[13] and ligand-binding,[14] etc. Voltage-dependent ion channels are activated or influenced by changes in transmembrane potential.[6] This class of ion channels is especially critical for the propagation of an impulse in neurons. For example, the Na^+ channels in neurons can go through conformational distortion in response to a change to the resting transmembrane potential so that the channels open to admit Na^+ ion influx across the membrane into the cells. The cell membranes are then quickly depolarized to generate a nervous impulse traveling along the cell membrane of axon, to synapses, and then to other neurons.[15, 16] The Na^+ ion influx eventually generates a reversed transmembrane potential which then triggers K^+ channels to open for the efflux of K^+ ions out of cells to counter the effect of Na^+ ion influx, returning the transmembrane potential back to normal. Na^+ and K^+ channels are also rectified ion channels through which the passage of ions in one direction is favored relative to the other direction. Therefore, outward-rectified Na^+ channels prevent the back flow of Na+ ions out of the cells when the transmembrane potential is reversed. The inward-rectified K^+ channels, on the other hand, prevent back flow of K+ ions into the cells when the normal resting transmembrane potential of the neurons is reestablished.[17]

Chemists have been long interested in natural ion channels and have synthesized enormous number of artificial ion channel compounds and systems that can reproduce many functions of natural channels (reviews,[18-24] recent examples[25-33]). There are high conductance channels,[2, 4, 24] highly selective channels,[34] channels for protons, small ions, large ionic species,[24] channels that act in sensors, in drug delivery,[2, 4] and as cytotoxic agents.[2, 4]

Developing synthetic ion channels that mimic natural voltage-dependent ion channels becomes an attractive area of research as these channels are the better analogs of natural voltage-dependent channels. Despite the recognition of the importance of voltage-dependence and rectification of natural ion channels, the large majority of synthetic ion channel systems are not voltage-dependent but simply follow Ohm's law (Ohmic channel behavior). Figure 1-1A shows the current and conductance behavior of an Ohmic channel. The conductance of these channels is a constant in response to various applied potentials, and ions pass in either direction through the channels with no energetic difference related to direction of passage. It is not surprising to observe Ohmic behaviours for synthetic compounds since the most of the reported channels are centrosymmetric structures and are expected to insert to the membrane in a symmetric fashion. Therefore, creating a synthetic voltage-dependent ion channel seems facile by bringing dissymmetry into ion channel designs. Figure 1-1B shows a non-linear, voltage dependent response in which the positive and negative current patterns are centrosymmetric in the current-voltage plot. The conductance of this type of channels appears a minimum at low potential and increases in both positive and negative directions. This might be due to a voltage-dependent change in the structure of the channel, or the initiation of more channels as the potential increases. The alternative voltage-dependent case is the rectified ion channel shown in Figure 1-1C. In this case current does not flow under some conditions of applied potential but above a threshold increases rapidly. The conductance plot shows that there is no conducting structure at some potential. This is a rectifier as the energy profile for ions flowing at potential above the threshold is clearly different from the profile at values below the threshold.

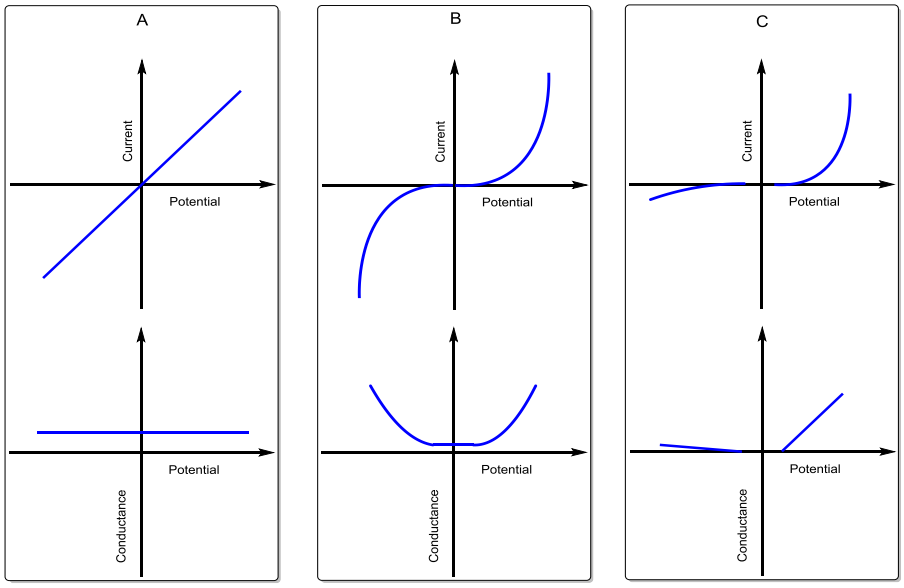

Figure 1-1. A) Current and conductance behavior of a voltage-independent ion channel. B) Current and conductance behavior of a voltage-dependent ion channel. C) Current and conductance behavior of a voltage-dependent rectified ion channel.

1.2 Synthetic Voltage-Dependent Ion Channels

Before going into the survey of synthetic ion channels that are voltage-dependent, it is worth mentioning a well studied natural occurring small peptide ion channel, alamethicin. The peptide chain of alamethicin forms an α-helical structure which then aggregates into multimer (usually tetra or hexamer) in the membrane, forming highly efficient and stable ion channels.[8] The channel pores vary with the aggregation level of the monomer in a voltage-dependent manner, but each of the pores allows passage of ions in either direction with similar energetics.[5, 8] The size of the natural ion channel is close to that of synthetic ion channels but it exhibits non-rectifying behavior and voltage-dependence (Figure 1-1B).

Gramicidin A is another well-studied low molecular weight pentadecapeptide ion channel, consisting of alternating D- and L-amino acids.[2, 4] In membranes and non-polar solvents it forms a centrosymmetric *β*-helix. The Koert group modified the gramicidin by covalently linking an ammonium ion to the N-terminus which desymmetrizes the structure to give compound **1**.[10] The positive charge on the ammonium ion linker was expected to be repelled by a positive potential and thread into the adjacent opening of the *β*-helix, thus creating a plugging effect if a positive potential is applied. As a result, non-linear current-voltage response was observed and the intensity of current decreased up to 50% when a positive potential (cis to the compound addition) was applied (Figure 1-1C).[4, 10]

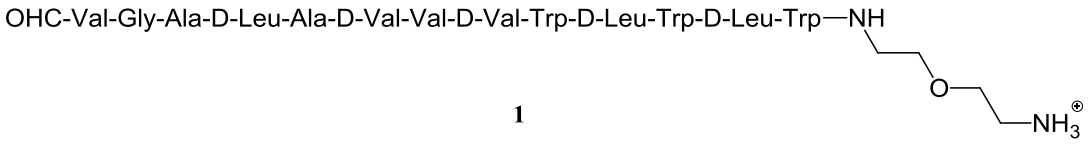

1

Schlesinger reported a chloride-selective, membrane-anchored peptide channel **2** that exhibits voltage gating in 2002. In a liposome media experiment this compound showed rapid, concentration dependent chloride release. The planar bilayer membrane experiment showed voltage-dependent behavior at low potential (-3 to 10mV) (Figure 1-1B).[12]

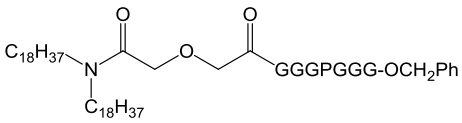

2

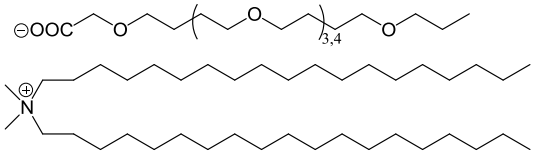

3

In 1992, Kobuke reported the first non-peptide ion channel.[9] This simple design **3** consists of a carboxylate core and an ammonium cation with two hydrophobic alkyl chains. The dissymmetric ion pair is one half of the thickness of the membrane. The channel was evidently formed from asymmetric aggregates and was both K^+-selective

and voltage dependent.[2, 9] The current-voltage response of the small simple compound was quite irregular with large variety. This kind of behavior is considered time-dependent.

In 2001, the Kobuke group reported another set of compounds showing voltage-dependent and rectified current behavior using the planar bilayer experiment. Asymmetries were introduced by terminal hydrophilic groups, carboxylic acid and phosphoric acid for **4** and hydroxyl and carboxylic acid for **5**. The current-voltage plots were fitted by curves through a zero point to show clear rectification properties. Parallel alignment of terminal headgroups directed by the dipole- potential interactions is essential for giving voltage-dependent rectified ion channels (Figure 1-1C).[35]

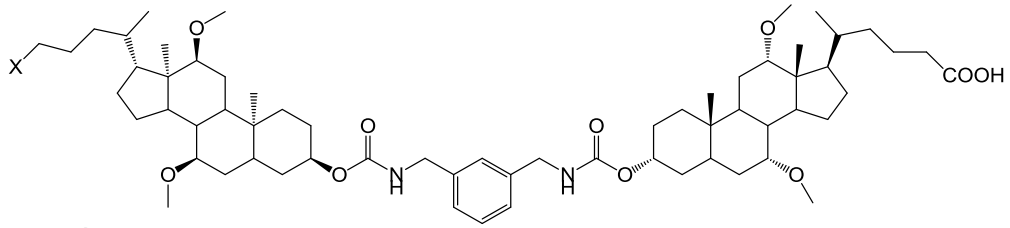

4: X=H_2PO_4
5: X=OH

In 2002, Sakai and Matile reported a voltage-dependent ion channel **6** constructed by a *p*-octiphenyl rod equipped with amphiphilic cationic tripeptide strands and polarized with methoxy π-donor and methylsulfone π-acceptor at either end.[11, 34] The polarization provides asymmetry to the structure which results in dramatic difference with respect to the symmetric version of the molecule **7** i.e. a symmetrical *p*-octiphenyl rod equipped with methoxy π-donor at both ends (push-push).[11, 34] This rigid rod monomer **6** tetramerizes into polarized (push-pull) β-barrel channels in response to the applied transmembrane potential according to fluorescence depth quenching and circular dichroism studies (Figure 1-2). The spherical bilayer experiments showed the channel was highly voltage-dependent and slightly anion-selective (OH^-/Cl^- selective). The planar bilayer experiments showed exponential relationships between the average current and the applied potential and between the channel open probability and the applied potential (Figure 1-1C). In contrast, the symmetric push-push β-barrel channels did not show facilitated membrane incorporation at applied potentials and presented only strong Ohmic behaviour.[34]

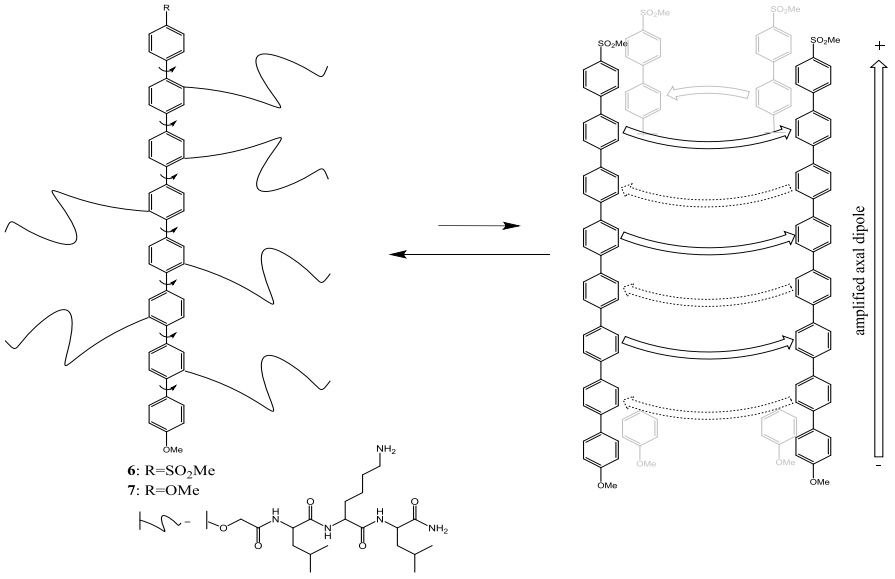

Figure 1-2. Structure of rigid push-pull rod 6 and push-push rod 7, and putative suprastructure of parallel β-barrels.

The recent research in Fyles group has uncovered a series of oligoester bolaamphilphile compounds that have shown ion conducting activities.[3, 6-7, 36-41] Our attention has been drawn to the design and synthesis of structurally simple compounds as increasing evidences suggest that simple compounds, with facile syntheses, can be as active as the other synthetic ion channels with more complex and defined structures.[3, 6-7, 36-41] The channel formation mechanism from these simple compounds is believed to be the aggregation of the compounds in the membrane.[40] In 1998, Fyles and Loock reported an early example of a synthetic voltage-gated ion channel **8** in our group. Bilayer-clamp experiments gave rectified current-voltage responses in which current is carried only at cis-negative potentials (Figure 1-1C). Voltage orientation-dependent irregular single-channel activity was also observed.[6] The axial macrodipole of the molecule was introduced by asymmetric distribution of terminal negative charges and was believed to account for voltage-gating.[6, 34] In 2011, Genge reported an asymmetrical diphenylacetylene-derived diester ion channel **9** that exhibited voltage-dependence at higher potentials. The overall profile is symmetric indicating that conductance is not rectifying (Figure 1-1B).[7]

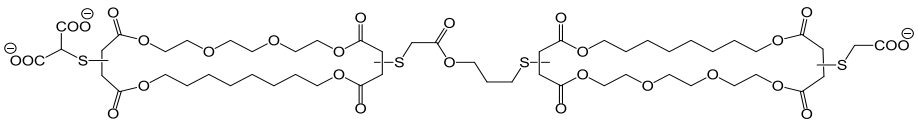

8

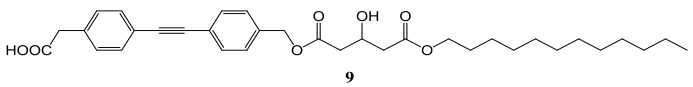

9

Also in 2011 Chui reported two oligoester compounds **10** and **11** exhibiting voltage-dependent behavior based on planar bilayer experimental results.[1, 4] The current patterns of the two compounds at positive and negative sides of the applied potentials are concluded by Chui to be non-rectifying and centrosymmetrical. The current branch at the negative potential is therefore folded to the positive side, and together with the positive current branch, they are fit successfully into several exponential regression curves. i.e. the two compounds exhibit exponential voltage-dependent behaviors.[1] However, the two compounds behave different from time to time and between trials. Therefore, the activities of two compounds are possibly time-dependent. The results are very surprising as compound **10** and **11** are symmetrically constructed compounds. This novel observation revolutionizes the designing criteria of a synthetic voltage-dependent, rectified ion channel, i.e. overall asymmetry in the structure.

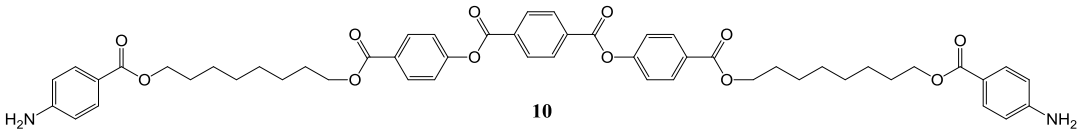

10

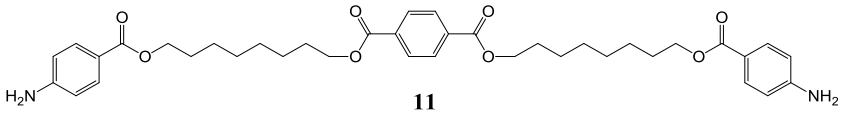

11

1.3 Techniques for Studying Synthetic Ion Channels

There have been a few methods developed for studying the transport activity of synthetic ion channels in the past few years, and these methods fall into the two main categories: spherical bilayer membrane or planar bilayer membrane based experiments. Both of these techniques are used extensively in the Fyles group and below are detailed discussions of these techniques.

1.3.1 Spherical Bilayers Based Experiments

Spherical bilayers based experiments utilize spherical lipid sacks known as liposomes or vesicles, ranging from 20nm to above 1 μm in diameter, to enclose an analyte containing aqueous buffer. The internal aqueous content is isolated from the external medium at this point (in absence of ion channels). The preparation of these vesicles with a wide variety of lipid compositions and sizes follows well known procedures and is quite facile.[42] The size distribution of the vesicles, the overall lipid concentration, and the number of bilayers (uni- or multi-lamellar vesicles) can be characterized using well-developed techniques.[42] Ion channels as catalysts of ion translocation are capable of incorporating themselves into the vesicle membrane and then accelerating the diffusion of ions from one side of the membrane to the other. The experiments usually start by the addition of an ion channel compound, followed by the observation of the collapse of the concentration

gradient of the analyte between the internal and external environments of the lipid vesicles.[43] There have been a number of methods developed for detecting the concentrations of an analyte in either the interior or exterior of the vesicles. Some commonly used methods include using sodium NMR spectroscopy to monitor the transport of sodium ion with a vesicle-entrapped, membrane-impermeable paramagnetic shift reagent,[44] using ion-selective electrodes to monitor the diffusion of specific ions such as chloride or protons from the interior to the exterior of the vesicles,[45] and using UV/Vis or fluorescence spectroscopy to monitor the changes of concentration of a pH-sensitive dye induced by transport activity.[46]

The most extensively used dye based detection is the pH-sensitive pyranine dye HPTS (8-hydroxypyrene-1,3,6-trisulfonic acid). The illustration of this technique is shown in Figure 1-3. Vesicles are prepared in the presence of HPTS to ensure the entrapment of HPTS. An ion channel compound is then added into the vesicle medium for a standard period of equilibrium which allows the incorporation of the compound into the vesicle membrane, forming active ion channels. At this point, the pH levels in the interior and exterior of the vesicles are identical, so the proton transport should not happen even though the internal and external protons are able to exchange through the channels. HPTS has two excitation wavelengths; one for the hydroxyl form at 403nm and the other for the conjugated base at 460nm; both forms emit at 510nm. The experiment starts with monitoring the fluorescent emission wavelength of both forms which are alternately excited by the two excitation wavelengths. For a short period before addition of NaOH, there should be no transport activity as indicated by the short black baseline at zero transport. A pH-gradient is then established by the addition of NaOH to the external medium, which initiates the proton transport. The collapse of the pH-gradient is reported by the change in fluorescence as the hydroxyl form of HPTS gradually shifts to the conjugated base form in response to the increasing internal pH (red curve). At end of the experiment, the vesicles are lysed by the addition of a surfactant (Triton-X 100) to give the maximal response which ensures that the transport activity was not due to membrane disruption. On the other hand, if the blank control experiment in absence of ion channels or a normal experiment with an inactive compound is performed, the transport activity should remain very low as indicated by the blue curve.[2, 42]

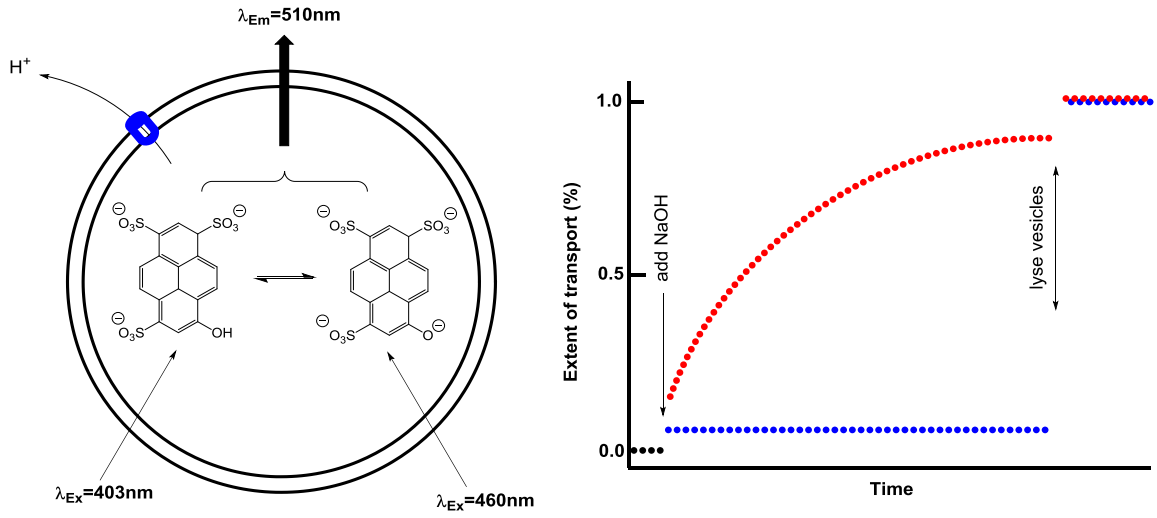

Figure 1-3. The vesicle with HPTS dye experiment: an active ion channel incorporates into the vesicle membrane and initiates the diffusion of internal protons to the exterior due to the establishment of a pH-gradient with the addition of NaOH. As a result, the excitation fluorescent wavelength of the entrapped HPTS switches from 403nm to 460nm (both species are monitored at the same emission wavelength 510nm) in response to the internal pH changes to more basic level. The transition in the excitation wavelength can be converted to the extent of proton transport over time (the plot on the right). The blue curve represents the blank control in which the experiment proceeds in absence of an ion channel compound. The red curve represents the experiment proceeds with vesicles containing an ion channel compound.

1.3.2 Planar Bilayers Based Experiments

Planar bilayers based experiments are also referred as voltage clamp or bilayer clamp experiments. Figure 1-4A, a set of voltage is applied into the two compartments filled with aqueous electrolyte solution in a cell holder. A planar bilayer membrane can be formed across a small hole that connects the two compartments by painting a small amount of lipid in a nonpolar solvent such as decane over the small hole and further gentle brushing or other manipulation. The planar bilayer membrane then creates a hydrophobic barrier between the two compartments, separating the electrolyte solutions filled within. The integrity of the membrane can be frequently checked with a capacitance test.[1-2] The voltage-clamp generates a constant transmembrane potential, and the resultant current can be monitored over time; change in the corresponding potential and conductance can also be monitored over time. In the absence of an open channel, the bilayer membrane itself is a good resistor which prevents the flow of current in response to the applied transmembrane potential, so very little current should be observed (Figure 1-4B). If an ion channel compound is introduced into the solution in either side or both sides of the membrane, successfully forming channels in the membrane, a simple electric circuit is complete, and current as the representation of channel activity starts to be observed (Figure 1-4C).

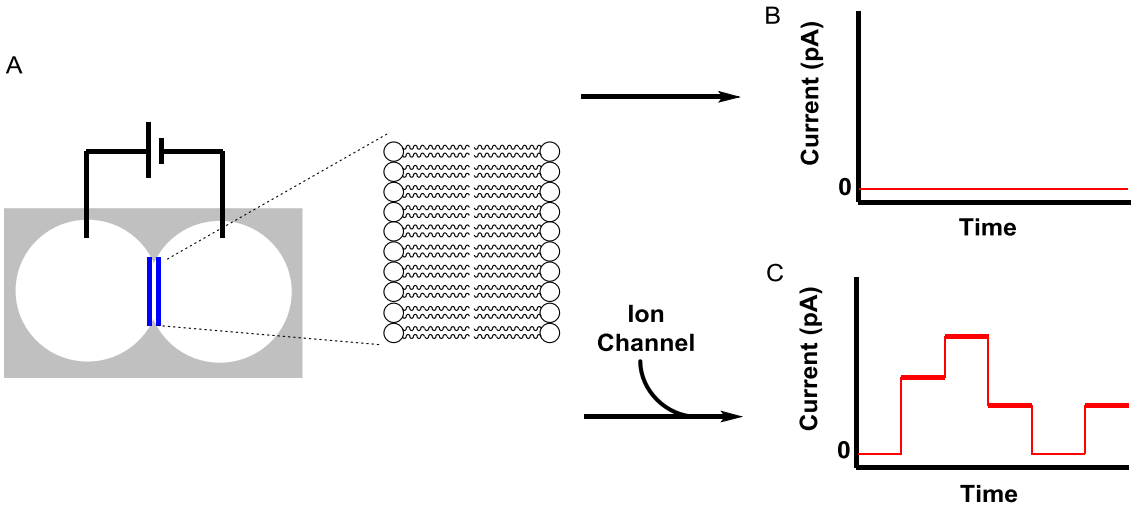

Figure 1-4. Voltage clamp experiment: A) a bilayer membrane is formed between the two compartments of the holding cell filled with aqueous electrolyte solutions (blue lines). A voltage is applied creating a transmembrane potential, B) and if the membrane is intact, very little current should be observed, C) but if an ion channel compound added with successfully incorporation into the membrane, current should be observed.

The resting potential at the membrane of the voltage clamp can be determined from Nernst potential equation (1):

$$E = \frac{RT}{nF} ln(\frac{[I]o}{[I]i}) \quad (1)$$

R is the gas constant; *T* is the absolute temperature; *F* is the Faraday constant; n is the charge on the ion; [I]o and [I]i represent the ion concentrations on either side of the membrane. In this case, the ion concentrations on either side are the same. The resting potential at the membrane is 0mV, meaning the current direction reverses at 0mV.

The "square-top" activity presented in Figure 1-4C occurs only in rather ideal situations. In a real experiment, current activities can be completely random upon the addition of ion channel compounds. There are many more complex current activities can be observed for active compounds, and between the periods with activities there are the "quiet" periods that have no activity. In other words, the channel behaviors in terms of the channels' "on" and "off" states, current intensity and current pattern are time-dependent. In the past these irregular behaviors are usually separated and ignored in favor of analyzing the easier regular "square-top" behaviors. The Fyles group has recently developed a method called activity grids for cataloging and categorizing all potentially observable behaviors in a statistically meaningful way.[4]

The general method for analyzing the transport behaviors of a certain ion channel compound is by averaging the resultant current at various potentials in a fixed period of time, regardless its complex current behaviors. Although this method lacks the specific representation for the distinct behavior of an ion channel compound, it is still the easiest

way to generate overall activity from variable time-dependent activity. However, this method is very sensitive to the experimental environment. Any noise, vibration, electrical interference or capacitance discharge could result artifacts that obscure the real activities. Consequently, before each experiment, membrane integrity and connections in the experimental setup must be tested free of ion channel compounds for a period of time to ensure the exclusion of any above artifacts.

1.4 Goal of the Project

As discussed before, Chui's discovery of exponential voltage-dependence of compounds **10** and **11** is a quite surprising result as the two compounds are structurally symmetrical. Chui's focus by then was only an activity survey of a number of compounds including **10** and **11** as a prelude to test activity grids. The research documented in this thesis focuses on confirming Chui's observation for compound **10** and **11** as well as further synthesizing and testing seven additional derivatives (**12**, **13**, **14**, **15**, **16**, **17** and **18**) of the parent compounds **10** and **11**. Based on the results obtained from the study, we are hoping to address the following questions that were left unanswered from Chui's preliminary discovery: Is the current-voltage response truly exponential? Are current patterns at the negative and the positive potentials symmetrical (non-rectifying ion channel) or asymmetrical (rectifying ion channel)? Are these observations time-dependent? Are there more compounds that behave the same? With some clear answers to these questions, it may be possible to propose a mechanism that allows symmetrical compounds to show voltage-dependent behavior.

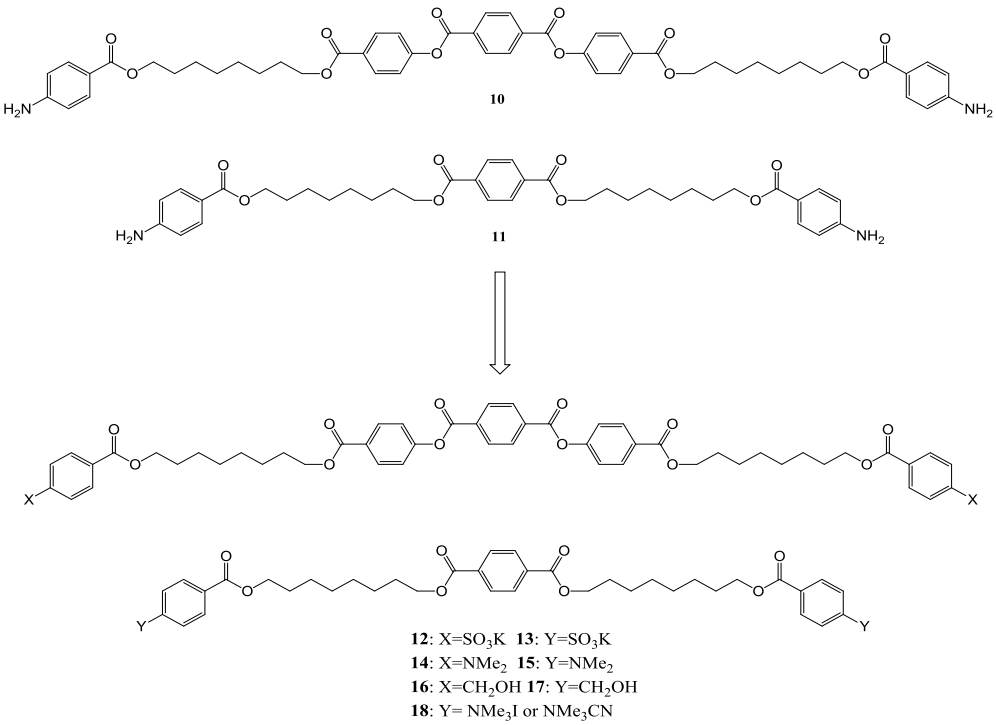

Figure 1-5. Proposal of the extended series of compounds (12-18) from the parent compounds 10 and 11.

2 Results and Discussion

2.1 Synthesis of Linear Oligoester Bolaamphiphilies

To be able to address these questions that emerged from Chui's discovery of voltage dependent ion transport observed for compound **10** and **11**, an extended series of compounds (**12, 13, 14, 15, 16, 17 and 18**) was synthesized. The main backbones of the compounds were kept intact so that their transporting functions would be presumably preserved. The various head groups were then installed onto the two ends of the backbones.

2.1.1 Synthesis of backbones

The synthetic methods for these compounds are mainly adapted from Chui's work.[1] The methods begin by constructing a triaromatic diacid core **21** by reaction of terephthaloyl chloride **19** and 4-hydroxybenzoic acid **20**, and subsequent conversion to the triaromatic dichloride **22**. Terephthaloyl chloride **19** or the triaromatic dichloride core **22** was then reacted with bromoalcohol **5** prepared by mono-brominating 1, 8-octanediol. This gave the mono-aromatic or tri-aromatic *bis*-bromides (**25** and **26**) which were subsequently reacted by various head group precursors.

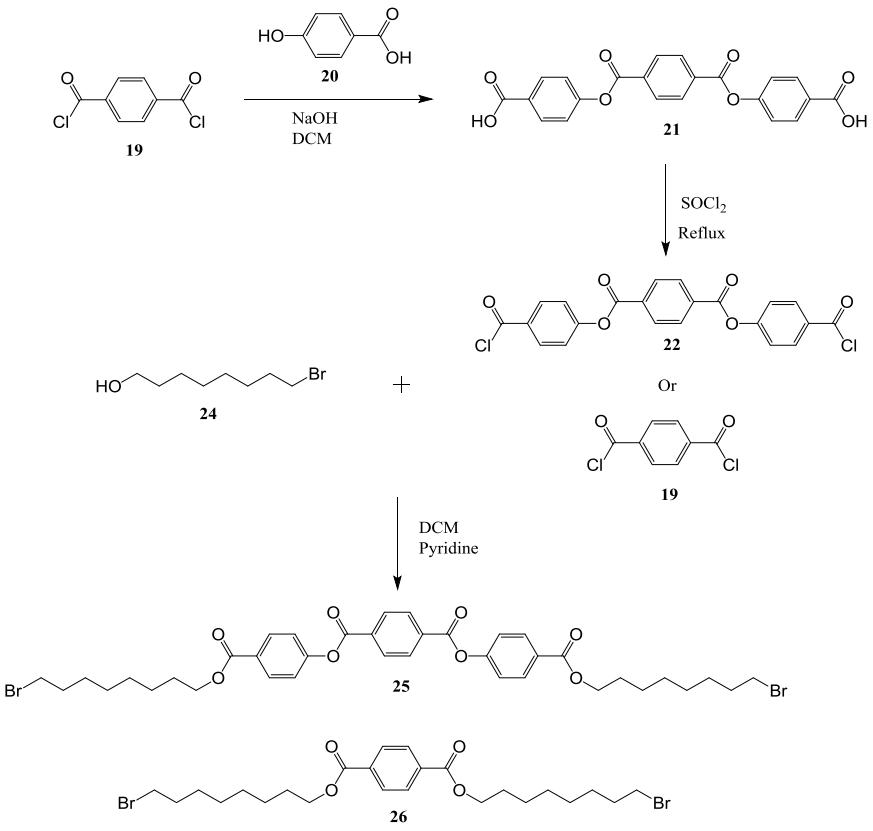

Scheme 2-1. Synthesis of the Backbones, Mono and Triaromatic Dibromide Core 25 and 26

2.1.2 Synthesis of Parent Compounds 10 and 11

Chui's method as he described in his thesis[1] was followed to prepare the parent compounds **10** and **11**. The mono and triaromatic dibromide **25** and **26** were first reacted with BOC protected 4-aminobenzoic acid **27** to give BOC-protected **28** and **29**. Removal of Boc-protecting group was achieved using TMSCl-phenol reagent in DCM to give compound **10** and **11** as described in Chui's thesis. The purification of the compounds by recrystallization or column chromatograph was also adapted from Chui's work. The resulting compounds were confirmed with ^{1}H and ^{13}C NMR spectra which were identical to those in Chui's thesis.

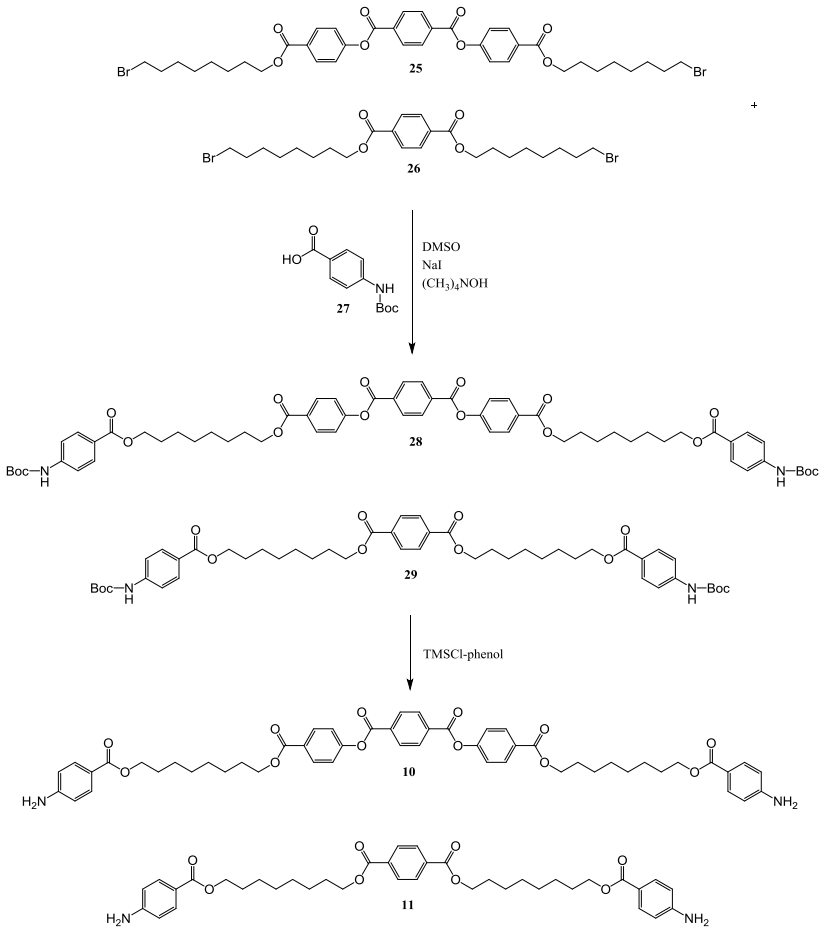

Scheme 2-2. I--catalyzed Nucleophilic Displacement and Deprotection in Preparation of 10 and 11

The ^{1}H NMR spectra showed the expected number of signals and chemical shifts and were identical to Chui's spectra. The ^{1}H NMR spectrum for **10** showed five types of aromatic protons at δ 8.33 (s, 4H), 8.13 (d, J=8.9Hz, 4H), 7.83 (d, J=8.8Hz, 4H), 7.32 (d, J=8.8Hz, 4H) as well as two types of methylene protons next to ester oxygen observed at 4.32 (t, J=6.7Hz, 4H), 4.24 (t, J=6.7Hz, 4H). The key amino protons were showed as a broad peak at 6.61 (br, s, 2H). For **11**, there were three types of aromatic protons at δ 8.09 (s, 4H), 7.84 (d, J=8.9Hz, 4H), 6.64 (d, J=8.9Hz, 4H) along with two types of methylene

protons next to ester oxygen observed at δ 4.36 (t, J=6.7Hz, 4H), 4.25 (t, J=6.7Hz, 4H). The key amino protons were showed as a broad peak at 4.03 (s, br, 4H).

The ^{13}C NMR spectrum for compound **11** was also consistent with the assigned structures and identical to Chui's spectra. Three types of aromatic protons observed at δ 166.8, 165.9, 150.8 along with two types of methylenes next to ester observed at δ 65.5, 64.4.

2.1.3 Synthesis of Sulfonate Compounds 12 and 13

The sulfonate compounds **12** and **13** were synthesized by reacting the dibromide cores **25** and **26** with 4-sulfobenzoic acid potassium salt **30** in the standard conditions as used for **10** and **11** (DMSO, Bu_4NOH, NaI, overnight). At the end of the reaction, DCM was added into the reaction mixture. The sulfonate compounds were precipitated out of the reaction solution due to their low solubility in DCM. The precipitates were then filtered and washed with methanol to remove residual tetramethyl ammonium hydroxide. The resulting compounds were confirmed with Mass spectroscopy, ^{1}H and ^{13}C NMR.

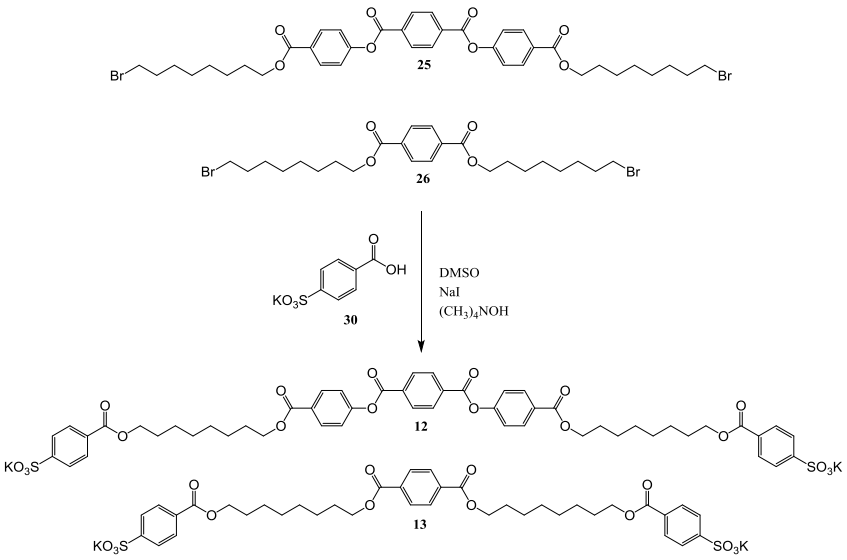

Scheme 2-3. I--catalyzed Nucleophilic Displacement in Preparation of 12 and 13

By negative ESI mass spectrometry, the m/z calculated for **12** dianion $[C_{52}H_{52}O_{18}S_2]^{2-}$ was 514.5, and this ion was observed as 514.6. Also, a monoanion corresponding to the monopotassium salt was observed ($[C_{52}H_{52}O_{18}S_2+K]^-$ =1068.1; found 1067.7). Similarly for **13**, the calculated dianion mass was observed along with the monopotassium salt (the m/z calculated $[C_{38}H_{44}O_{14}S_2]^{2-}$ =394.4 and $[C_{38}H_{44}O_{14}S_2+K]^-$ =827.9; found 394.8 and 827.8 respectively).

The ^{1}H NMR spectra showed the expected number of signals and chemical shifts. For **12**, five types of aromatic protons were observed at δ 8.34 (s, 4H), 8.07 (d, J=8.9Hz, 4H) 7.91 (d, J=8.8Hz, 4H), 7.71 (d, J=8.9Hz, 4H) and 7.51 (d, J=8.9Hz, 4H) along with two types of methylenes adjacent to ester oxygen at δ4.30-4.23 (m, 8H). Compound **13**

showed three types of aromatic protons at δ 8.07 (s, 4H), 7.91 (d, J=8.8Hz, 4H) and 7.71 (d, J=8.8Hz, 4H) along with two types of methylenes next to ester oxygen at 4.31-4.21 (m, 8H).

The ^{13}C NMR spectra were also consistent with the assigned structures. For **12**, three types of carbonyl carbons were showed at δ165.5, 165.0, 163.5, and two types of methylene carbons next to ester carbons at δ 64.8 and 64.7. For **13**, there were two types of carbonyl carbons at δ165.4, 165.0 along with the two types of methylene next to ester at δ 65.1, 64.7.

2.1.4 Synthesis of Dimethylamino Compounds 14 and 15

The dimethylamino compounds **14** and **15** were synthesized by reacting the core **25** and **26** with 4-dimethylamino benzoic acid **31** in the standard conditions overnight. The resulting compounds were recrystallized from DCM/EtOAc and confirmed with mass spectroscopy, ^{1}H and ^{13}C NMR.

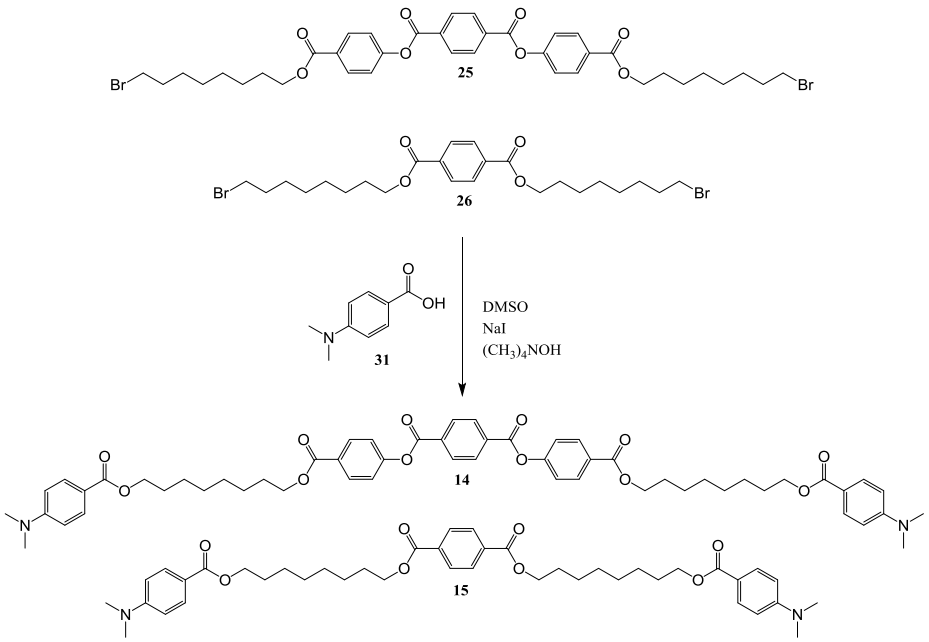

Scheme 2-4. I--catalyzed Nucleophilic Displacement in Preparation of 14 and 15

By positive ESI mass spectrometry, the m/z calculated for **14** cation $[C_{56}H_{64}O_{12}N_2+H]^+$ was 957.1, and this ion was observed as 957.1. Similarly, for **15** the m/z calculated cation monosodium salt $[C_{42}H_{56}O_8N_2+Na]^+$ was 739.5, and this ion was found 739.5.

The ^{1}H NMR spectra showed the expected number of signals and chemical shifts. The ^{1}H NMR spectrum for **14** showed five types of aromatic protons observed at δ 8.35 (s, 4H), 8.16 (d, J=8.8Hz, 4H), 7.92 (d, J=8.8Hz, 4H), 7.34 (d, J=8.8Hz, 4H) and 6.64 (d, J=8.8Hz,

4H) as well as two types of methylene protons next to ester oxygen at δ 4.34 (t, J=6.7Hz, 4H), 4.26 (t, J=6.7Hz, 4H). The identifier methyl protons on the amino nitrogen were showed at δ 3.03 (s, 12H). The ^{1}H NMR spectrum for **15** showed three types of aromatic protons at δ 8.09 (s, 4H), 7.91 (d, J=8.8Hz, 4H), 6.64 (d, J=8.8Hz, 4H) along with two types of methylene protons next to ester oxygen at δ 4.34 (t, J=6.7Hz, 4H), 4.26 (t, J=6.7Hz, 4H). The identifier methyl protons were showed at δ 3.03 (s, 12H).

The ^{13}C NMR spectra were also consistent with the assigned structures. For **14**, the spectrum showed three types of carbonyl carbons at δ165.8, 163.7, 154.2 as well as two types of methylene next to ester carbons at δ 65.3, 64.2. The identifier methyl carbons showed at δ 40.1. Similarly, for **15** the spectrum showed two types of carbonyl carbons at δ167.1, 165.9 along with two types of methylene next to ester at δ 65.5, 64.2. The identifier methyl carbons were observed at δ 40.0.

2.1.5 Synthesis of Hydoxymethyl Compounds 16 and 17

There were several trials to optimize the synthesis of the hydroxymethyl compounds **16**. In the early trials, the compounds were synthesized by reacting the core **25** with 4-hydroxymethyl benzoic acid **32** in the same condition overnight as the previous compounds. However, we think the hydroxyl group of **32**, hydrolysis and transesterification occurred around ester bonds in the core **25** during the reaction. This generated a mixture of compounds that were difficult to be characterized using ^{1}H NMR spectroscopy or to be purified through silica column chromatography or LH-20 gel column (size exclusion column).

We decided to protect the hydroxyl group on **32** so that prevents any side reactions. The hydroxyl protection was achieved using TBDMS. Compound **32** was reacted with tert-butylchlorodimethylsilane and imidazole in THF and 2M K_2CO_3 solution for 18 hours. The TBDMS protected **33** was then installed onto the core **25** using the previous condition to generate the TBDMS protected compound **34**. Although, hydrolysis still occurred, the TBDMS protected compound **34** was able to be isolated using silica column chromatography. The deprotection of TBDMS was carried out by combining and stirring DCM solution of the TBDMS protected **34** with 1 equivalent tetra-n-butylammonium fluoride in room temperature for 20minutes. However, the deprotection process also resulted the hydrolysis of the ester bonds in the molecule. Considering the effort and the time required of deprotecting the TBDMS protected compound **34**, the further exploration of an optimal deprotection condition was on hold.

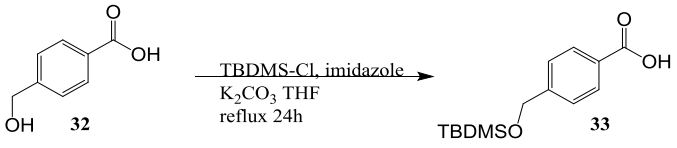

Scheme 2-5. TBDMS protection of 4-Hydroxymethyl Benzoic Acid

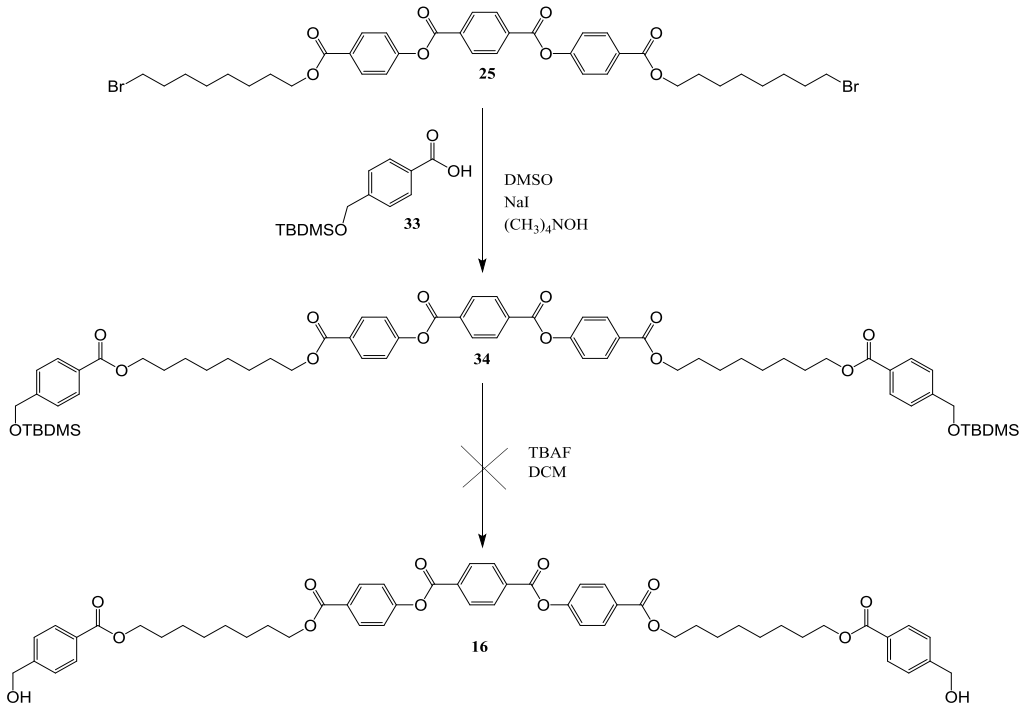

Scheme 2-6. Synthesis of Hydroxymethyl Compound 16 with 14

The last attempt of making the compound **16** was carried out using the similar condition as the previous compounds except the reaction time was kept short under 2 hours. The generated compound was purified through silica column chromatography. It was later discovered that the compound **16** could be purified by recrystallization from DCM/EtOAc. The synthetic method was also suitable for making the compound **17** which was also purified by recrystallization from DCM/EtOAc (Scheme 2-7). The two compounds did not generate decent ESI-MS spectra; therefore, both compounds were confirmed by ^{1}H and ^{13}C NMR.

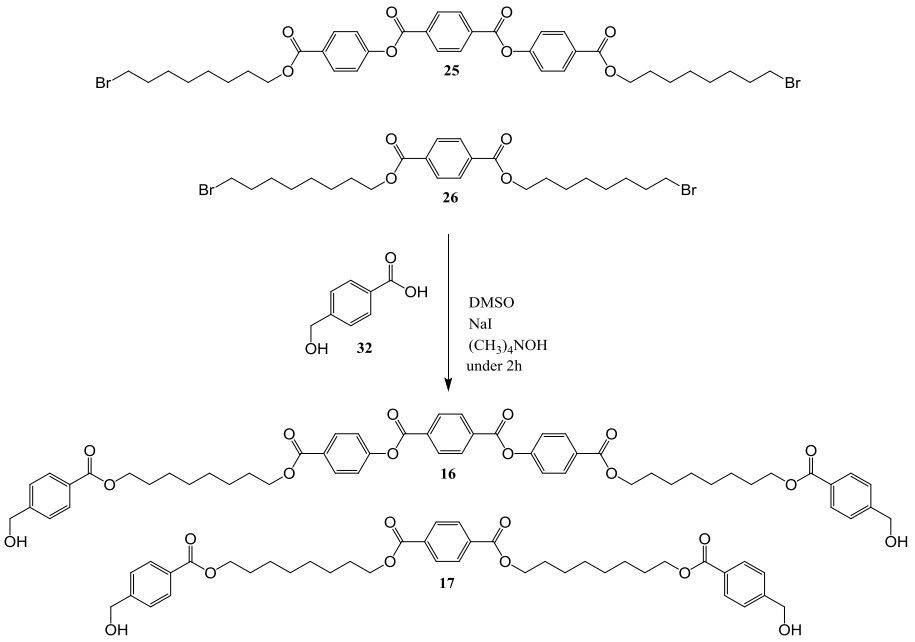

Scheme 2-7. I--catalyzed Nucleophilic Displacement in Preparation of 16 and 17

The ^{1}H NMR spectra showed the expected number of signals and chemical shifts. The ^{1}H NMR spectrum for **16** showed five types of aromatic protons observed at δ 8.35 (s, 4H), 8.14 (d, J=8.8Hz, 4H), 8.04 (d, J=8.8Hz, 4H), 7.43 (d, J=8.8Hz, 4H), 7.34 (d, J=8.8Hz, 4H). The methylene protons next to hydroxyl were observed at δ 4.77 (s, 4H) and two types of methylene protons next to ester oxygen were showed at δ 4.35-4.30 (m, J=6.7Hz, 8H). Similarly, for **17**, three types of aromatic protons were showed at δ 8.07 (s, 4H), 8.01 (d, J=8.8Hz, 4H), 7.41 (d, J=8.8Hz, 4H) and methylene protons next to hydroxyl were observed at δ 4.75 (s, 4H) as well as two types of methylene protons next to ester oxygen observed at δ 4.34-4.29 (m, 8H).

The ^{13}C NMR spectra were also consistent with the assigned structures. For **16**, three types of carbonyl carbons were showed at δ166.5, 165.8, 164.0 along with three methylene carbons next to hydroxyl and next to ester oxygen observed at δ 65.3, 65.0 and 64.7. For **17**, two types of carbonyl carbons were showed at δ166.5, 165.9 along with three types of methylene carbons next to hydroxyl and next to ester at δ 65.5, 65.0, 64.6.

2.1.6 Synthesis of Trimethylamino Compounds 18

There were several attempts of optimizing the synthesis of the trimethylamino compound **18**. In the early trials, the dimethylamino mono-aromatic core compound **15** was methylated by refluxing it in iodomethane to make the trimethylamino compound **18**. However, there were two problems with this reaction. First, the methylation reaction was in equilibrium between dimethyl and trimethyl amino heads. Second, the ester bonds of the molecule started to break in long reflux (over 24 hours) in high heat (about 70^{o}C). The resulting product was a mixture of compounds that contains dimethyl and trimethylamino compounds as well as the fragments resulting from breakage of the ester bonds in the molecule. The mixture was difficult to analyze by ^{1}H NMR spectroscopy. The ESI-MS spectrum showed a pentamethyl mono-cation, m/z=731 as the major abundant ion and the required hexamethyl dication, m/z=373 as the minor abundant ion.

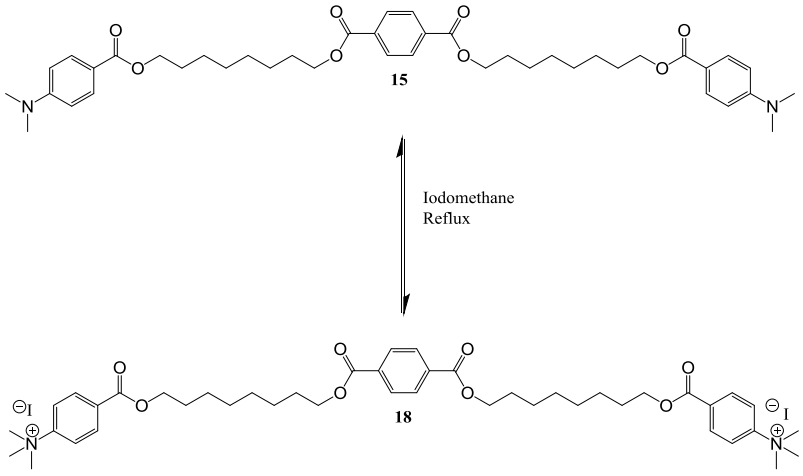

Scheme 2-8. Methylation of Compound 15 to prepare Compound 18

To detour the previous problems, the trimethylamino benzoic acid was first synthesized from dimethylamino benzoic acid by methylation, and was then installed onto core compound **26** using iodide catalyzed nucleophilic displacement, the usual method for making the series of compounds. However, the reaction also yielded a mixture of compounds which was as complex as the mixture that resulted from the methylation of compound **15**. The purification was difficult to perform on silica column chromatography, and the identification of the mixture was difficult with ^{1}H NMR. However, the dimethyl amino and trimethyl amino proton signals at about δ 3.3 and 3.7 were obvious. The ESI-MS spectrum also showed pentamethyl and hexamethyl ions (731 mono-cation and 373 dication) almost equally abundant.

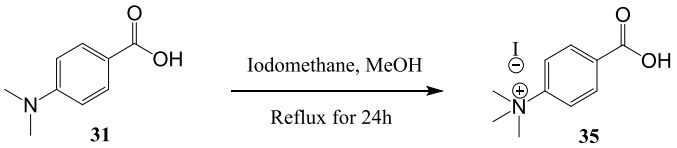

Scheme 2-9. Synthesis of Trimethylamino Benzoic Acid

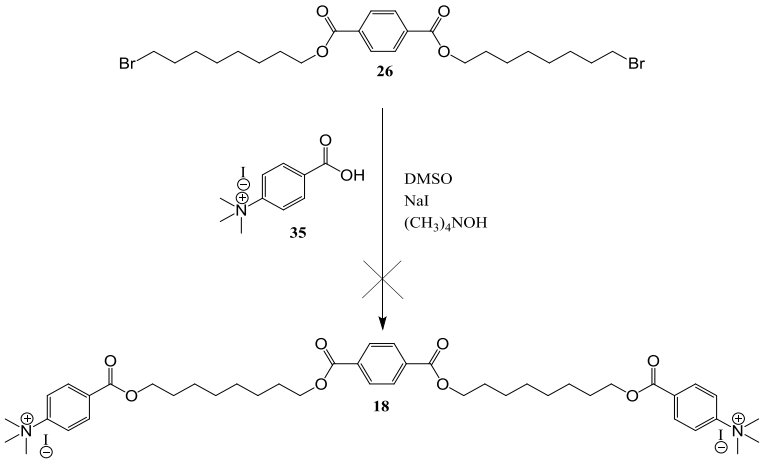

Scheme 2-10. I--catalyzed Nucleophilic Displacement in Preparation of 18

Alternatively, to push the methylation equilibrium to the completion, iodide ions could be removed from the system. Celite-$AgNO_3$ was, therefore, added to react with the iodide ions and remove from the reaction as the AgI precipitates. In addition, to prevent the degradation of the ester bonds, the reaction mixture was stirred under 45^{o}C over two days. Although these changes yielded a better result, the methylation had not gone to completion (or the proper length of methylation reaction was never found). The ESI-MS spectrum showed the hexamethyl ion (m/z 373 dication) as the major abundant ion, but there still significant pentamethyl mono-cation at m/z 731 left. Considering the time frame of the research project, the synthetic effort for the compound **18** was on hold at this point. The summary of the synthetic effort and results of the trials are listed in Table 2-1.

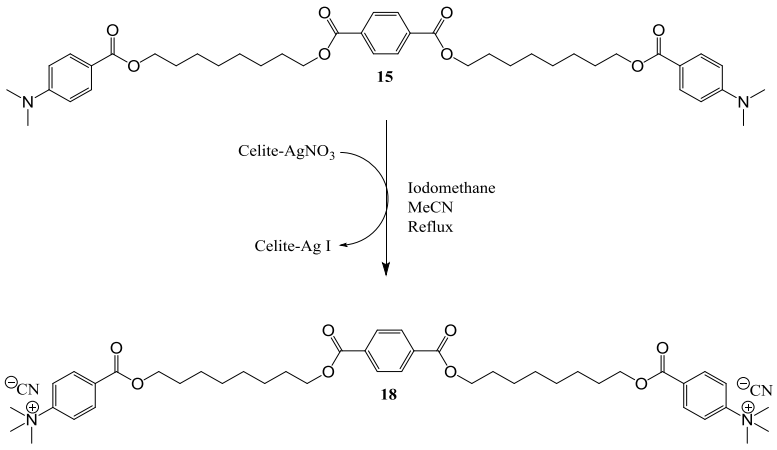

Scheme 2-11. Methylation with the Addition of Celite-$AgNO_3$

Trials	Conditions	Strategies	Results
1	Dissolve 20mL MeI Reflux at 60°C for 2 days	Methylation of compound **17**	Mixture of compounds; Equilibrium in methylation; ^{1}H NMR Me_2N:Me_3N = 1: 3
2	DMSO solvent NaI 0.2 eqv. 60-70°C 2hrs	Synthesize trimethylamino benzoic acid **15** and then attach to the core **26**	Mixture of compounds; Difficult to separation or analyze using ^{1}H NMR
3	Dissolve 20mL MeI Reflux at 45°C for 2 days	Methylation of compound **17** with Celite-AgNO3 to remove iodide ions to push the equilibrium to the right	Better results but still a mixture of dimethylamino and trimethylamno compounds ^{1}H NMR Me_2N:Me_3N = 1: 10

Table 2-1. Summary of Synthetic Attempts to Prepare Compound 18

2.2 Voltage Clamp Results

These compounds were analyzed using both techniques mentioned in the introduction. However, no of the compounds were active in the HPTS assay. Consequently, the study solely relied on the voltage-clamp technique. A voltage clamp is one of the techniques for studying ion channel activity. It applies constant transmembrane potentials and the resultant changes in current, potential and conductance can be monitored as functions of time.[2] The bilayer membrane which acts as a hydrophobic barrier is a good resistor, so in the absence of ion channel molecules, the membrane should be able to block the passage of ions so that only very little current can be observed. When a single ion channel opens with the addition of ion channel molecules, the current resulting from the flux of ions in response to the applied potential should be observed.

2.2.1 Sample Preparation and Experimental Setup

The voltage clamp apparatus consists of a bilayer clamp probe, electrolyte-filled holding cells with two connected compartments, a polystyrene cup (with a 250um aperture), Ag/AgCl electrodes and KCl/Agar salt bridges. The cup was placed in one of the compartments of the holding cell with its aperture facing the other compartment. The lipid bilayer membrane was added around the aperture by painting a small amount of lipid in decane over the aperture with a small brush and drying with argon gas. The aqueous CsCl electrolyte solution was then filled inside and outside the cup, and the aperture and the lipid were both immersed in the aqueous electrolyte solution. A stable membrane could form from lipids on the cup by lifting the cup out of the electrolyte solution and then dipping it back in, or sometimes by repainting a small amount of lipid in decane over the aperture with a small paint brush. Without membrane, the electrolyte solutions inside and outside the cup connect through the aperture. Once a stable membrane formed in the middle of the aperture, the two compartments of the holding cell are isolated. Through two KCl/Agar salt bridges, the two compartments were separately connected to two KCl reference electrolytes which were contacted electrically to the digital input of the apparatus via two of Ag/AgCl electrodes. The apparatus applies a potential, amplifies, and measures any current. The current is typically pico-Amperes so the signal needs to be isolated from electrical and mechanical interferences. It is quite noisy so the signal is filtered before being digitized. The signal was acquired using pClamp software to control the instrument.

All test compounds were prepared in 1mM and 5mM concentrations in 5mL of water-miscible organic solvents. The sulphonate compounds **12** and **13** were dissolved in DMSO, and the rest of compounds (**10**, **11**, **14**, **15**, **16** and **17**) were dissolved in THF. Once the stable membrane is formed, the test compounds were injected with a 10uL syringe in proximity of both sides of the bilayer membrane. Injection of compound **10**, **11**, **12**, **13**, **16** and **17** did not generate immediate transport activities, so these compounds were assisted by physical transfer on one side of the cup with a brush. Physical transfer

usually resulted membrane breakage; therefore, a lift/dip motion was required to reform the membrane and the capacitance needed to be checked again to ensure the integrity of the membrane. In some trials, compound **14** and **16** were premixed in 1mol% with the lipid before loading them on both sides of the membrane; however, the pre-mixing of these compounds with the lipid did not result in particularly more activity or any easier way of generating activities.

The data was surveyed with various positive and negative potentials in a continuous recording mode after the addition of the test compounds. This allowed the activity to be explored under operator control to ensure the activity was as expected and reliable. In order to record data automatically after stable activities were observed, the system was switched to instrument control of the applied potential where a potential was set for a fixed period of time, shifted to a new potential at the end of each period, and then repeated over the range of potential required. Under these conditions the acquisition is automated and no operator intervention or perturbation is possible. However, the amplification of current gain was difficult to estimate or preset in automated recording; as a result, the large current spikes in response to major ion channel openings at higher potentials would sometime overflow the digitizer scale. This problem seemed unsolvable using the current experiment setup. Nevertheless, the experiments were conducted in the automated and unbiased condition.

2.2.2 Voltage Clamp Data

The following table summarizes the total experiment trials and the trials for the observable activity for each compound.

Compound	No. of trials	Trials with observable activity	Voltage dependent or Ohmic
10	16	11	Voltage dependent
11	8	5	Voltage dependent
12	10	4	Voltage dependent and Ohmic
13	10	6	Voltage dependent and Ohmic
14	8	0	-
15	7	4	Voltage dependent
16	8	6	Ohmic
17	8	5	Ohmic
18	-	-	-

Table 2-2. Summary of Voltage Clamp Experiment

2.2.2.1 Voltage Clamp Data for the Parent Compound 10 and 11

The instrument controlled modes display real-time data on three panels corresponding to changes of the current, the potential and the conductance for a certain compound. The current-time perspective was recorded as shown in the top panel. The automated corresponding potential changes were shown in the middle panel. The bottom panel was the conversion to conductance-time perspective using division of the current by the potential at each data point. An experiment recorded in this fashion is given in full in Figure 2-1.

The Figure was one of the recordings of the parent compound **10**. As shown in the middle panel, the potential change was set from150mV to -150mV. Each potential level was maintained 11seconds and was then increased to a new level by 20mV at the end of each period (stepping up). The resultant current was measured on a scale of 200 to -200pA. The activity was very strong at very positive and very negative potentials in terms of the magnitude of the current spikes (close to 200pA) and in terms of a higher frequency of observations (very dense spikes at 0-20 seconds and 160-176 seconds). The activity quickly diminished as the potential dropped below ±130mV and appeared to die off at very low potential (around ±10mV). Correspondingly, the conductance appeared to be very high at very positive and very negative potential and diminished as the potential got smaller. However, near zero potential, there was a big block of conductance which resulted from significant noise being divided by a very small potential. At zero current, of course, the conductance should be zero, so all this section shows is the amplified system noise.

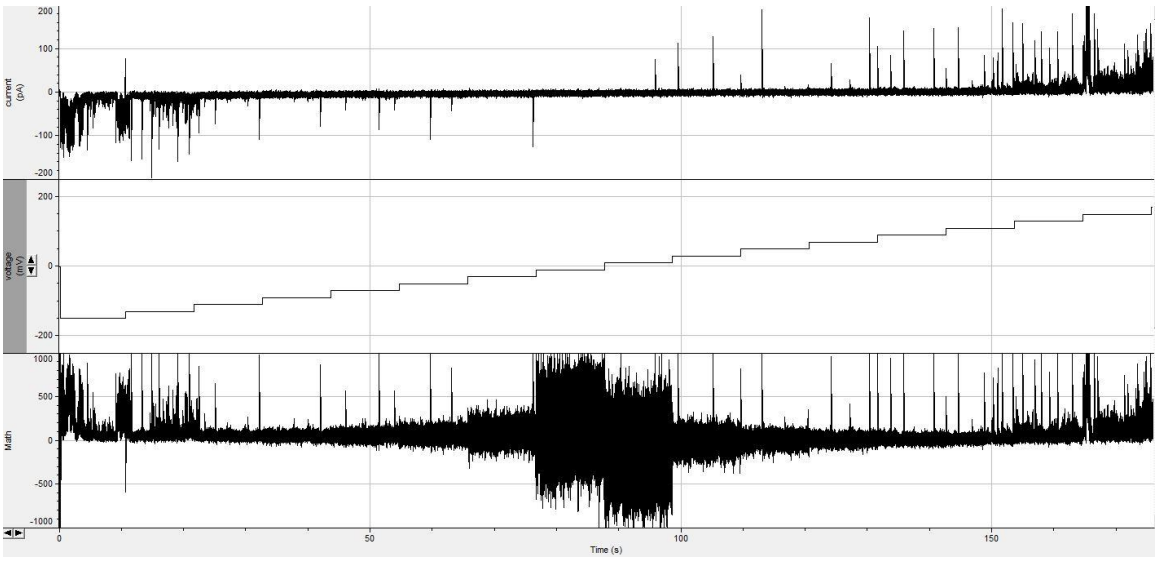

Figure 2-1. Voltage Clamp Data for Parent Compound 10. Condition: 1M CsCl buffered to pH 7.0, -150mV to 150mV in steps of +20mV; total experiment time 176 seconds with total 6uL of 1mM solution added on both sides of the membrane (total 12nmole of 10). Top panel: current-time perspective with full scale -200 to +200pA; middle panel: potential-time perspective with full scale -220 to +220mV; bottom panel: conductance-time perspective with full scale of -1 to +1nS.

The time-dependent data in Figure 2-1 was not useful for the analysis of the activity of the compounds. The average current data at the different potential levels was used to plot against the applied potentials to generate Figure 2-2 (left). The average current was calculated for only 10 seconds of data at each potential to avoid the current surges that occurred at the times when the applied potential was changed. As shown, the activity concentrated at very positive and very negative potentials (±150mV) and diminished quickly when the potential dropped below ±130mV. This plot appeared to be a centrally symmetrical pattern with slight off-setting from the zero point due to the amplified noise. This symmetry was similar to what Chui had observed. Chui claimed the positive and negative current patterns were symmetrically related, so he thought he could combine and analyze both positive and negative branches on the same side of the axis. However, this symmetrical data was only one special case among the more common asymmetrical cases which will be shown in later examples. In the average conductance vs. applied potential plot (Figure 2, right), the four data points at ±30mV and ±10mV were omitted due to the unrealistic data points generated from the amplified noise near the zero potential. As shown, the conductance maintained relatively a stable value of about 60pS from -110mV to -50mV but increased from below 20pS to about 40pS from 50mV to 110mV. The conductance increased dramatically once the higher potential (150mV or 130mV) was reached.

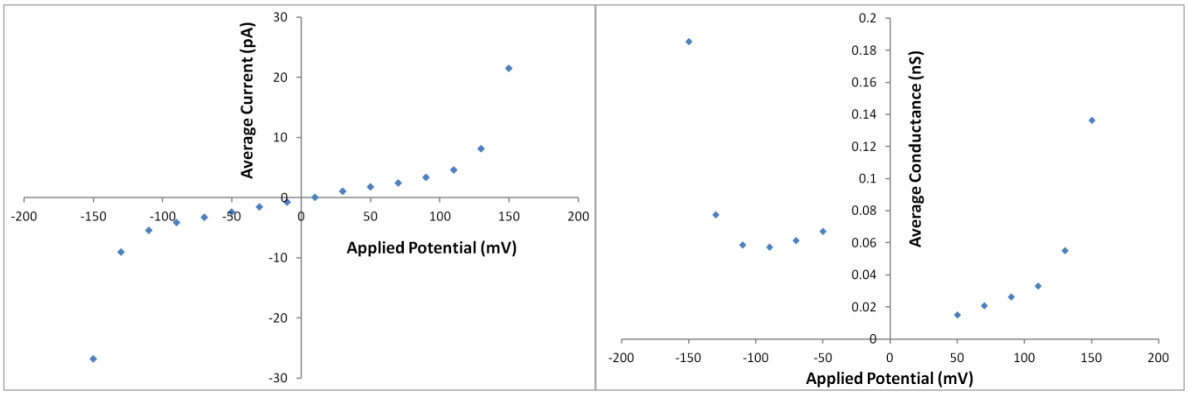

Figure 2-2. Left: Average Current vs. Applied Potential for Compound 10. Right: Average Conductance vs. Applied Potential for Compound 10; the unrealistic data points near the zero potential were not included.

In a different recording for compound **10** which was a few minutes later from the previous recording, the activity was recorded in step-down of potential levels that maintained 110 seconds per level (Figure 2-3). Similarly to the previous case, the activities concentrated at the high positive and high negative potentials (dense spikes at ±150mV) and diminished at lower potentials.

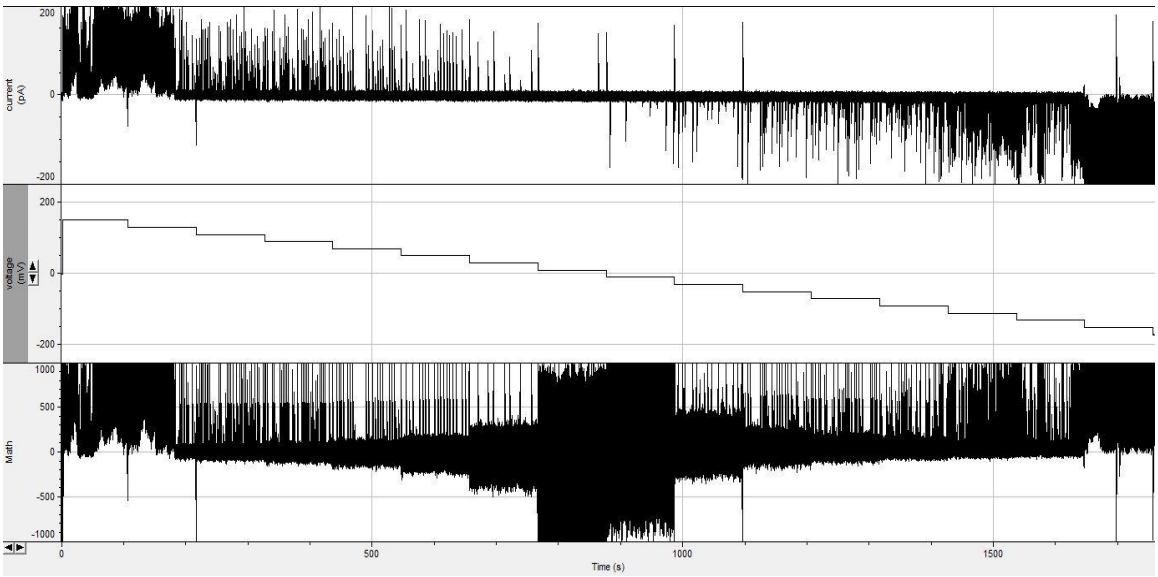

Figure 2-3. Voltage Clamp Data for Parent Compound 10. Condition: 1M CsCl buffered to pH 7.0, +150mV to -150mV in steps of -20mV; total experiment time 1760 seconds with total 6uL of 1mM solution added on both sides of the membrane (total 12nmole of 10). Top panel: current-time perspective with full scale -200 to +200pA; middle panel: potential-time perspective with full scale -220 to +220mV; bottom panel: conductance-time perspective with full scale of -1 to +1nS.

The average current vs. applied potential was used to analyze the current patterns at the positive and negative potentials. The average current was calculated for only 100 seconds of data at each potential to avoid the current surge that occurred at the times when the applied potential was changed. As shown in Figure 2-4 (left) the current activity was very low from -130 to 110mV; whereas, the current started to take off as the potential reached ±150mV. Similarly, using the average conductance data to plot against the applied potential generated Figure 2-4 (right). It is also worth mentioning that the region near the zero point had a few off-set data points which were again due to the amplified noise at low potentials in the conductance vs. potential plot, and these are not included in the plot. The conductance maintained relatively the one level (about 50pS) from -130 to -50 and a range from about 20pS to 50pS from 50mV to 110mV. The conductance increased dramatically once the potential reached ±150mV. Obviously the conductance on the positive branch was not in central symmetry with the negative branch. This was one of common cases observed in the experiments, which contradicts Chui's symmetry conclusion.[1]

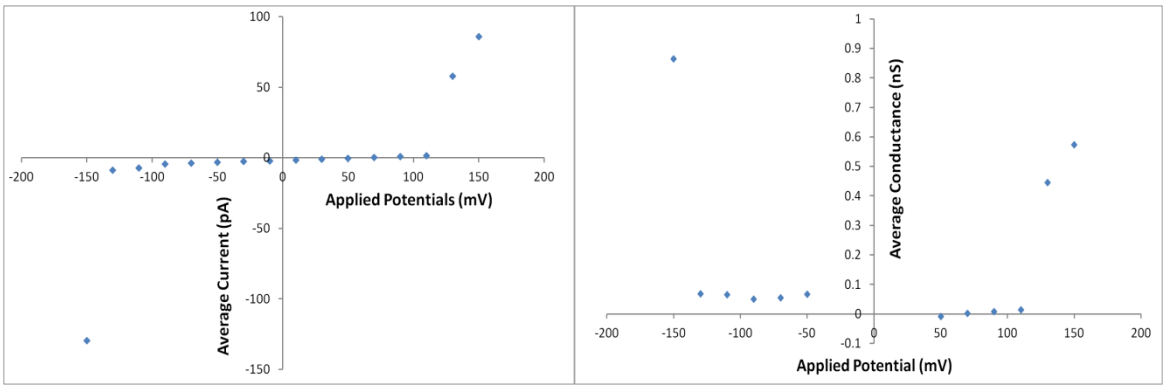

Figure 2-4 Left: Average Current vs. Applied Potential for Compound 10. Right: Average Conductance vs. Applied Potential for Compound 10; the unrealistic data points near the zero potential were not included.

The following Figure 2-5 was one of the current recordings for compound **11** under similar experiment settings but with the potential set from 110 to -110mV and each level maintained only 11 seconds. There were also periodic current surges corresponding to each change of the potential level. The average current was calculated for only 10 seconds of data at each potential to avoid the current surge that occurred at the times when the applied potential was changed. There were some overflows of the digitizer scale at the negative potential. Similar to compound 10, the activities concentrated at very positive (+110mV) and especially at negative potentials (-110mV) while the activity diminished quickly once the potential reached below ±90mV and then died off near zero potential (Figure 2-6, left). The symmetrical pattern for compound **11** between the current data on the positive and negative potential was not observed. The data patterns for this compound observed were asymmetrical. This contradicts to Chui's conclusion.[1]

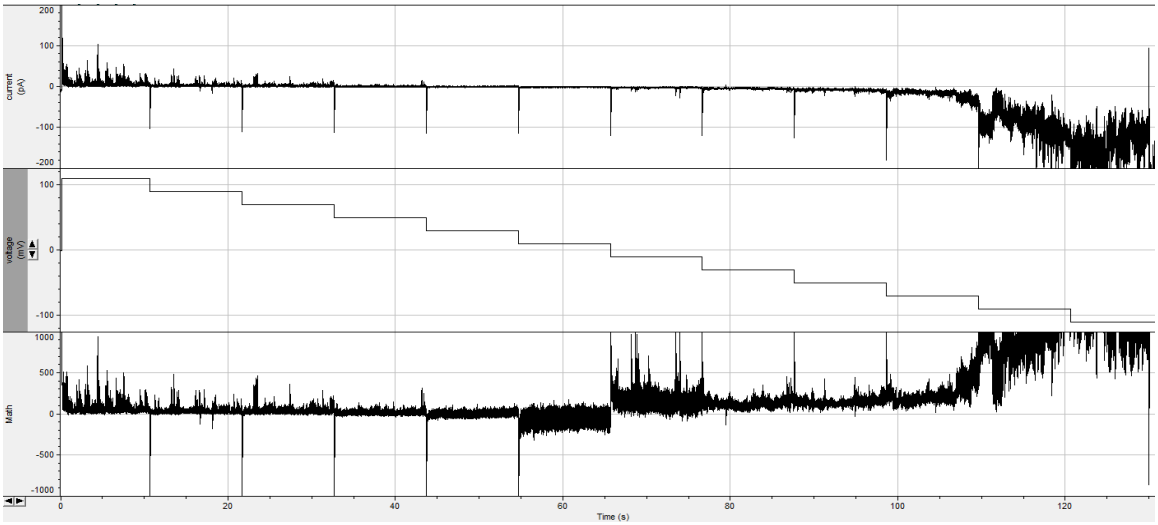

Figure 2-5. Voltage Clamp Data for Parent Compound 11. Condition: 1M CsCl buffered to pH 7.0, +110mV to -110mV in Steps of -20mV; total experiment time 132 seconds; 1mol% of 11 was premixed with lipid followed by total 6uL of 1mM solution added on both sides of the membrane (total 12nmole of 11). Top panel: current-time perspective with full scale -200 to +200pA; middle panel: potential-time perspective with full scale -120 to +120mV; bottom panel: conductance-time perspective with full scale of -1 to +1nS.

The conductance vs. potential plot (Figure 2-6, right) had the unrealistic data points at ±10mV which were omitted from the plot. The conductance maintained relatively one level (200pS) from -70mV to -30mV as well as a different level (35-50nS) from 30mV to 90mV with slight change. A large conductance change was observed at high negative potential while the changes in positive potential were not very obvious compared to the negative side. The two branches of the conductance were not in central symmetry. This

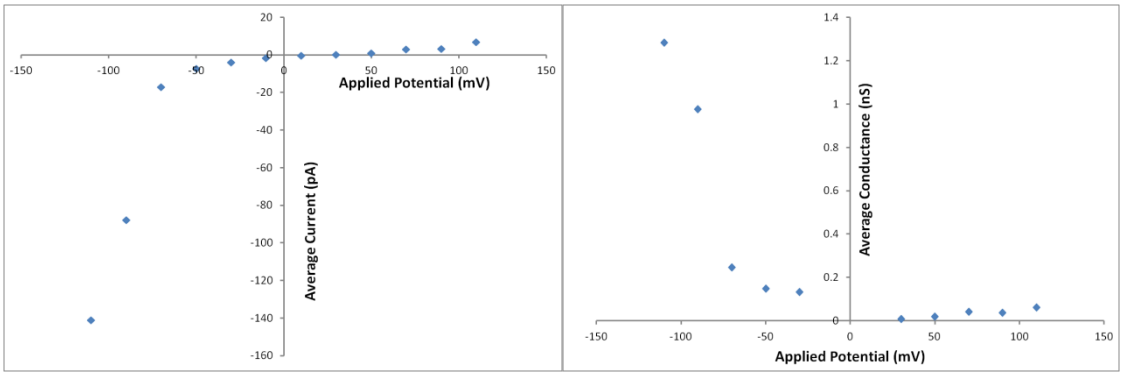

Figure 2-6. Left: Average Current vs. Applied Potential for Compound 11. Right: Average Conductance vs. Applied Potential for Compound 11; the unrealistic data points near the zero potential were not included.

summary of the two compounds calls into question Chui's conclusion. First, as reported by Chui, the activities of both compounds on voltage clamp were voltage dependent. However, the summary shows they were also time-dependent. An activity recording usually differed from the previous recording or the next recording. Therefore, the similar activities, in terms of similar current magnitude and similar pattern, were very difficult to reproduce on regular basis. Second, the positive and negative branches were not centrosymmetrical. The asymmetrical current patterns of both branches were very obvious in the current vs. potential plot (Figure 2-4 left and 6 left). The conductance changed differently on the positive and negative potentials. Therefore, the two branches of current needed to be analyzed separately (Figure 2-4 right and Figure 2-6 right). Thus, Chui's method of combining and analyzing two branches together would no longer work on the extended series of compounds.

2.2.2.2 Voltage Clamp Activity Survey for the Other Compounds

To develop a better understanding of the activities involved with the new compounds compared with compound **10** and **11**, we decided to survey these compounds in the voltage clamp under the same conditions as discussed above, but we would mainly focus on their current-time activity as this gives a quick overview of the compound behavior.

2.2.2.2.1 Voltage Dependent Activity of Compound **12** and **13**

The following activity recordings showed voltage-dependent activities for **12** (Figure 2-7) and **13** (Figure 2-8) using similar experimental conditions. As shown, the activities concentrated on higher positive and negative potentials and diminished quickly at low

potentials. However, the activities were under 50pA which were not as strong as those observed in **10** and **11**. Also, the magnitude of activity at the positive and the negative potentials were obviously not in symmetry. The average current vs. applied potential plots showed a great current change at high potential dependence while the current was very low at lower potentials. The magnitude and patterns of the activities on both sides of potentials were clearly not in symmetry.

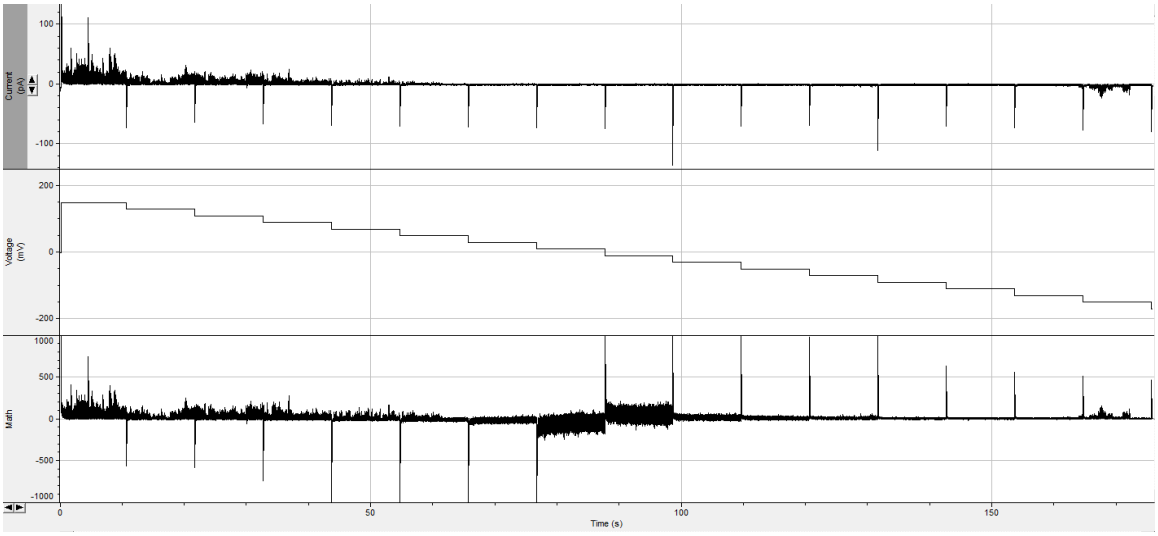

Figure 2-7. Voltage Clamp Data for Compound 12. Condition: 1M CsCl buffered to pH 7.0, +150mV to -150mV in steps of -20mV; total experiment time 176 seconds with total 6uL of 1mM solution added on both sides of the membrane (total 4nmole of 12). Top panel: current-time perspective with full scale -200 to +200pA; middle panel: potential-time perspective with full scale -220 to +220mV; bottom panel: conductance-time perspective with full scale of -1 to +1nS.

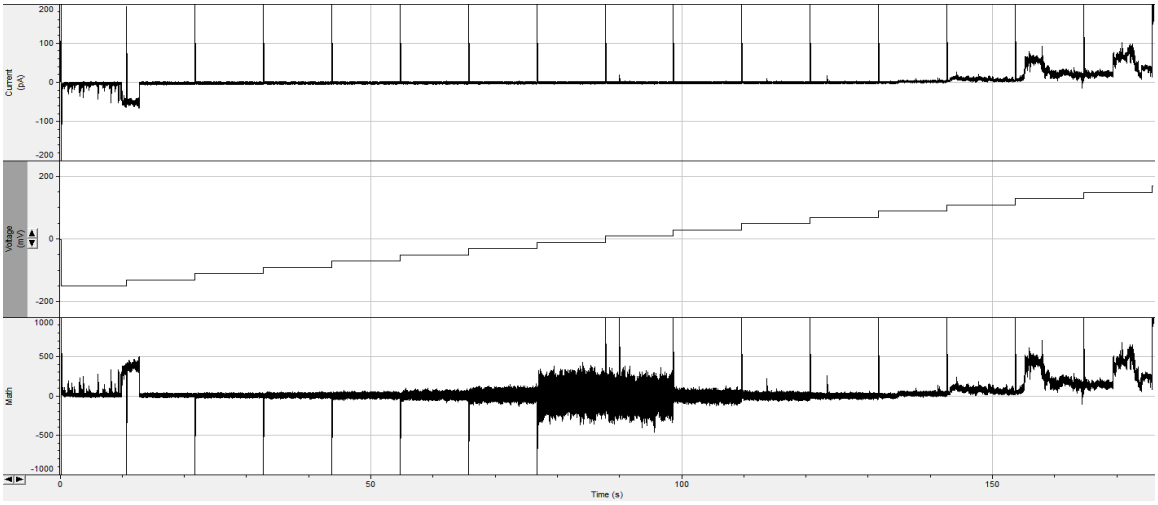

Figure 2-8 Voltage Clamp Data for Compound 13. Condition: 1M CsCl buffered to pH 7.0, -150mV to +150mV in steps of +20mV; total experiment time 176 seconds with total 6uL of 5mM solution added on both sides of the membrane (total 60nmole of 13). Top panel: current-time perspective with full scale -200 to +200pA; middle panel: potential-time perspective with full scale -220 to +220mV; bottom panel: conductance-time perspective with full scale of -1 to +1nS.

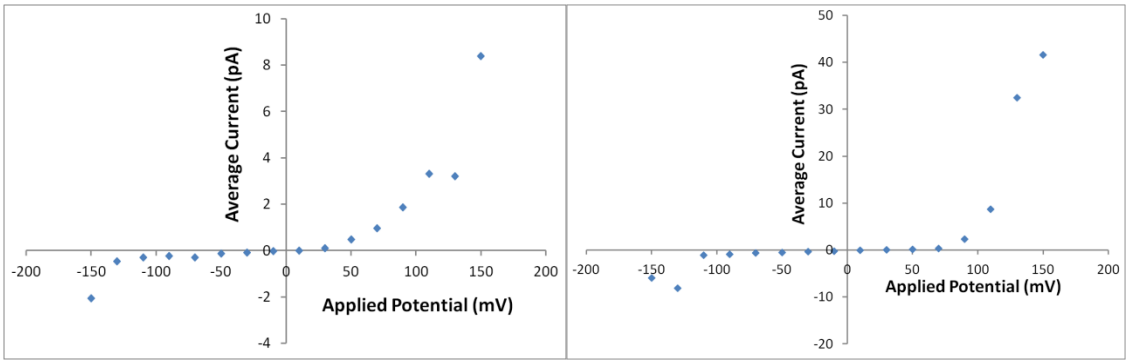

Figure 2-9 Left: Average Current vs. Applied Potential for Compound 12. Right: Average Current vs. Applied Potential for Compound 13.

When the initial injection did not result immediate activities, more would be injected on both sides of the membrane, and often, the compounds required physical transfer which would assist compounds to incorporate into the membrane. The capacitance was checked to ensure the integrity of the membrane. When 10uL of compound **12** or 8uL of **13** were added on both sides of the membrane (total 20nmole of **12** and 80nmole of **13**), the observed activity appeared to be voltage-independent in which the channel maintained continuously "on" state as shown in Figure 2-10 and 2-11. The current change nicely corresponded to the potential change from 150mV to -150mV. The average current vs. applied plot in Figure 2-10 and 2-11 showed the Ohmic relationship. Also, the slopes of the plots were the conductances of **12** and **13** (1.2nS and 460pS, respectively).

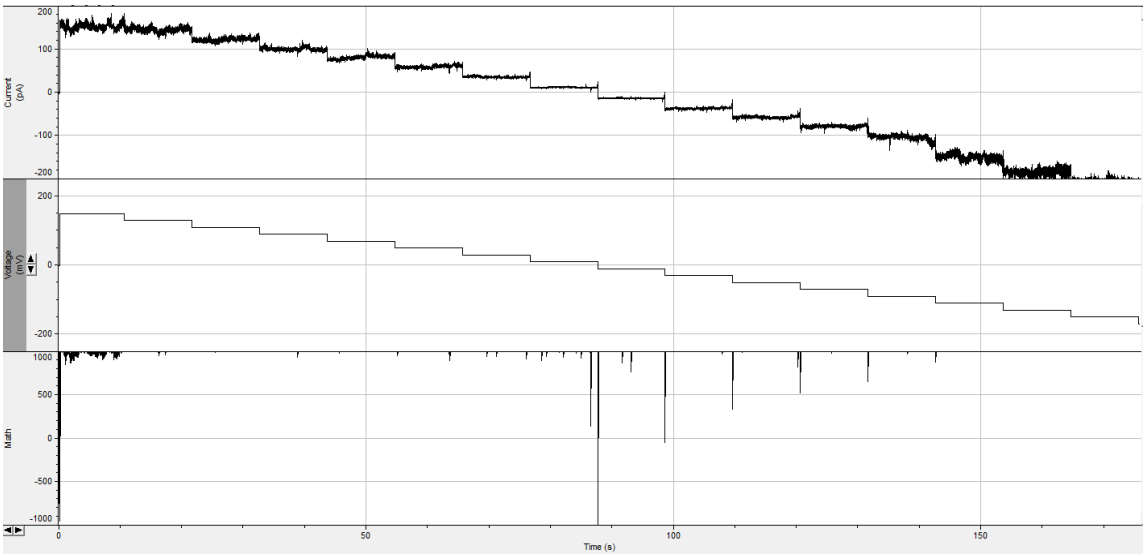

Figure 2-10. Voltage Clamp Data for Compound 12. Condition: 1M CsCl buffered to pH 7.0, +150mV to -150mV in steps of -20mV; total experiment time 176 seconds with total 10uL of 1mM solution added on both sides of the membrane (total 20nmole of 12). Top panel: current-time perspective with full scale -200 to +200pA; middle panel: potential-time perspective with full scale -220 to +220mV; bottom panel: conductance-time perspective with full scale of -1 to +1nS.

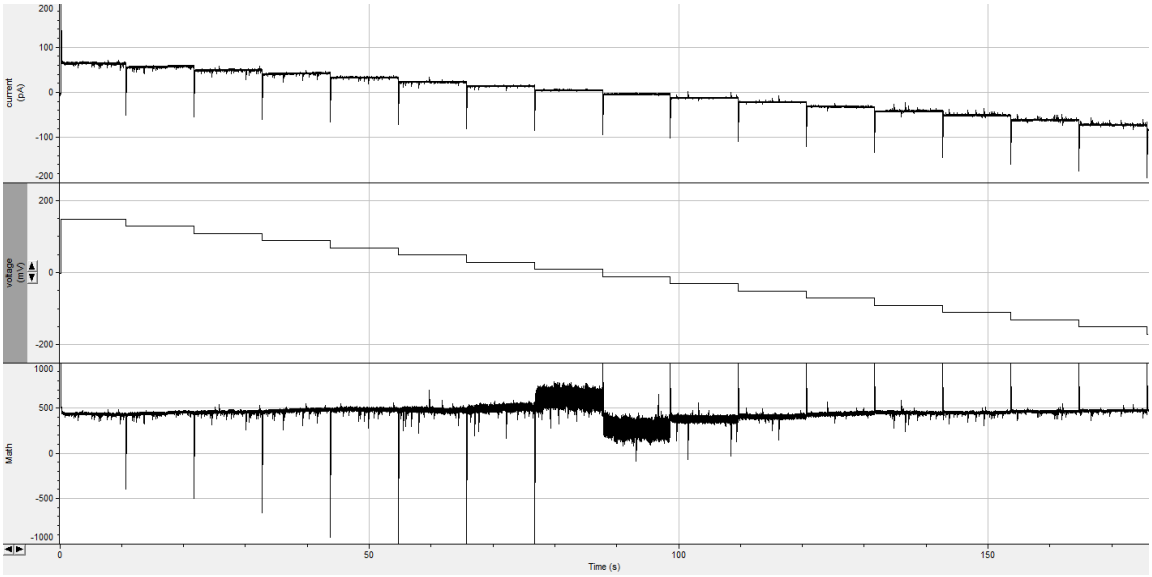

Figure 2-11. Voltage Clamp Data for Compound 13. Condition: 1M CsCl buffered to pH 7.0, +150mV to -150mV in steps of -20mV; total experiment time 176 seconds with total 8uL of 5mM solution added on both sides of the membrane (total 80nmole of 13). Top panel: current-time perspective with full scale -200 to +200pA; middle panel: potential-time perspective with full scale -220 to +220mV; bottom panel: conductance-time perspective with full scale of -1 to +1nS.

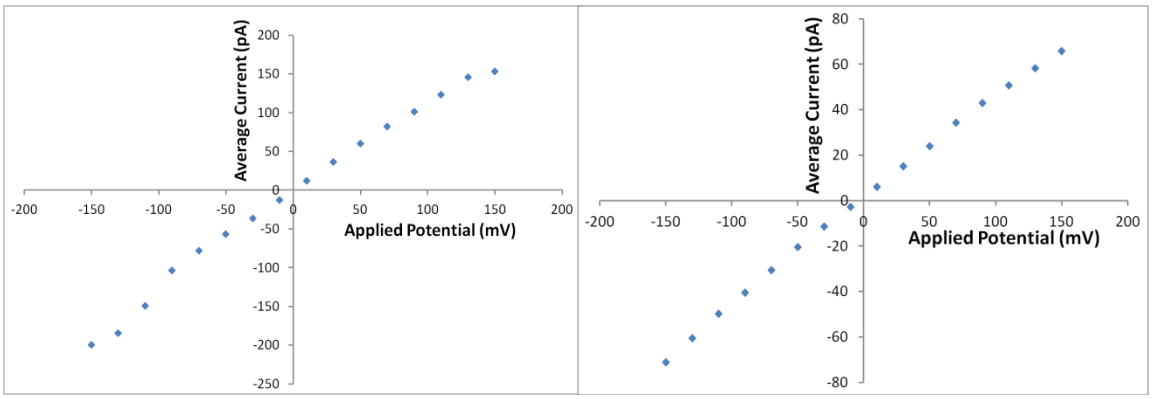

Figure 2-12. Left: Average Current vs. Applied Potential for Compound 12 (Linear Relationship). Right: Average Current vs. Applied Potential for Compound 13 (Linear Relationship

2.2.2.2.2 Voltage Dependent Activity of Compound **15**

Although activity was not observed for compound **14**, compound **15** with the similar structure was about as active as the parent compounds **10** and **11**. The activity for compound **15** could be observed in every two or three trials, while for compound **14**, activity was not observed in all five trials. The activity for compound **15** was quite strong as shown in Figure 2-13. The activity at the positive potential concentrated at about 110mV while the activity started low at the highest positive potential. The activity at the negative potential mostly concentrated at the highest potential as usual. However, there were also some activities at low negative potentials from -10mV to -50mV and then a drop from -60mV to -110mV before reaching higher negative potentials. These observations were clearly due to time-dependency. The conducting structure was clearly changing during the experiment.

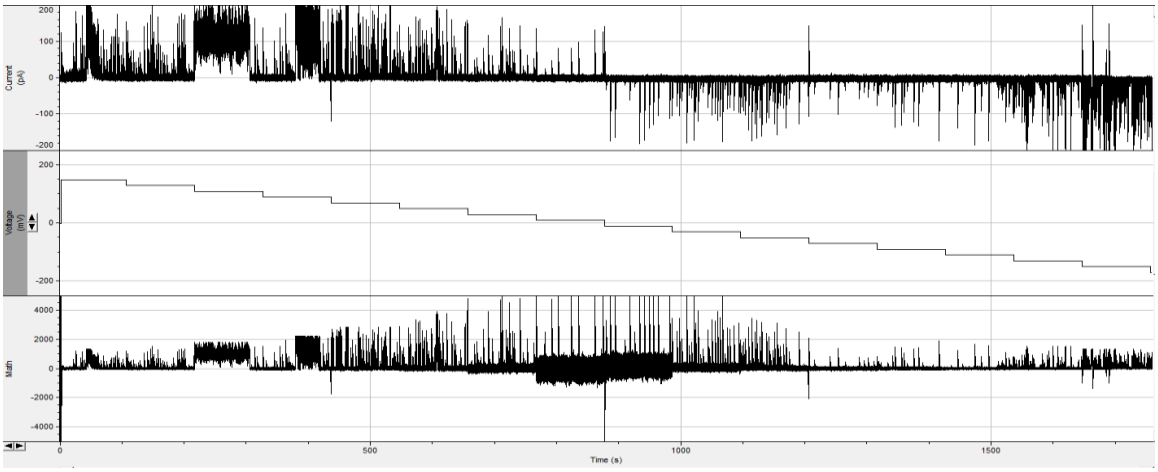

Figure 2-13. Voltage Clamp Data for Compound 15. Condition: 1M CsCl buffered to pH 7.0, +150mV to -150mV in steps of -20mV; total experiment time 1760 seconds with total 6uL of 1mM solution added on both sides of the membrane (total 12nmole of 15). Top panel: current-time perspective with full scale -200 to +200pA; middle panel: potential-time perspective with full scale -220 to +220mV; bottom panel: conductance-time perspective with full scale of -4 to +4nS.

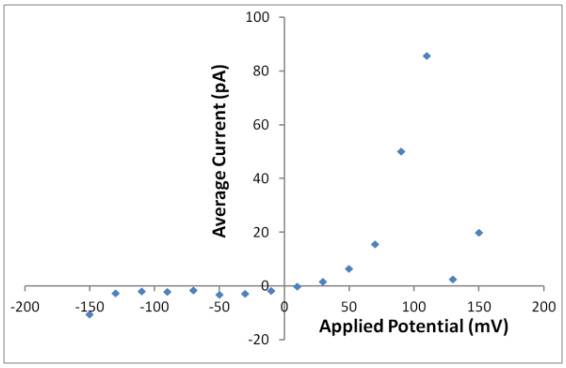

Figure 2-14. Average Current vs. Applied Potential for Compound 15

2.2.2.2.3 Voltage-Independent Activity for Compound **16** and **17**

Both compounds were premixed at 1mol% with lipid in decane before the experiments. Compound **16** was then added 2uL on both sides of the membrane (total of 4uL, 4nmole) with physical transfer before voltage-independent activity in which the channel maintained continuously "on" state was observed (Figure 2-15). Similarly compound **17** was gradually added upto10uL on both sides the membrane (total of 20uL, 20nmole) with physical transfer before the voltage-independent activity was observed (Figure 2-16). The average current vs. applied potential plot showed linear relationships (Figure 2-17). The slopes of the best fit lines were the conductances (445pS for **16**; 580pS for **17**).

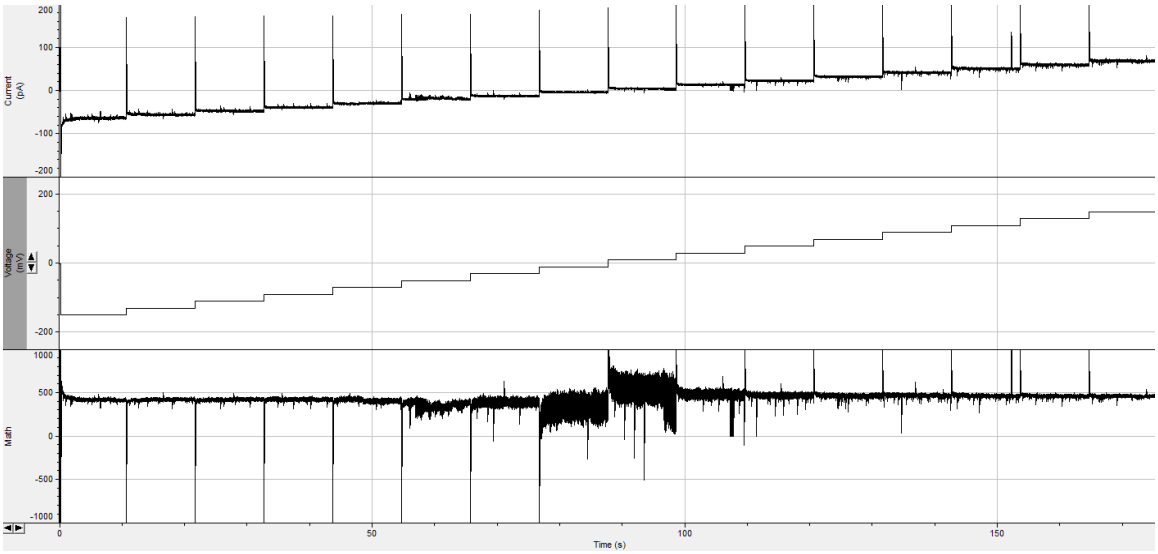

Figure 2-15. Voltage Clamp Data for Compound 16. Condition: 1M CsCl buffered to pH 7.0, -150mV to +150mV in steps of +20mV; total experiment time 176 seconds. 1mol% of 16 premixed with lipid, followed by total 2uL of 1mM solution added on both sides of the membrane (total 4nmole of 16, minimum amount added before activity observed) by physical transfer. The minimum Top panel: current-time perspective with full scale -200 to +200pA; middle panel: potential-time perspective with full scale -220 to +220mV; bottom panel: conductance-time perspective with full scale of -1 to +1nS.

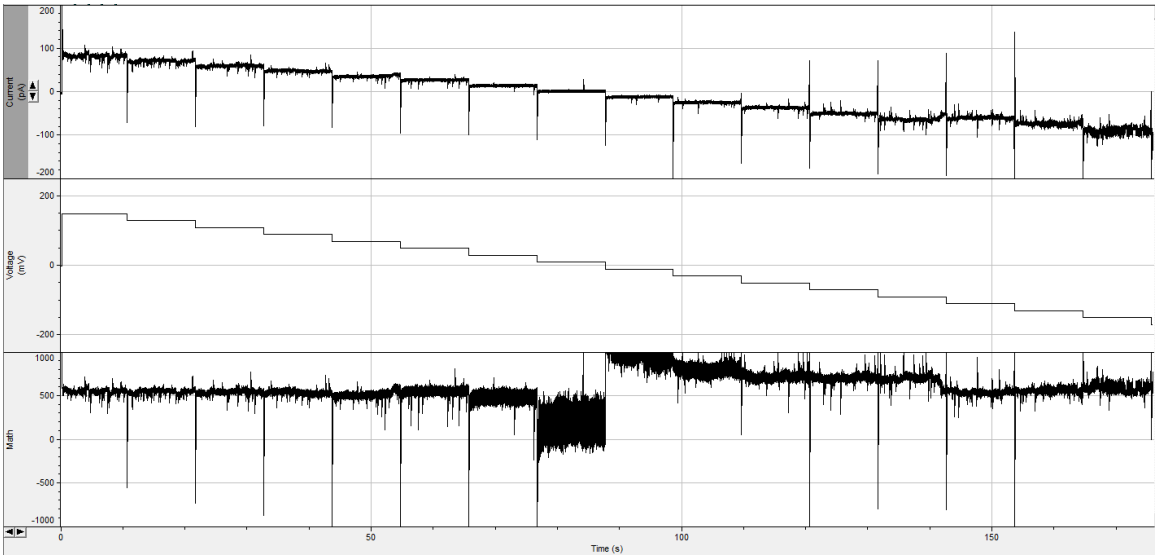

Figure 2-16. Voltage Clamp Data for Compound 17. Condition: 1M CsCl buffered to pH 7.0, -150mV to +150mV in steps of -20mV; total experiment time 176 seconds; 1mol% of 17 premixed with lipid, followed by total 10uL of 1mM solution added on both sides of the membrane (total 20nmole of 17, minimum amount added before the activity observed). Top panel: current-time perspective with full scale -200 to +200pA; middle panel: potential-time perspective with full scale -220 to +220mV; bottom panel: conductance-time perspective with full scale of -1 to +1nS.

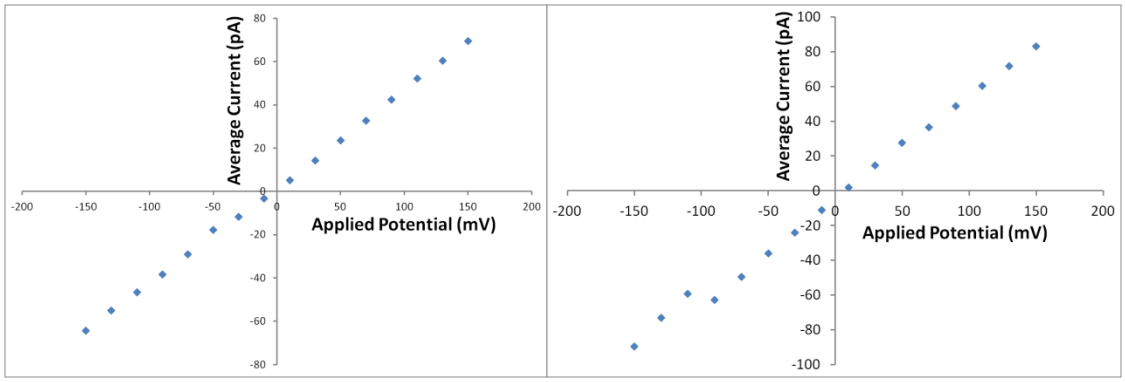

Figure 2-17 Left: Average Current vs. Applied Potential for Compound 16 (Linear Relationship). Right: Average Current vs. Applied Potential for Compound 17 (Linear Relationship).

In summary, the extended series of compounds except compound **14** were voltage clamp active and showed a number of activity types. Compound **12**, **13** showed the voltage-dependent activity at low concentrations as well as the voltage-independent Ohmic activity at relatively high concentrations. Compound **12** also presented unidirectional activity in most of its experiments even if it was injected on both sides of the membrane, but this could also be due to the time-dependency of the conductance. Compound **15** mostly showed the voltage-dependent activity while the triaromatic core compound **14** did not show any activity. Compound **16** and **17** mostly showed voltage-independent Ohmic activity.

2.2.3 Findings and Proposed Mechanisms

With the above survey of the activity of compounds in the series, we are able to draw several conclusions based on the nature of their activities. Compound **12**, **13** formed Ohmic channels at fairly high concentration, and these channels were always open for the 176s or 1760s of the experiment. Compound **16**, **17** with premixing and fairly high concentration also formed Ohmic channels which were always open for the 176 seconds of the experiment.

To better view and analyze the Ohmic channels, a 5-second zoom-in section of Figure 2-10 (compound **12**) at 150mV was generated as Figure 2-18A. The current pattern generated from Ohmic channels, like this, was more regular compared to the erratic current from voltage-dependent channels. These channels are very stable, suggesting that the injection of high concentrations of the compounds may result an incorporation of many molecules that forms a good ion conductor with a tightly clustered channel structure. The structure constantly opens in the membrane and is strong enough to survive through the potential changes and reversals. As proposed in Figure 2-18B using the mono-aromatic core version of molecules (triaromatic core molecule should have the similar mechanism), the orientations of the incorporated molecules could be completely random; some could be straight insertions (red); some could be twisted into a U-shaped orientation (blue). The U-inserts are commonly observed for the oligoester compounds partitioned in a bilayer membrane. Our previous group member, Moszynski concluded a fast U-inserts formation of her oligoester compounds in the bilayer membrane based on her fluorescence data.[41] The existence of the U-inserts is highly possible in the current bilayer experiment and could more likely count for the other observations in the survey.

The conductance of a Ohmic channel can be used to calculate the Hille radius derived for a hemisphere-capped cylinder of length l and radius r containing a sample of electrolyte with bulk resistivity ρ according to eqn (2)

$$\frac{1}{g} = \left(l + \frac{\pi r}{2}\right)\left(\frac{\rho}{\pi r^2}\right) \qquad (2)$$

Eqn (2) thus allows an estimation of the radius of Ohmic ion channel spanning the bilayer membrane. The conductance, 1.2nS was obtained from the slope of the current vs. potential plot. We assume a length of 3.5nm and use the resistivity of 1.0M CsCl equal to 0.089Ωm to derive the Hille radius of 0.37nm. By processing similarly the data for compound **13**, **16** and **17**, we were able to get their Hille radii of 0.22nm, 0.22nm, and 0.25nm respectively. In a few other recordings for compound **13** and **16**, Hille radius of 0.34nm and 0.40nm were also obtained. The discrepancy in the Hille radii of **13** and **16** were due to time dependency. Since the radius of cesium ion is about 0.18nm the channels with smaller radii (0.22nm and 0.25nm) for compound **13**, **16** and **17** allow single cesium ions passing through. The channels with larger radii (0.34nm, 0.37nm and

0.40nm) for compound **12**, **13**, **16** and **17** were big enough for the passage of hydrated cesium ions.

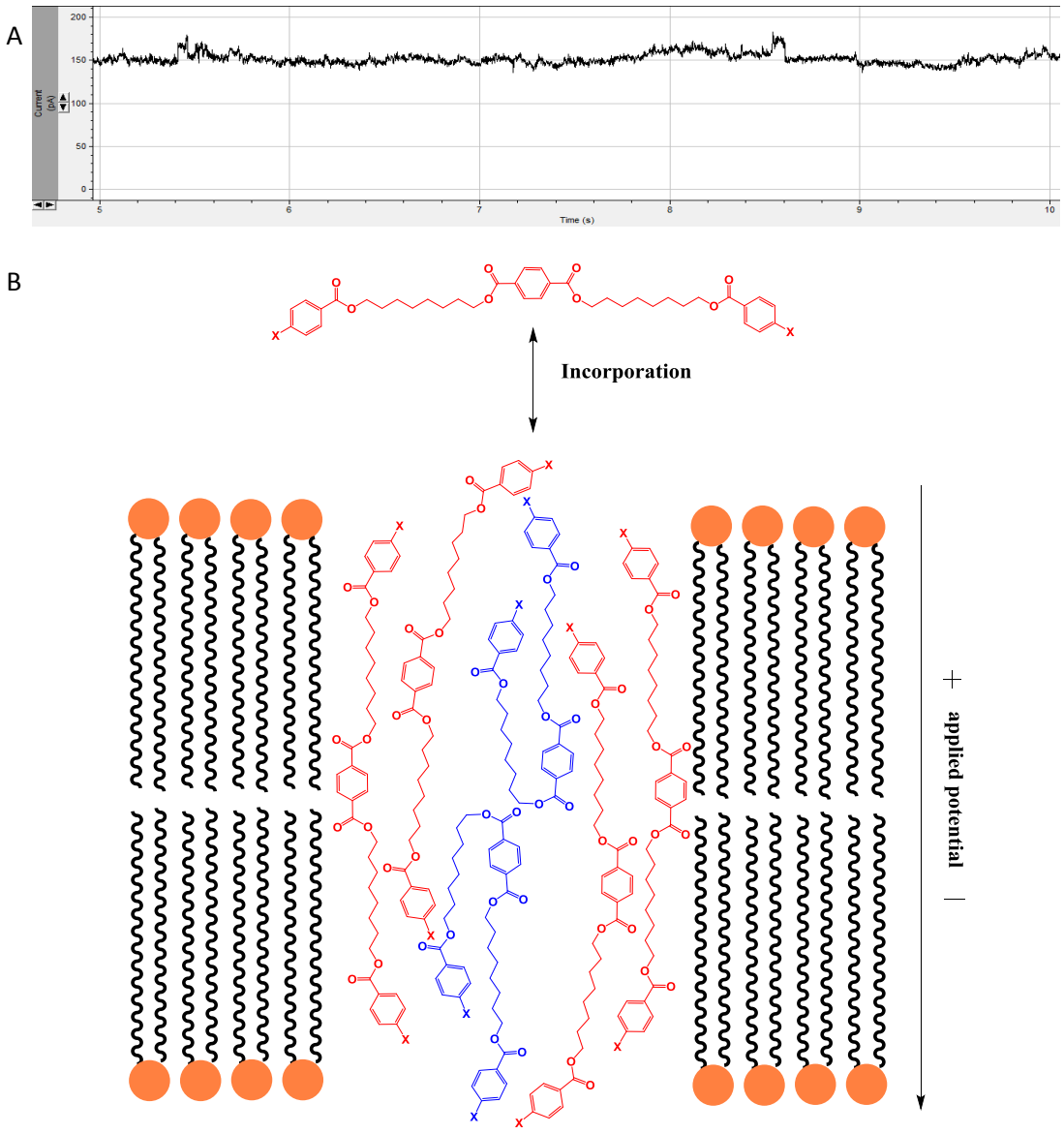

Figure 2-18. A) 5-second zoom-in section from 5s to 10s of Fig. 10 at potential of 150mV with a full scale of 0 to 200pA. The current pattern of the Ohmic channel appeared to be relatively regular. B) Using the monoaromatic core version of the ion channel as a representation of membrane incorporated channel molecules which form a tightly clustered channel structure that is able to survive through potential changes and reversals; The "X" at the ends of the molecules represents the various head groups.

Low conductance channels with about 50pS conductance levels were observed at relatively lower concentrations and relatively low potentials. Figure 2-19A shows a current pattern of compound **10** at a moderate potential of -110mV. This is a 5-second zoom-in section of Figure 2-3 from 1535s to 1540s. The channel frequently shifted "on" and "off" with the resultant current spikes ranged from -10pA to -180pA. The more erratic behavior suggested these channels were obviously less stable compared to the

Ohmic channels and maybe involved fewer molecules incorporated in the membrane. As proposed in Figure 2-20A&B using tri-aromatic core version of molecules (mono-aromatic core molecules should have the similar mechanism), the incorporation of a small number of molecules (both straight insertion and U orientation are possible) may not open the channels for long periods of time which would present as frequent switching between "on" and "off" states of the channel.

The higher conductance channels with more than 400pS are frequently erratic as shown Figure 2-19B but sometimes have some regular-looking patterns shown in Figure 2-19C. These channels were only stable when the potential was high which suggested that they involve electrostatic repulsions within the active structures which are overcome at the higher potential that creates a higher field gradient across the membrane. It is pretty clear the high conductance channels grow from previous unstable or less stable channels. With higher potential one arm of a U-shaped insert could be pushed over to the other leaflet of the membrane as indicated by the blue U-insert pushed straight in the membrane (Figure 2-20C). Similarly, one arm of a straight-insert could also be pushed into the same leaflet of the membrane as the other arm with increased potential. Both situations are equally possible and could either significantly enhance the integrity of the channel structure or increase the conductance of the channel, thus generating higher activity at high potentials (Figure 2-20B).

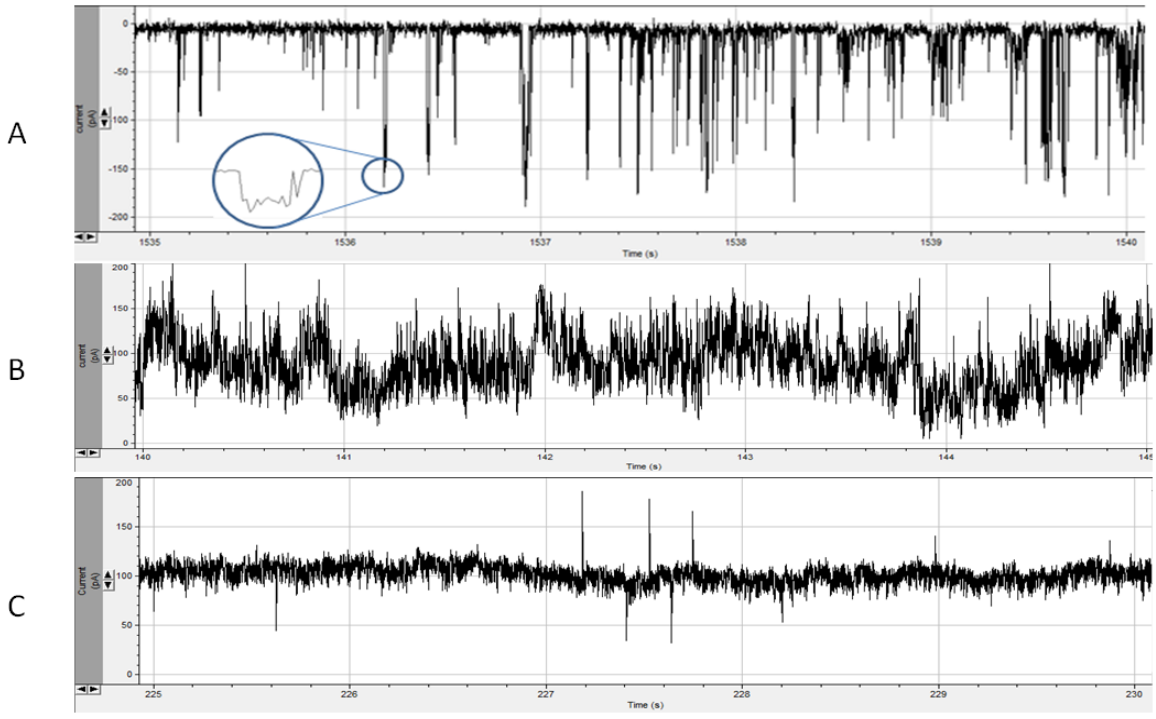

Figure 2-19. A) 5-second zoom-in section (1535s to 1540s) from Figure 2-3 at potential of -110mV with a full scale of 0 to -200pA; A zoom section for one of the peaks. B) 5-second zoom-in section (140s to 145s) from Figure 2-3 at potential of 130mV with a full scale of 0 to 200pA. C) 5-second zoom-in section (225s to 230s) from Figure 2-13 at potential of 110mV with a full scale of 0 to 200pA.

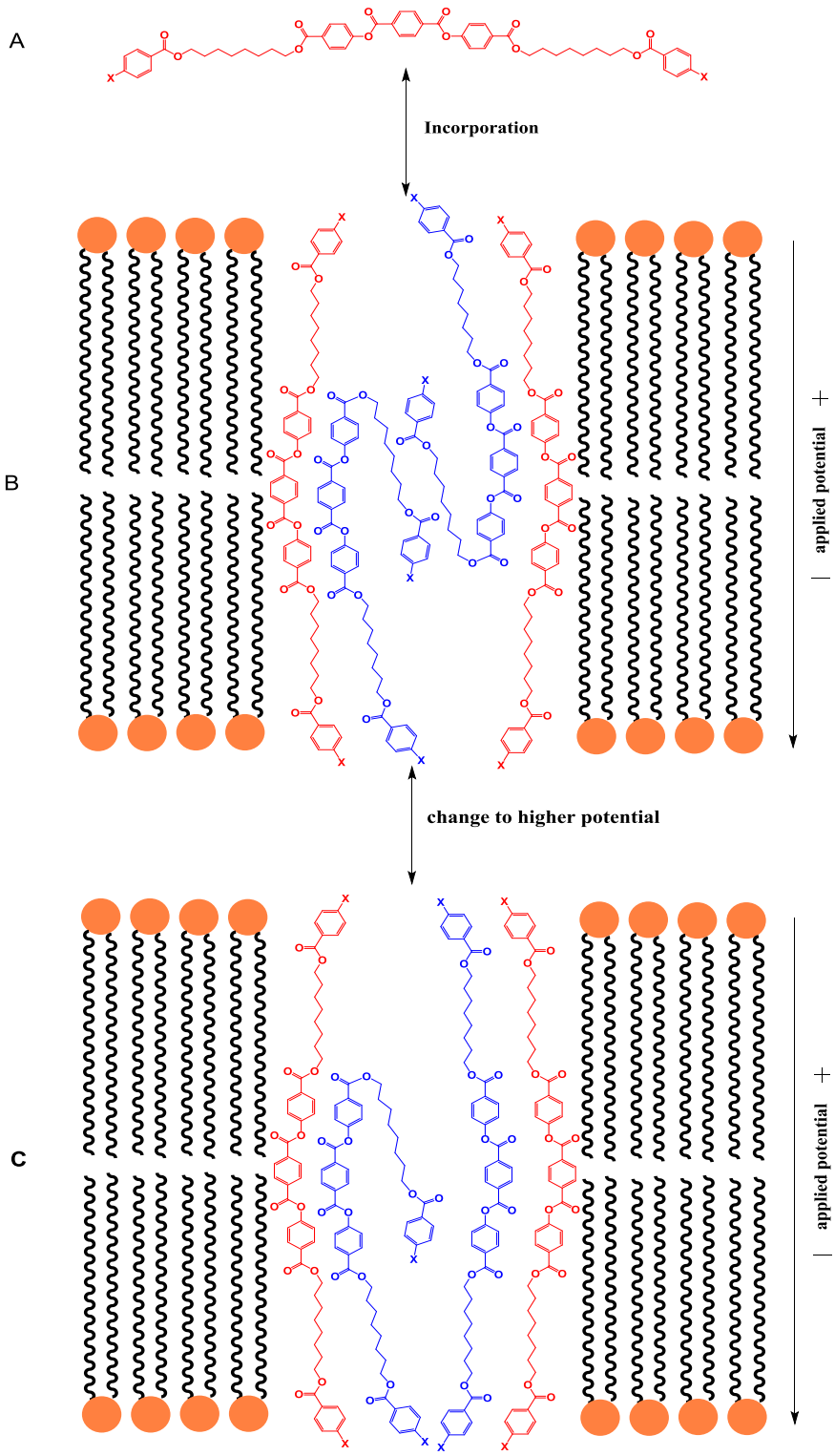

Figure 2-20. A) A representation of channel molecules which are incorporated to the membrane and B) form a less stable channel structure that cannot stay open for long periods of time; C) At high potentials U-inserts could straighten up or straight inserts could be pushed to U orientation. The "X" at the ends of the molecules represents the various headgroups.

As shown in many examples above, the positive and the negative current branches were asymmetrical, opposing to Chui's symmetry conclusion. This suggests that the compounds incorporate and aggregate asymmetrically in the membrane as the result of the unidirectionally applied potential during the manual mode of the experiment. Even though the same amount of the compounds is added on both sides of the membrane, the compound molecules on either side of the membrane obviously experience a different sign of the transmembrane potential, in which the potential field directs into the membrane perpendicularly on one side of the membrane while on the other side the potential directs out of the membrane perpendicularly. The current branches have to be asymmetrical as current cannot pass through such the asymmetrical structure with a symmetrical current-voltage response. Figure 2-20C shows one possibility that a U-insert provides such asymmetry into the aggregated structure. The applied potentials acting on a U-insert in one leaflet of the bilayer membrane take an opposite sign on the other leaflet. If electrostatic stabilization is important, then the asymmetrical structure experiences different forces depending on whether it faces to the positive or the negative potential sides of the membrane.

3 Conclusion

The goals we set in the beginning of the thesis were to examine Chui's preliminary discovery of the two symmetric bolaamphiphilic oligoester compounds **10** and **11** exhibiting exponential voltage-dependent non-rectified behaviors, to test if other structurally symmetrical compounds showing the same behaviors, and to propose a mechanism explaining symmetrical compounds showing voltage-dependent behaviors. In order to answer these questions, the parent compounds **10** and **11** were resynthesized, and an extended series of compounds based on the parent compounds were also synthesized. The backbone structures of these compounds remain the identical to those of **10** and **11**. The structural variance was provided by the installation of the four different functionalized headgroups to the backbones. The synthetic processes of these compounds were similar and adapted from Chui's synthetic method for compound **10** and **11**. However, there were some complications for synthesizing the trimethylamino compound **18**, in which several tried methods always yield the slight contamination of product containing dimethylamino headgroup. Considering the time frame of the project, the synthetic effort for compound **18** was on hold. With that, there were eight compounds including the parent compounds synthesized and ready for transport experiments.

The synthesized compounds were tested using both the vesicle experiment with HPTS indicator and the voltage-clamp experiment. The compounds were tested inactive in the HPTS-vesicle experiment, and therefore, the experimental data were solely collected from the voltage-clamp experiments. The voltage-clamp data for **10** and **11** suggest their current behavior is clearly time-dependent as their current behaviors vary greatly through different trials. Most experiment data suggest the current data branches at positive potentials and negative potentials are asymmetrical; as the result, the negative and positive current branches need to be analyzed separately. The conductance-potential plots suggest exponential voltage-dependence is possible at higher potential but it seems to be voltage-independent at lower potential. The new observations and data for **10** and **11** call into question Chui's analyzing methods. The remaining compounds were therefore set for general activity surveys.

The remaining compounds except compound **14** showed a number of activity types which were still time-dependent. Compound **12** and **13** showed the voltage-dependent at low concentrations, but voltage-independent Ohmic activity at relatively high concentration. Compound **15** mostly showed the voltage-dependent activity at low concentration while there was no activity observation for compound **14**. Compound **16** and **17** mostly showed voltage-independent Ohmic activity. Combining these observations with the observations for compound **10** and **11**, it seems that voltage-dependent behaviors form at low concentrations while Ohmic behaviors form at high concentrations. The activity at low potentials showed relative erratic behavior but the channel frequently switched between

the opening and closing states; whereas, the activity at high potential lasted longer as the channel maintained longer state of opening.

We conclude that the higher level aggregation derived from the addition of more compounds generates the structurally stable ion channels that can resist the potential change and reversal, exhibiting stable Ohmic behavior. In contrast, the lower level aggregation derived from the addition of less compounds generate the low conductance, less stable or unstable channels that show relatively erratic behaviors with frequent "on" and "off" switches. As the applied potential increases, the previous less stable channels evolve into more stable aggregating structures which have higher conductance and exhibit longer open state. The actual change in the aggregating structure, we believe, highly depends on the structural change of U shaped insert. With the increasing potential, one arm of the U-inserts could be pushed over to the other leaflet of the bilayer membrane. Similarly, the one arm of the straight inserts can be pushed into the same leaflet where the other arm lies. Both situations are equally possible, creating the stable high conductance channels. Furthermore, these channels are stable only at higher potential, suggesting they involve electrostatic repulsion within the active structures which are overcome at the higher potential that creates a higher field gradient across the membrane. The change in U-inserts also provides asymmetry to the aggregating structure which generates asymmetrical current-voltage response.

In conclusion, a series of bolaamphiphilic oligoester compounds showing voltage-dependent ion channel behaviors have been synthesized and tested. The exponential voltage-dependent behaviors possibly occur at higher potential while the voltage-independent Ohmic behaviors occur at low potential. These channel behaviors are highly time-dependent as there is no control over the stability and the aggregation level for the compounds forming active channels in the membrane. Their current-voltage responses are asymmetrical between the positive and the negative potentials.

4 Experimental

4.1 Synthesis of triaromatic Core 21 and Conversion to 22[1]

4-hydroxybenzoic acid (5.78g, 41.8mmol, 3 eqv.) was dissolved in 40mL of 1M NaOH to give a colorless solution which was transferred into a 250mL two necked round bottom flask and cooled to 5°C in an ice bath. Terephthaloyl chloride (2.89g, 14.2mmol, 1.0 eqv.) was dissolved in 30mL 1,1,2,2 tetrachloroethane to give a colorless solution and then transferred into a 100mL dropping funnel which was attached to the two necked round bottom flask containing bis-anion of 4-hydroxybenzoic acid. While stir rapidly in the reaction flask, terephthaloyl chloride was added dropwise over 1 hour. The mixture was allowed stir continuously at room temperature over 4 hours. The reaction mixture turned to white and heterogenous. The reaction mixture was then acidified with 1M HCl to pH2, then vacuum filtered. The white precipitate was washed sequentially with water, ethyl ether, ethanol before drying at 60°C overnight. The precipitate was washed with acetone to remove possible residual 4-hydroxybenzoic acid and then re-filtered. The remaining solid was dried on vacuum line overnight yielding 3.95g white power (68.5%).

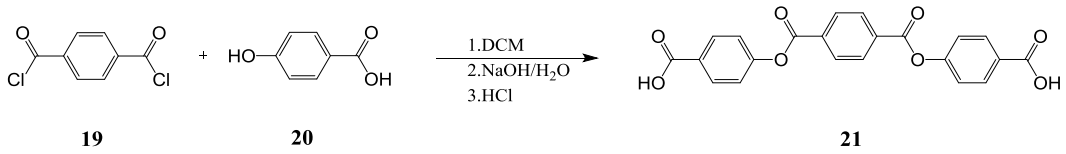

19 **20** **21**

To convert the bis-acid to the bis-acyl chloride, bis-acid core (1.465g, 3.61mmol, 1.0 eqv.) was refluxed overnight in 15mL of thionyl chloride. The condenser was then removed. The excess thionyl chloride was blow into NaOH with N_2 through tubing connection while the reaction was still heated. The residual thionyl chloride was removed under vacuum and the product was washed with ethyl ether to give 1.265g white powder (2.85mmol, 78.9%).

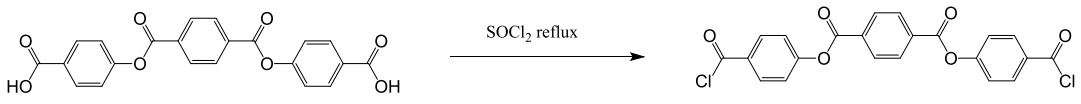

21 **22**

4.1.1 Characterization for 22

Reference NMR based on Jonathan Chui's Thesis:

^{1}H NMR – (250MHz; $CDCl_3$): δ 8.37 (s, 4H), 8.2 (d, J=8, 4H), 7.41 (d, J=8, 4H)

This sample:

^{1}H NMR – (300MHz; $CDCl_3$): δ 8.36 (s, 4H), 8.25 (d, J=8.8, 4H), 7.45 (d, J=8.8, 4H)

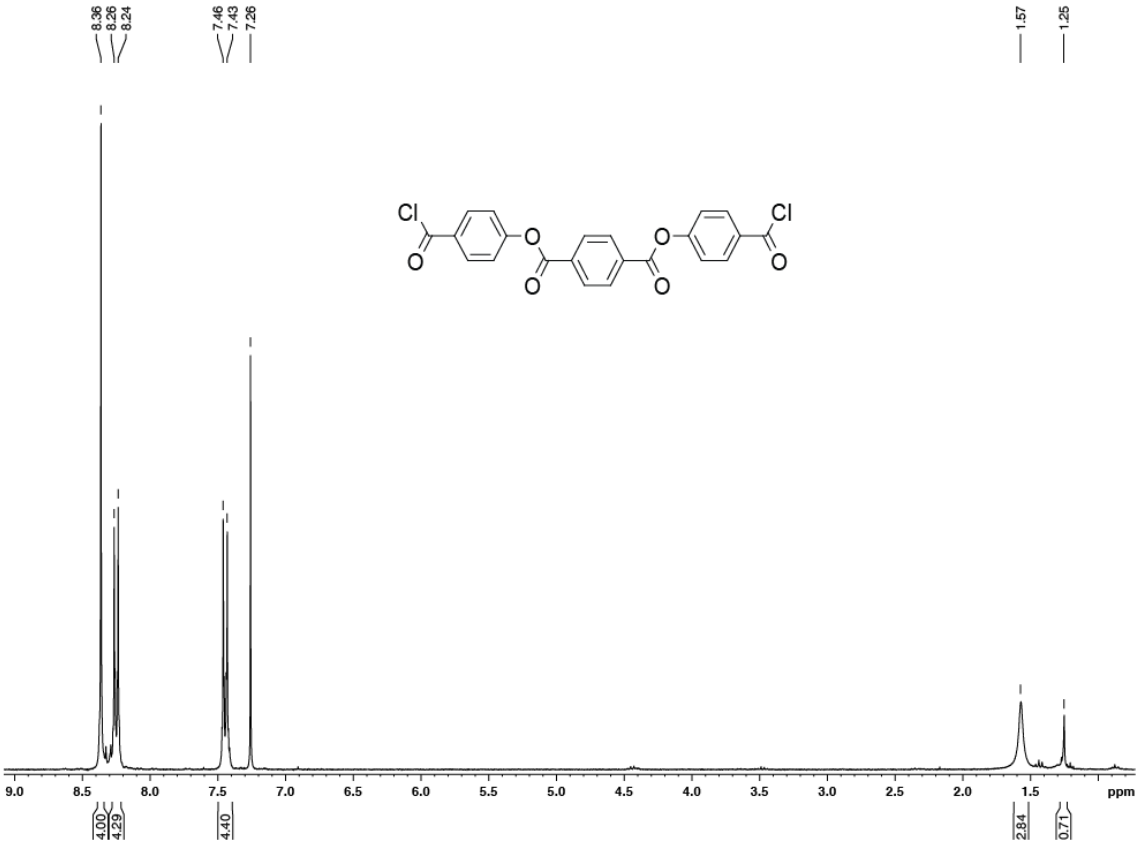

Figure 4-1. ^{1}H 300MHz NMR Spectrum for Compound 22 in $CDCl_3$

4.2 Synthesis of bromoalcohol 24

1,8-octanediol (15.0g, 103mmol 1.0 eqv.) was dissolved in 300mL toluene in a 500mL round bottom flask. HBr (27mL, 48%, 2.3 eqv) was added into the reaction flask. The mixture was refluxed overnight at 115°C. The mixture was washed two times with brine. The toluene layer was dried over $NaSO_4$, gravity filtered and concentrated to give dark orange oily liquid. Column chromatography 300mL silica gel with 1:1 hexane: ether as eluent yields 12.63g yellow oily liquid (60.4mmol, 60%).

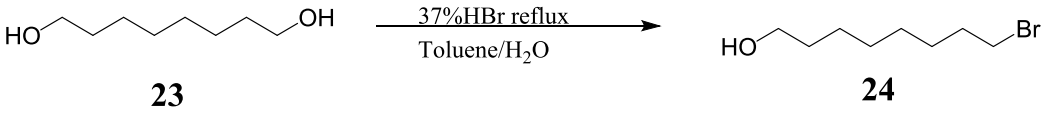

23 **24**

4.2.1 Characterization for 24

^{1}H NMR – (300MHz; $CDCl_3$): δ 3.61 (t, J=6.5, 2H), 3.39 (t, J=6.5, 2H), 1.84 (quin, J=7, 2H), 1.52 (quin, J=7, 2H), 1.44-1.31 (m, 8H)

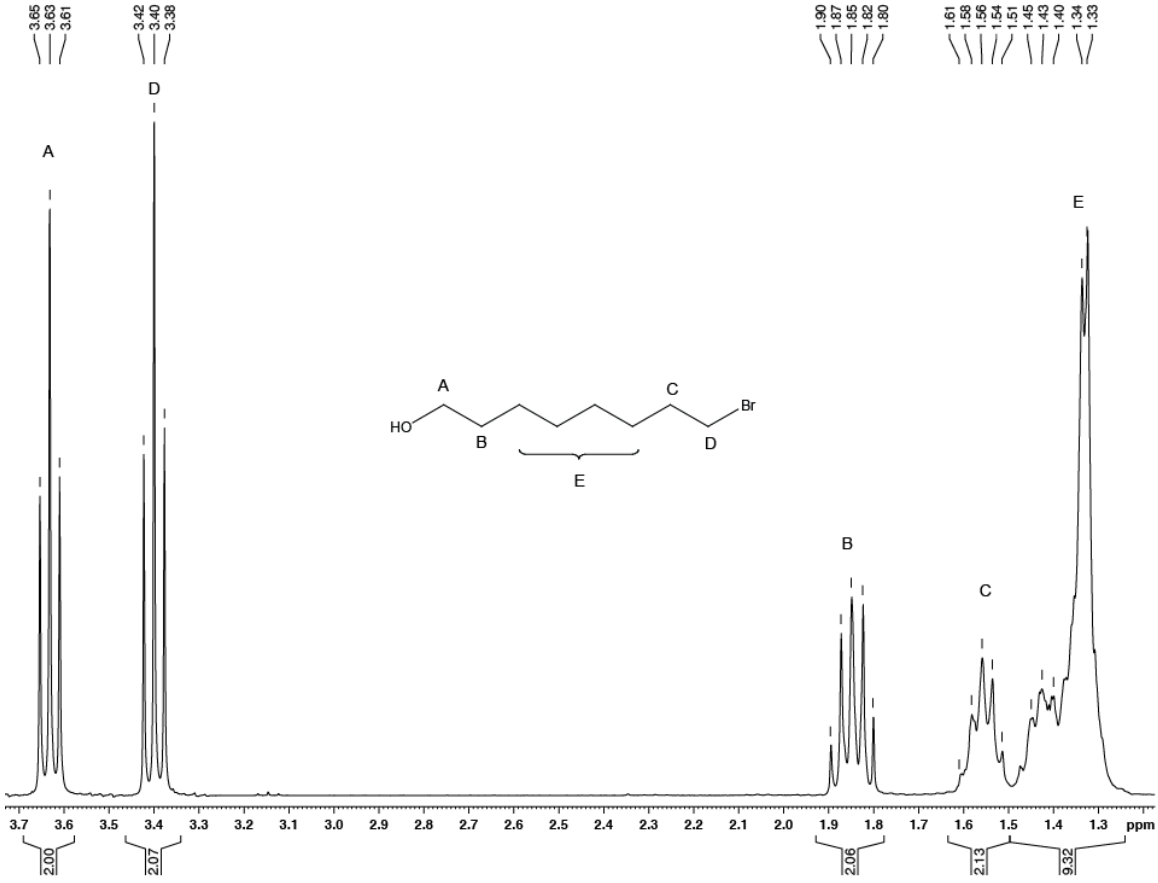

Figure 4-2. ^{1}H 300MHz NMR Spectrum for Compound 24 in $CDCl_3$

4.3 Coupling bromoalcohol 24 to triaromatic core 22[1]

A 100mL round bottom flask with a stir bar was dried in an oven overnight and was then cooled under N_2 atmosphere. Bis-acyl chloride (1.265g, 2.85mmol) and 20mL dichloromethane were quickly added into the flask and cooled in an alcohol-ice bath to -4°C. Bromoalcohol (1.80g, 8.61mmol, 3.0eqv.) and 0.6mL pyridine (7.45mmol, 3eqv.) were added sequentially via a syringe. The reaction became white milky homogeneous. The mixture was stirred at 0°C for 1 hour and then allowed to warm to room temperature overnight. The mixture was diluted with 20mL dichloromethane and washed with brine two times. The organic solution was dried over NaSO4, filtered and concentrated. Column chromatography 300mL silica gel with 1:4 ethyl acetate: hexane yields 0.780g white powder (0.989mmol, 34.7%).

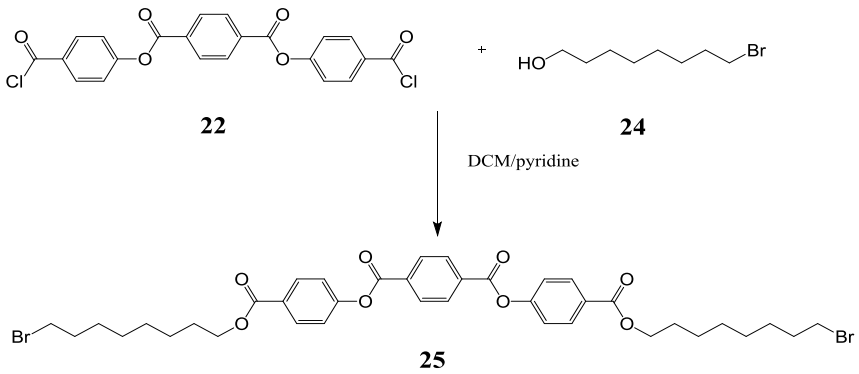

22 24 25

4.3.1 Characterization for 25

Reference NMR based on Johnathan Chui's Thesis

^{1}H NMR – (300MHz; $CDCl_3$): δ 8.28 (s, 4H), 8.08 (d, J=8.9, 4H), 7.27 (d, J=8.9, 4H), 4.27 (t, J=6.6, 4H), 3.35 (t, J=6.8, 4H), 1.82-1.68 (m, 8H), 1.39-1.30 (m, 16H)

^{13}C NMR – (75MHz; $CDCl_3$): δ163.5, 161.4, 152.1, 131.4, 128.9, 128.3, 126.2, 119.4, 62.8, 31.8, 30.4, 26.9, 26.51, 26.41, 25.7, 23.6

This sample:

^{1}H NMR – (300MHz; $CDCl_3$): δ 8.34 (s, 4H), 8.15 (d, J=8.8, 4H), 7.33 (d, J=8.8, 4H), 4.33 (t, J=6.8, 4H), 3.40 (t, J=6.8, 4H), 1.90-1.73 (m, 8H), 1.45-1.25 (m, 16H)

^{13}C NMR – (300MHz; $CDCl_3$): δ165.8, 163.7, 154.2, 133.7, 131.3, 130.4, 128.5, 121.6, 65.2, 33.9, 32.7, 29.0, 28.66, 28.62, 28.04, 25.91

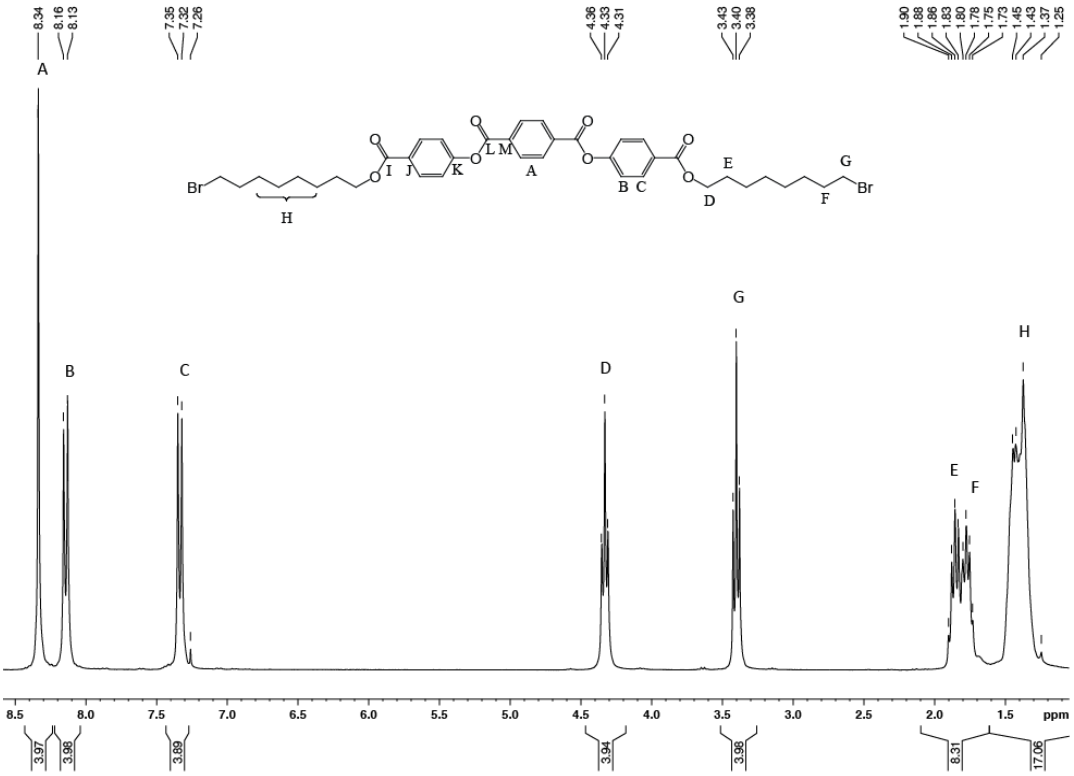

Figure 4-3.^{1}H 300MHz NMR Spectrum for Compound 25 in $CDCl_3$

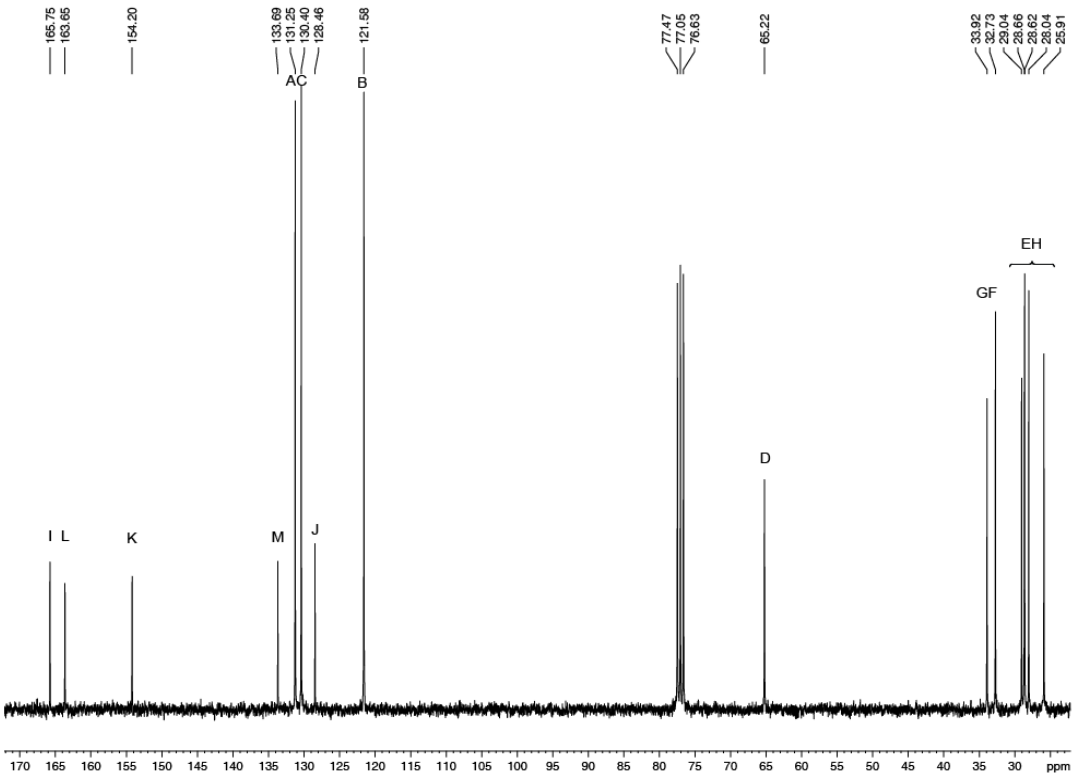

Figure 4-4.^{13}C 300MHz NMR Spectrum for Compound 25 in $CDCl_3$

4.4 Coupling bromoalcohol 24 to monoaromatic core 19[1]

A 100mL round bottom flask with a stir bar was dried in an oven overnight and was then cooled under N_2 atmosphere. In the flask, terephthaloyl chloride (500mg, 2.46mmol, 1.0eqv.) was dissolved in 10mL dry dichloromethane, and the solution was cooled in an ice bach. bromoalcohol (1.100g, 5.26mmol, 2.1eqv.) and 0.4mL pyridine (4.96mmol, 2eqv.) were added via a syringe. The solution becomes white cloudy in a few minutes. The reaction was allowed to warm to room temperature and stirred for 4 hours. The mixture was then diluted with 20mL dichloromethane and washed with 30mL of water. The aqueous layer was back washed with 20mL dichloromethane two times. The organic layers were combined, dried over $NaSO_4$, filtered and concentrated. Column chromatography, 200mL silica gel with 1:9 ethyl acetate: hexane yields 0.771g white-yellowish powder (1.41mmol, 57.3%).

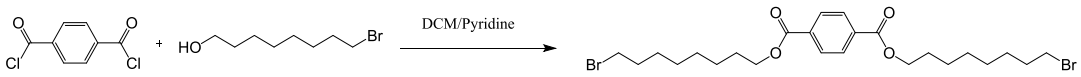

19 **24** **26**

4.4.1 Characterization for 26

Reference NMR based on Johnathan Chui's Thesis

^{1}H NMR – (300MHz; $CDCl_3$): δ 8.03 (s, 4H), 4.27 (t, J=6.7, 4H), 3.33 (t, J=6.9, 4H), 1.83-1.68 (m, 8H), 1.37-1.28 (m, 12H)

^{13}C NMR – (75MHz; $CDCl_3$): δ165.0, 133.3, 128.6, 64.6, 33.2, 28.70, 28.59, 28.40, 27.96, 27.86, 27.3

This sample:

^{1}H NMR – (300MHz; $CDCl_3$): δ 8.10 (s, 4H), 4.41 (t, J=6.7, 4H), 3.41 (t, J=6.9, 4H), 1.91-1.74 (m, 8H), 1.47-1.36 (m, 12H)

^{13}C NMR – (75MHz; $CDCl_3$): δ165.85, 134.16, 129.47, 65.46, 33.92, 32.72, 29.04, 28.61, 28.04, 25.89

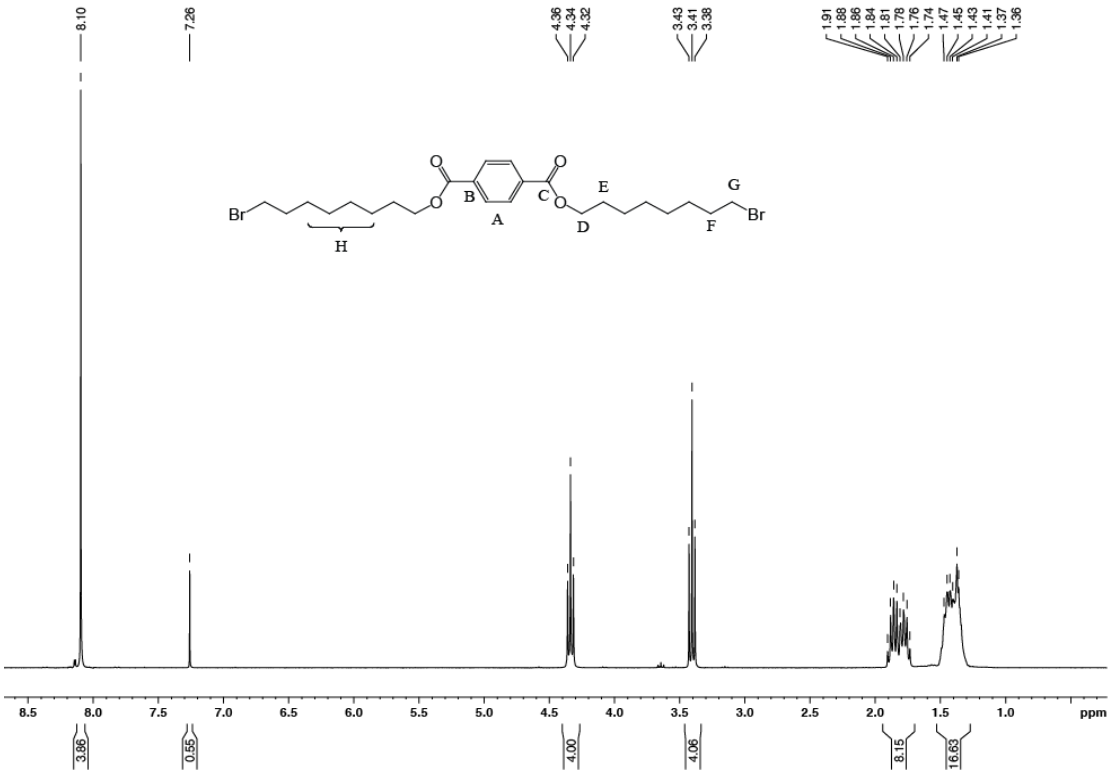

Figure 4-5.[1]H 300MHz NMR Spectrum for Compound 26 in $CDCl_3$

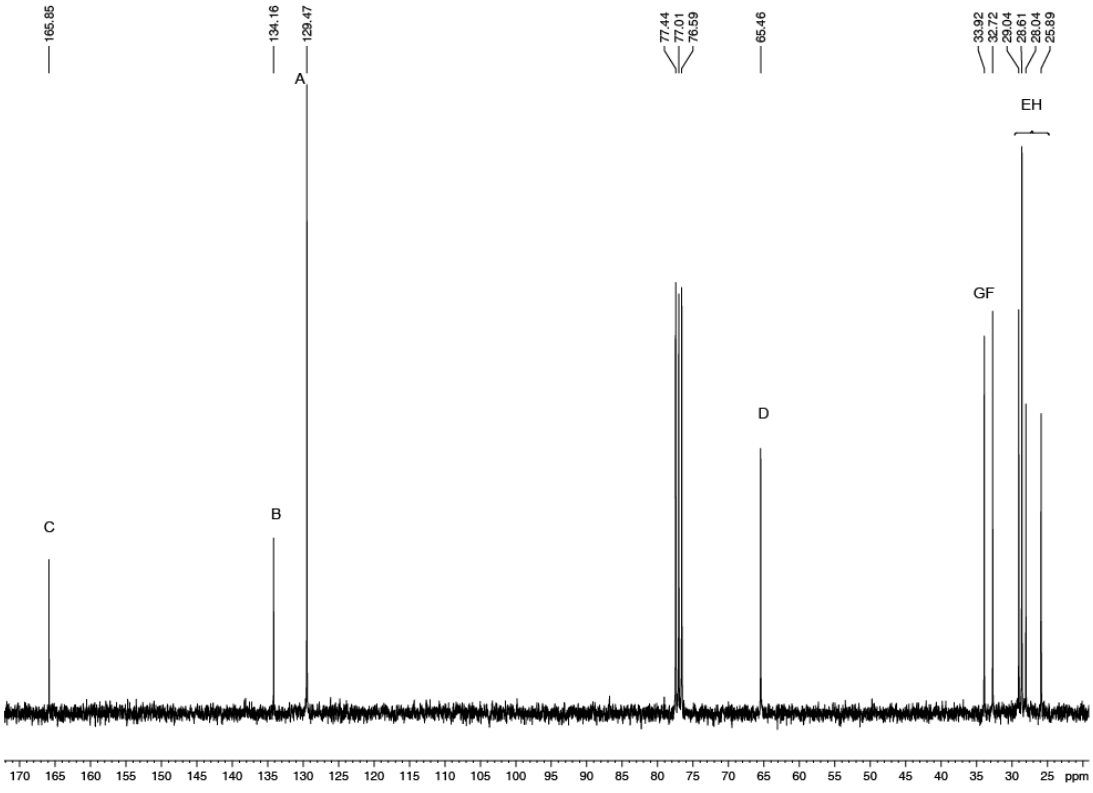

Figure 4-6.[13]C 300MHz NMR Spectrum for Compound 26 in $CDCl_3$

4.5 Iodide-catalyzed nucleophilic displacement to attach the head groups

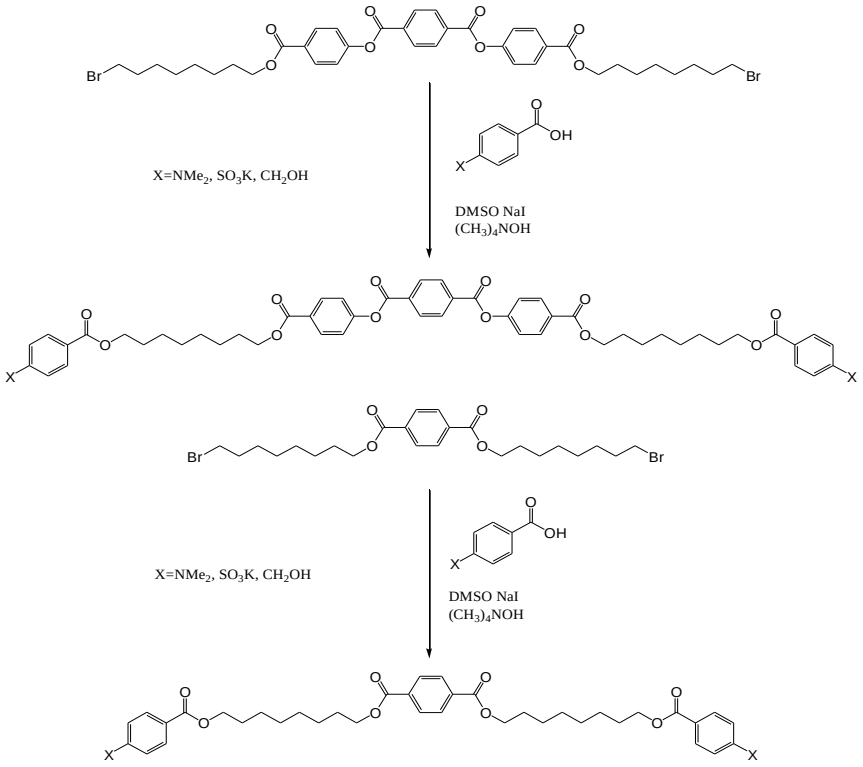

4.5.1 Attach 4-Sulfobenzoic Acid Potassium Salt

4.5.1.1 Attach 4-Sulfobenzoic Acid Potassium Salt to 25

Dibromide triaromatic core (200mg, 0.254mmol, 1eqv.), potassium 4-sulfobenzoic acid (134mg, 0.558mmol, 2.2eqv.) and NaI (9mg, 0.06mmol, 0.2eqv.) were dissolved in 20mL DMSO before tetramethyl ammonium hydroxide (101mg, 0.558mmol, 2.2eqv.) were added into the mixture. The reaction was heated to 60^{o}C overnight and then diluted with 30mL DCM. The resulting white precipitate was filtered out and washed with methanol to remove the remaining tetramethyl ammonium hydroxide giving 240mg white solid (0.217mmol, 85.3%).

4.5.1.2 Characterization for 12

Mass spectroscopy: m/z calculated for $[C_{52}H_{52}O_{18}S_2]^{2-}$ =514.5 and $[C_{52}H_{52}O_{18}S_2+K]^{-}$ =1068.1; found 514.6 and 1067.7 respectively.

^{1}H NMR – (300MHz; DMSO-d6): δ 8.34 (s, 4H), 8.07 (d, J=8.9, 4H) 7.91 (d, J=8.8, 4H), 7.71 (d, J=8.9, 4H), 7.51 (d, J=8.9, 4H), 4.30-4.23 (m, 8H), 1.72-1.69 (m, 8H), 1.37 (m, 12H)

^{13}C NMR – (300MHz; DMSO-d6): δ165.45, 165.04, 163.45, 154.13, 152.65, 133.23, 130.79, 130.36, 129.62, 128.74, 127.81, 125.84, 122.35, 64.80, 64.68, 28.53, 28.09, 26.37

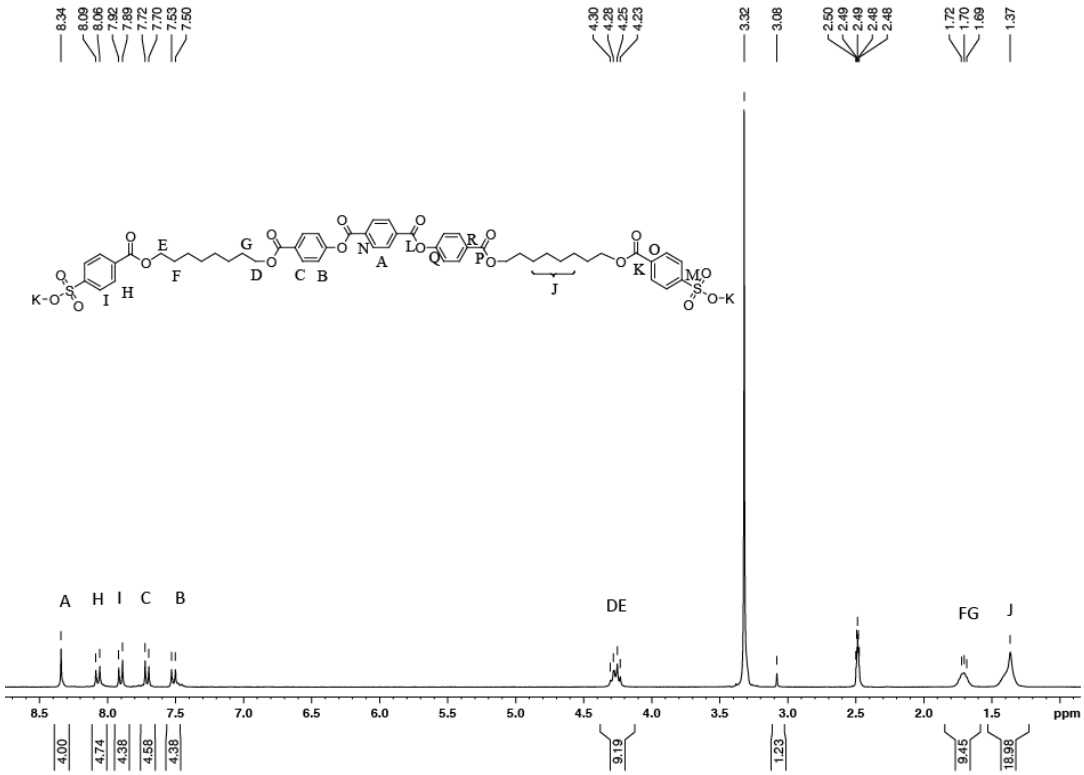

Figure 4-7.[1]H 300MHz NMR Spectrum for Compound 12 in DMSO-D_6

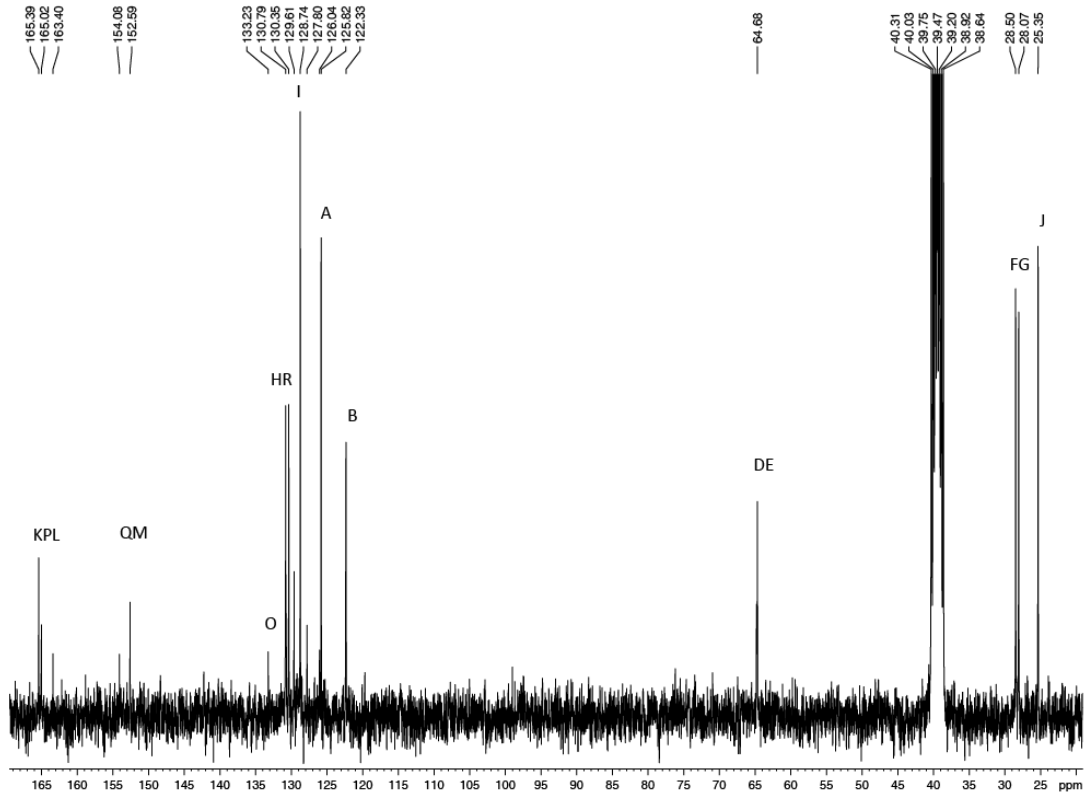

Figure 4-8.[13]C 300MHz NMR Spectrum for Compound 12 in DMSO-D6

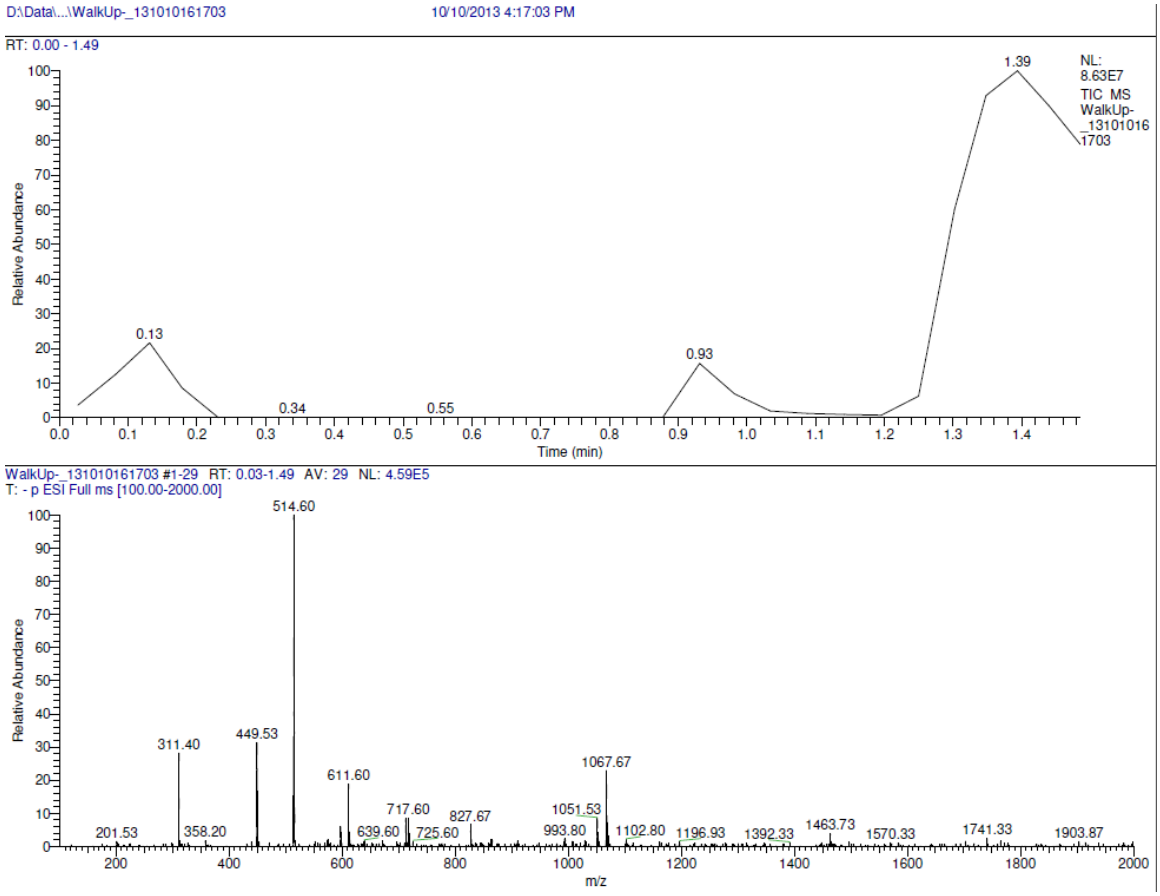

Figure 4-9. ESI-MS Spectrum for Compound 12

4.5.1.3 Attach 4-Sulfobenzoic Acid Potassium Salt to 26

Dibromide monoaromatic core (245mg, 0.446mmol, 1eqv.), potassium 4-sulfobenzoic acid (236mg, 0.983mmol, 2.2eqv.) and NaI (9mg, 0.06mmol, 0.2eqv.) were dissolved in 20mL DMSO before tetramethyl ammonium hydroxide (178mg, 0.980mmol, 2.2eqv.) were added into the mixture. The reaction was heated to 60^{o}C overnight and then diluted with 30mL DCM. The resulting white precipitate was filtered out and washed with methanol to remove the remaining tetramethyl ammonium hydroxide giving 280mg white solid (0.323mmol, 72.4%).

4.5.1.4 Characterization for 13

Mass spectroscopy: m/z calculated for $[C_{38}H_{44}O_{14}S_2]^{2-}$ =394.4 and $[C_{38}H_{44}O_{14}S_2+K]^{-}$ =827.9; found 394.8 and 827.8 respectively.

^{1}H NMR – (300MHz; DMSO-d6): δ 8.07 (s, 4H), 7.91 (d, J=8.8, 4H), 7.71 (d, J=8.8, 4H), 4.31-4.21 (m, 8H), 1.74-1.68 (m, 8H), 1.39-1.35 (m, 12H)

^{13}C NMR – (300MHz; DMSO-d6): δ165.38, 165.00, 152.61, 133.69, 129.59, 129.40, 128.73, 125.82, 65.10, 64.67, 28.48, 28.06, 28.00, 25.32

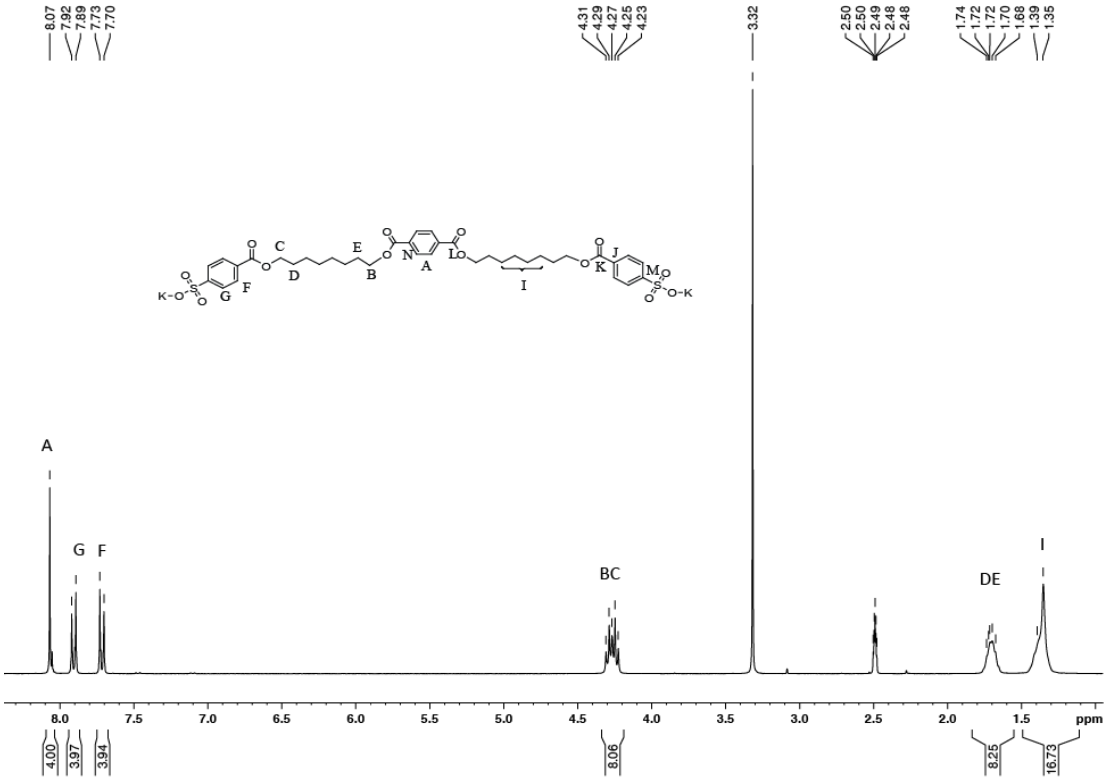

Figure 4-10. ^{1}H 300MHz NMR Spectrum for Compound 13 in DMSO-D_6

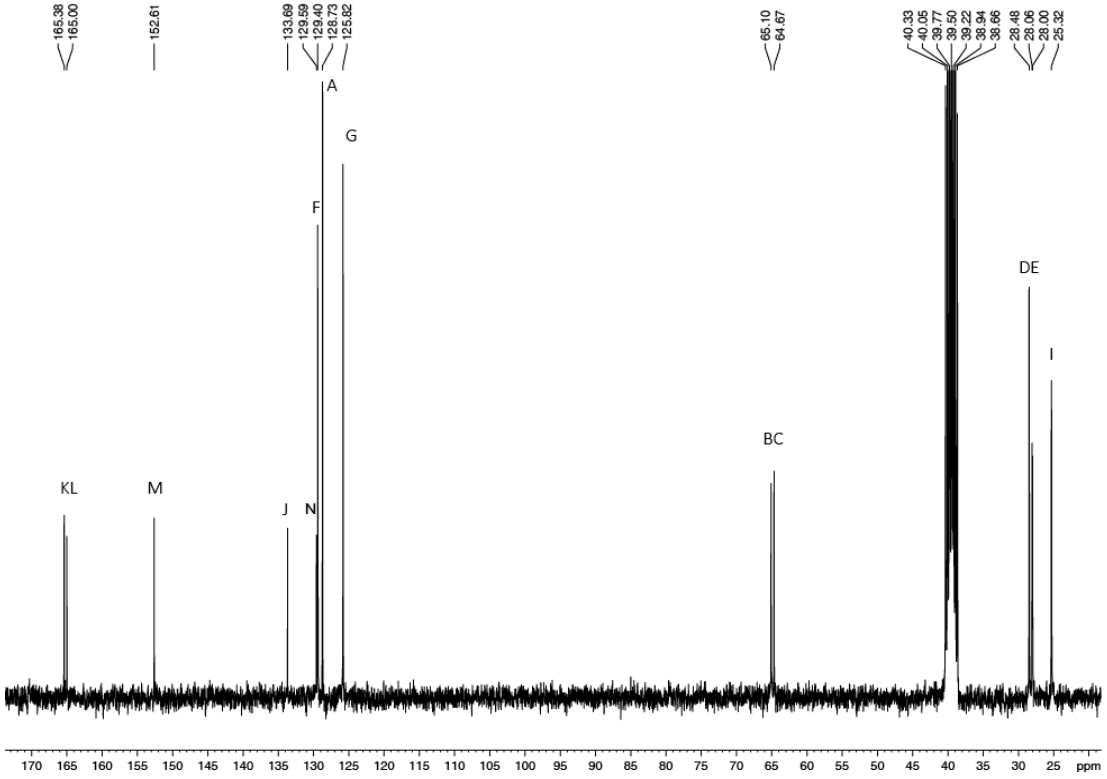

Figure 4-11. ^{13}C 300MHz NMR Spectrum for Compound 13 in DMSO-D_6

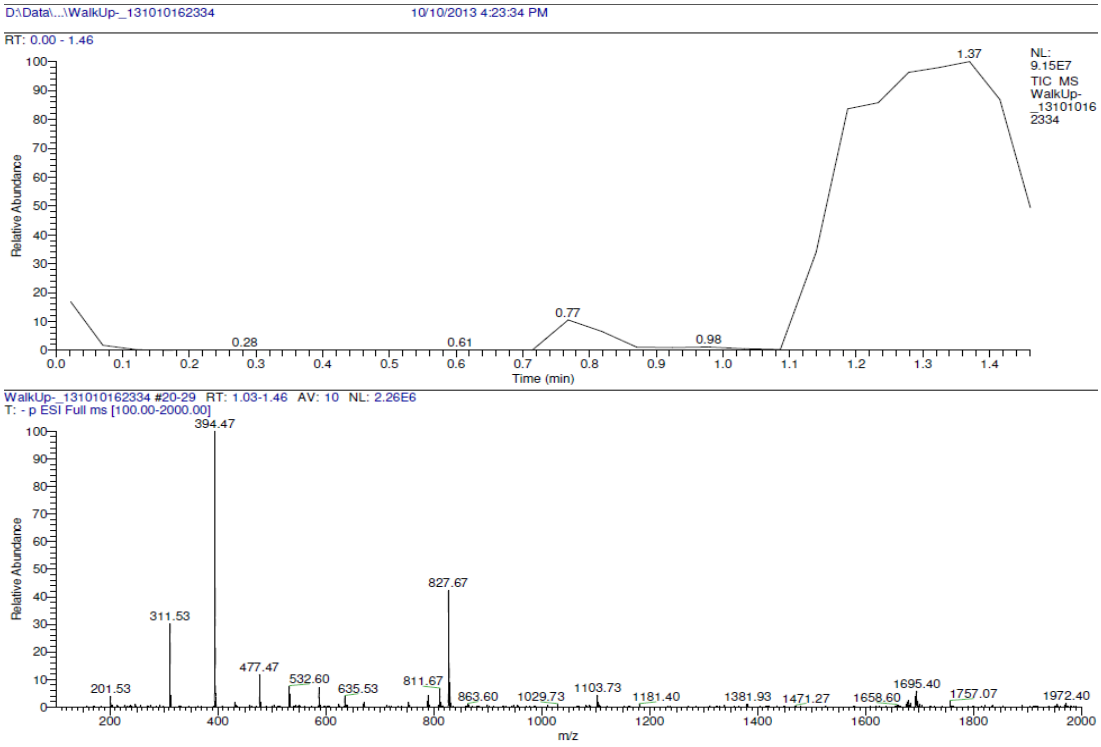

Figure 4-12. ESI-MS Spectrum for Compound 13

4.5.2 Attach 4-(Dimethylamino) Benzoic Acid

4.5.2.1 Attach 4-(Dimethylamino) Benzoic Acid to 25

Dibromide triaromatic core (200mg, 0.254mmol, 1eqv.), 4-dimethylamino benzoic acid (100mg, 0.605mmol, 2.4eqv.) and NaI (8mg, 0.05mmol, 0.2eqv.) were dissolved in 20mL DMSO in a 50mL RBF. The mixture was stirred rapidly before 114mg tetramethylammonium hydroxide was added into the mixture. The reaction was heated to 60^{o}C overnight, and then diluted with 30mL of dichloromethane before washed with 80mL water. Aqueous portion was backwashed with 30mL dichloromethane. The organic portions were combined and dried over Na_2SO_4, filtered and concentrated to give yellowish white solid. The solid was recrystallized from 8mL DCM/EtOAc to give 110mg white power (0.115mmol, 45.3%).

4.5.2.2 Characterization for 14

Mass spectroscopy: m/z calculated $[C_{56}H_{64}O_{12}N_2+H]^+$ =957.1; found 957.1

^{1}H NMR – (300MHz; $CDCl_3$): δ 8.35 (s, 4H), 8.16 (d, J=8.8, 4H), 7.92 (d, J=8.8, 4H), 7.34 (d, J=8.8, 4H), 6.64 (d, J=8.8, 4H), 4.34 (t, J=6.7, 4H), 4.26 (t, J=6.7, 4H), 3.03 (s, 12H), 1.81-1.71 (m, 8H), 1.42 (m, 12H)

^{13}C NMR – (300MHz; $CDCl_3$): δ167.16, 165.80, 163.69, 154.18, 153.0, 133.95, 131.27, 131.19, 130.41, 128.52, 121.58, 110.68, 65.30, 64.22, 40.05, 29.17, 28.83, 28.04, 26.01, 25.96.

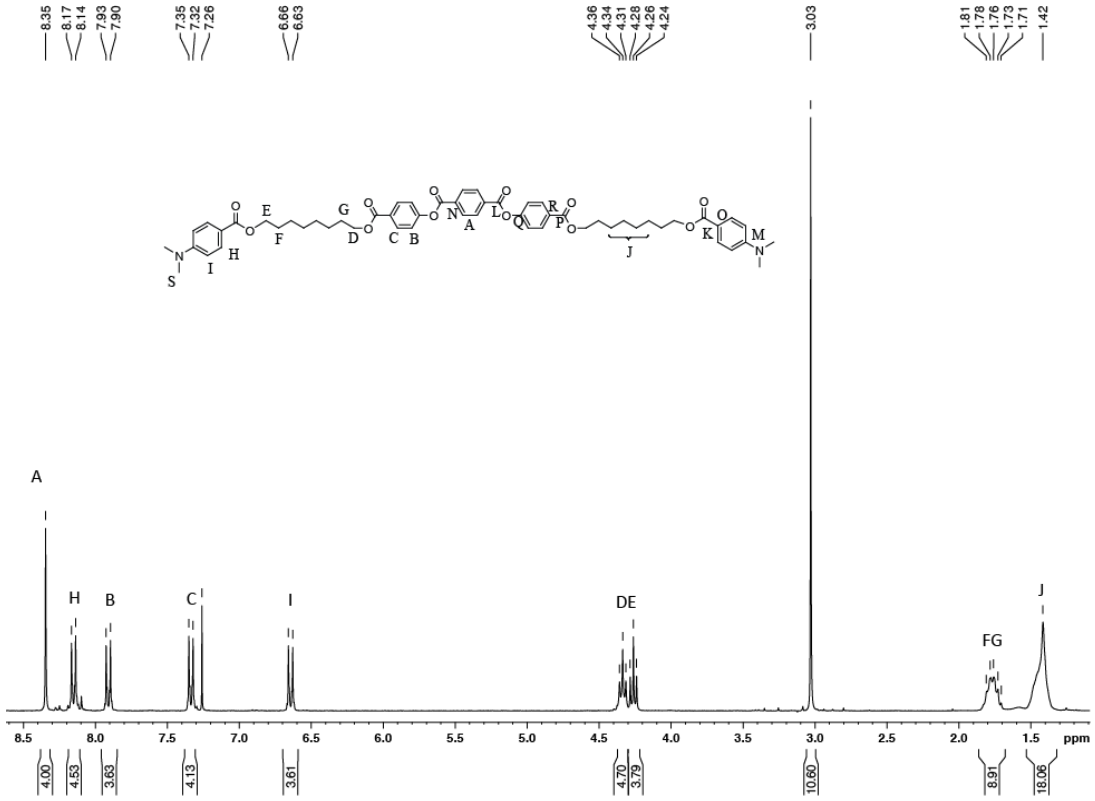

Figure 4-13. ^{1}H 300MHz NMR Spectrum for Compound 14 in $CDCl_3$

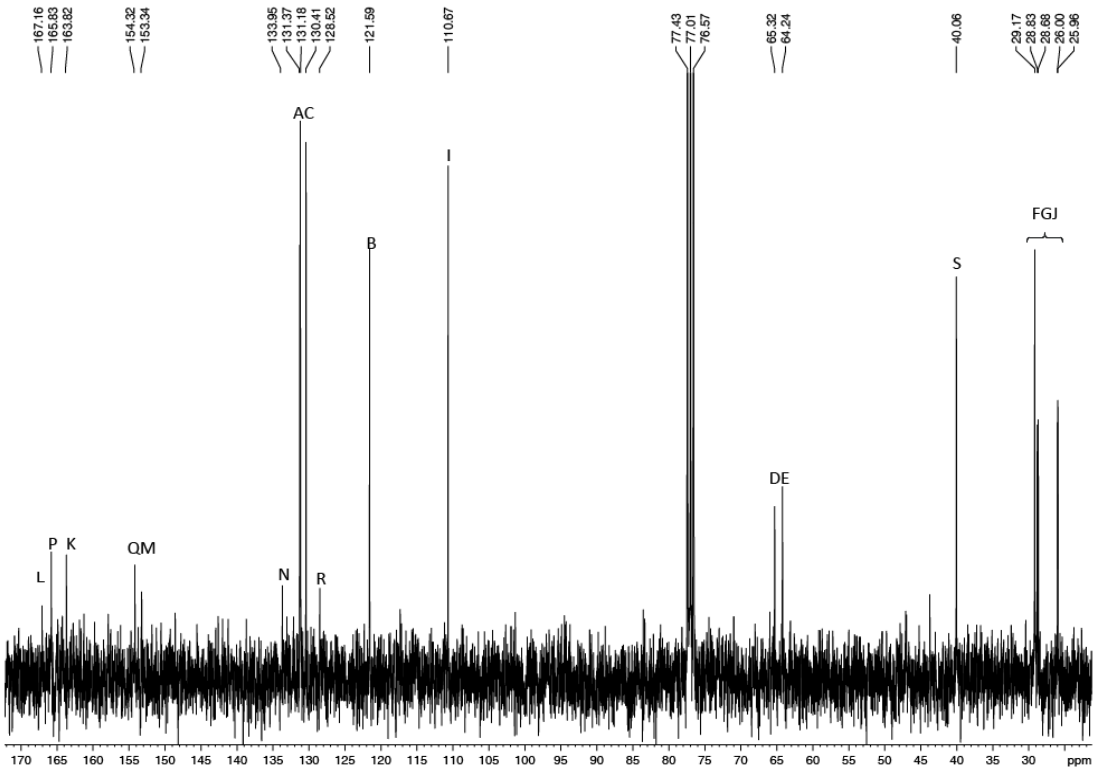

Figure 4-14. ^{13}C 300MHz NMR Spectrum for Compound 14 in $CDCl_3$

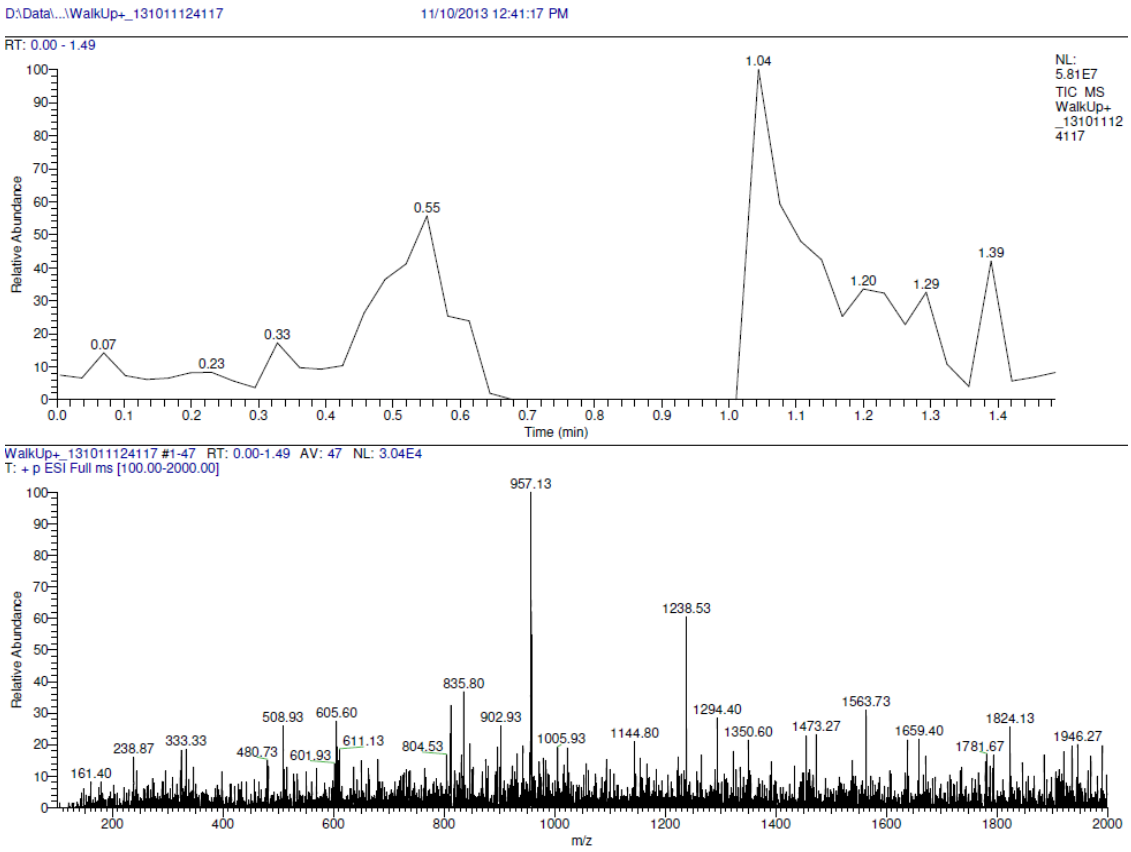

Figure 4-15. ESI-MS Spectrum for Compound 14

4.5.2.3 Attach 4-(Dimethylamino) Benzoic Acid to 26

Dibromide monoaromatic core (245mg, 0.447mmol, 1eqv), 4-dimethylamino benzoic acid (162mg, 0.980mmol, 2.2eqv.) and NaI (8mg were dissolved in 20mL DMSO in a 50mL RBF before tetramethyl-ammonium hydroxide (178mg, 0.980mmol, 2.2eqv.) was added into the mixture. The reaction was heated to 60^{o}C overnight, and then diluted with 30mL of dichloromethane before washed with 80mL water. Aqueous portion was backwashed with 30mL dichloromethane. The organic portions were combined and dried over Na_2SO_4, filtered and concentrated to give yellowish white solid. The solid was recrystallized from 8mL DCM/EtOAc to give 208mg white power (0.290mmol, 64.9%)

4.5.2.4 Characterization for 15

Mass spectroscopy: m/z calculated for $[C_{42}H_{56}O_8N_2+Na]^+$ =739.5; found 739.5

^{1}H NMR – (300MHz; $CDCl_3$): δ 8.09 (s, 4H), 7.91 (d, J=8.8, 4H), 6.64 (d, J=8.8, 4H), 4.34 (t, J=6.7, 4H), 4.26 (t, J=6.7, 4H), 3.03 (s, 12H), 1.83-1.70 (m, 8H), 1.47-1.41 (m, 12H)

^{13}C NMR – (300MHz; $CDCl_3$): δ167.07, 165.88, 153.22, 134.16, 131.18, 129.47, 117.28, 110.66, 65.51, 64.20, 40.04, 29.69, 29.16, 28.82, 28.63, 26.00, 25.93

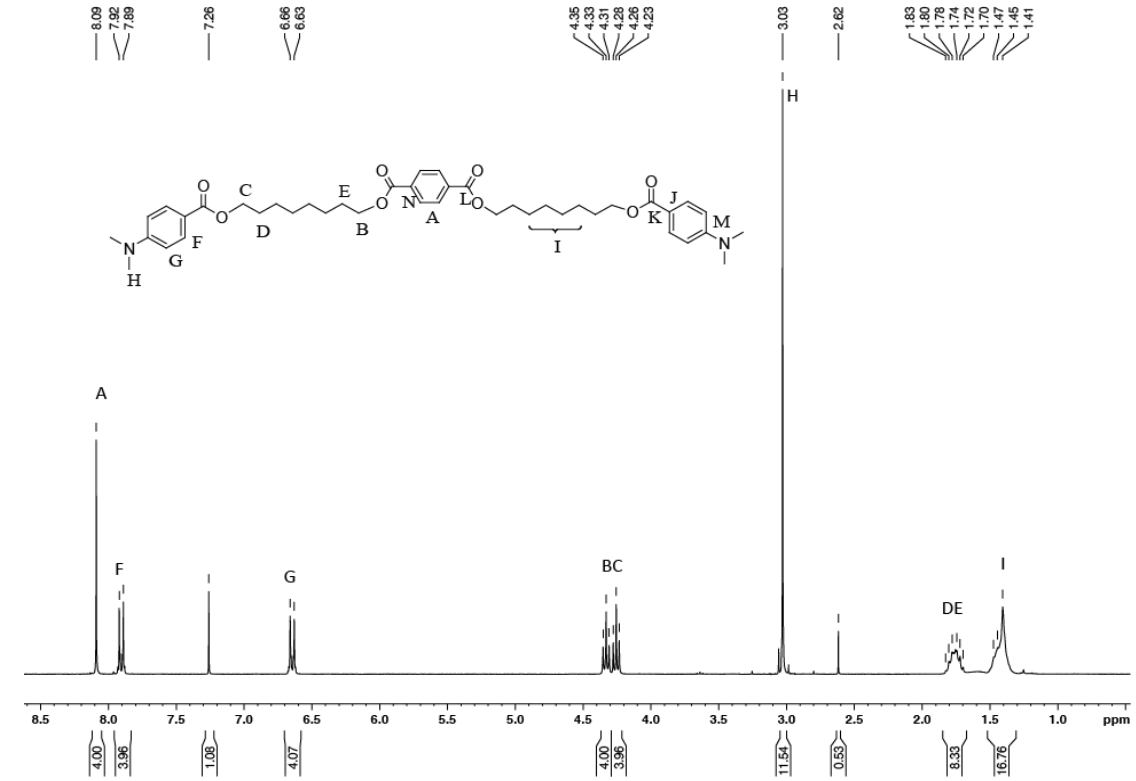

Figure 4-16. ^{1}H 300MHz NMR Spectrum for Compound 15 in $CDCl_3$

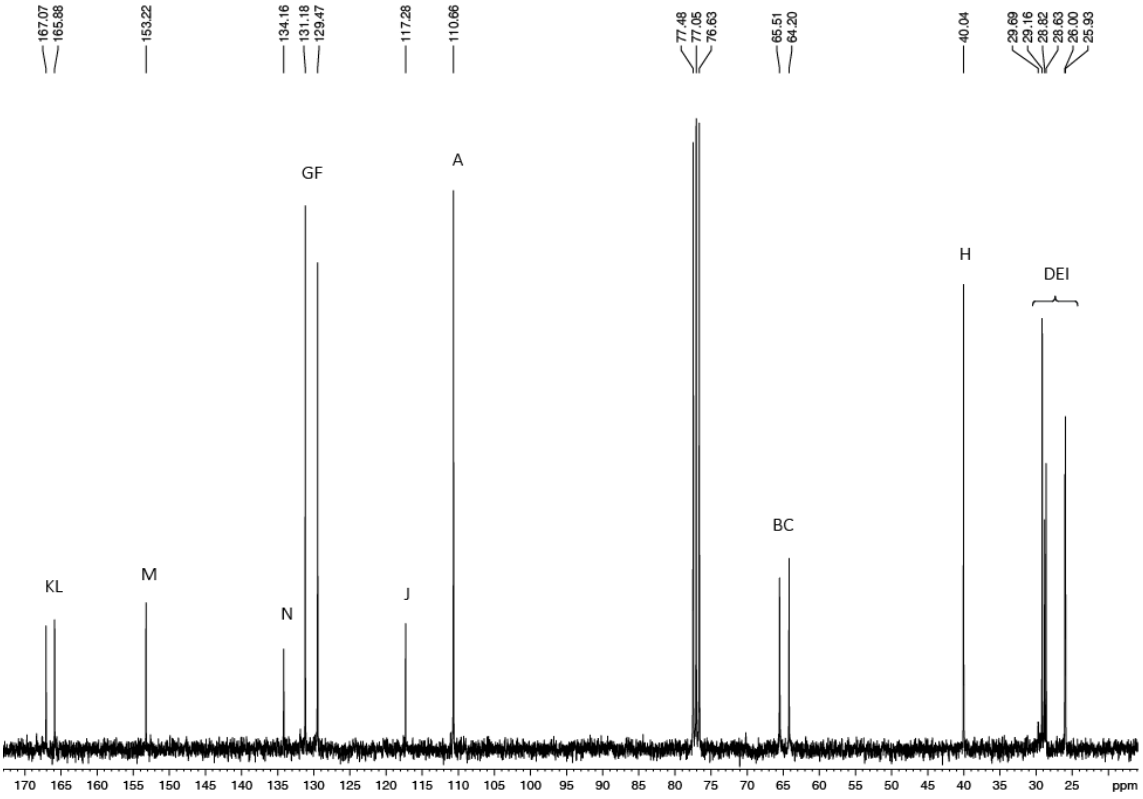

Figure 4-17. ^{13}C 300MHz NMR Spectrum for Compound 15 in $CDCl_3$

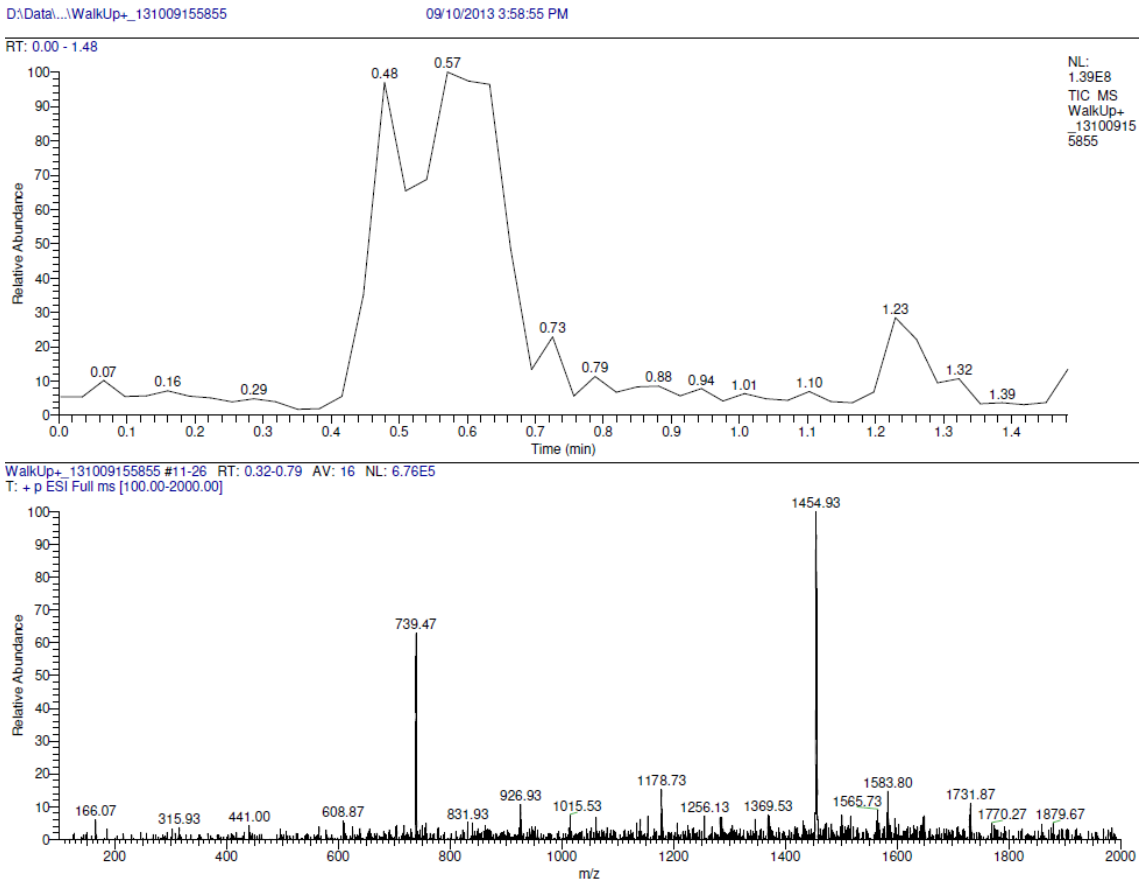

Figure 4-18. ESI-MS Spectrum for Compound 15

4.5.3 Attach 4-(Hydroxymethyl) Benzoic Acid

4.5.3.1 Attach 4-(Hydroxymethyl) Benzoic Acid to 25

Dibromide triaromatic core (200mg, 0.254mmol, 1eqv.), 4-hydroxymethyl benzoic acid (90mg, 0.559mmol, 2.2eqv.) and NaI (9mg, 0.06mmol, 0.2eqv.) were dissolved in 20mL DMSO before tetramethyl ammonium hydroxide (101mg, 0.558mmol, 2.2eqv.) were added into the mixture. The reaction was heated to 60^{o}C for 2 hrs and then diluted with 30mL chloroform and washed with brine once. Aqueous layer was backwashed with 40mL chloroform and the organic layers were combined, dried over Na_2SO_4, rotovapped down. Column chromatography with Hex:EtOAc =1:1 as elute then gradually increased to 3:7. The product came out last with 120mg white powder (0.174mmol, 68.5%).

4.5.3.2 Characterization for 16

^{1}H NMR – (300MHz; $CDCl_3$): δ 8.35 (s, 4H), 8.14 (d, J=8.8, 4H), 8.04 (d, J=8.8, 4H), 7.43 (d, J=8.8, 4H), 7.34 (d, J=8.8, 4H), 4.77 (s, 4H), 4.35-4.30 (m, J=6.7, 8H), 1.83-1.74 (m, 8H), 1.43 (m, 12H)

^{13}C NMR – (300MHz; $CDCl_3$): δ166.47, 165.79, 164.0, 154.20, 145.88, 133.71, 131.25, 130.40, 129.78, 128.49, 126.42, 121.56, 65.27, 65.02, 64.70, 29.08, 28.65, 25.91

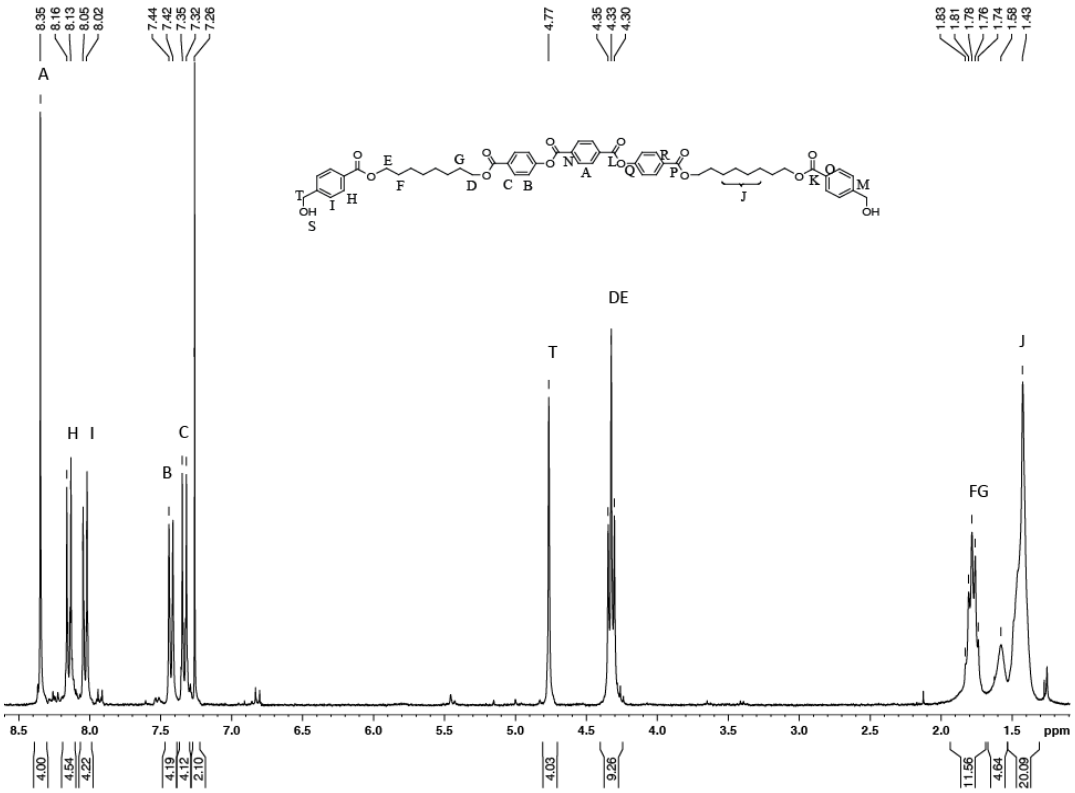

Figure 4-19. ^{1}H 300MHz NMR Spectrum for Compound 16 in $CDCl_3$

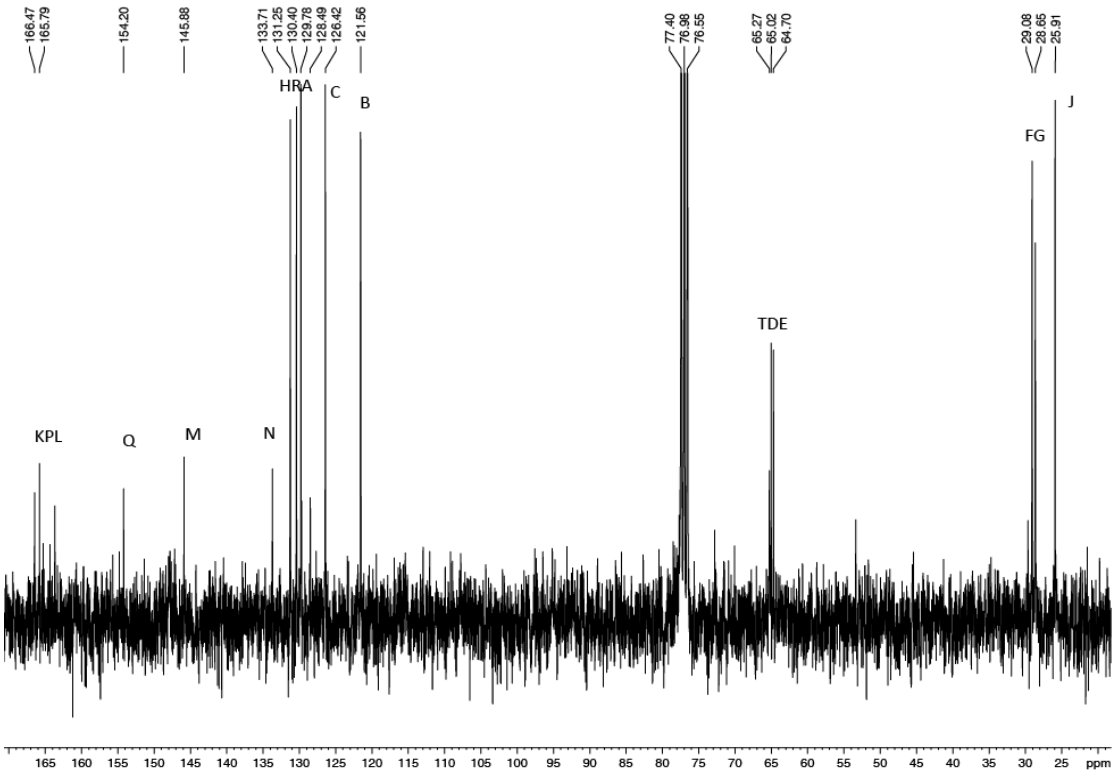

Figure 4-20. ^{13}C 300MHz NMR Spectrum for Compound 16 in $CDCl_3$

4.5.3.3 Attach 4-(Hydroxymethyl) Benzoic Acid to 26

Dibromide monoaromatic core (245mg, 0.446mmol, 1eqv.), 4-(hydroxylmethyl) benzoic acid (149mg, 0.993mmol, 2.2eqv.) and NaI (9mg, 0.06mmol, 0.2eqv.) were dissolved in 20mL DMSO before tetramethyl ammonium hydroxide (178mg, 0.980mmol, 2.2eqv.) were added into the mixture. The reaction was heated to 60^{o}C for 2 hrs and then diluted with 30mL chloroform and washed with brine once. Aqueous layer was backwashed with 40mL chloroform and the organic layers were combined, dried over Na_2SO_4, filtered and concentrated to give yellowish white solid. Column chromatography with Hex:EtOAc =4:1 as elute then gradually increased EtOAc composition to 1:1. The product came out last with white powder (0.320mmol, 71.7%).

4.5.3.4 Characterization for 17

^{1}H NMR – (300MHz; $CDCl_3$): δ 8.07 (s, 4H), 8.01 (d, J=8.8, 4H), 7.41 (d, J=8.8, 4H), 4.75 (s, 4H), 4.34-4.29 (m, 8H), 2.15 (s, 2H), 1.82-1.73 (m, 8H), 1.48-1.41 (m, 12H)

^{13}C NMR – (300MHz; $CDCl_3$): δ166.53, 165.94, 145.99, 134.13, 129.75, 129.58, 129.46, 126.42, 65.52, 65.03, 64.64, 29.09, 28.63, 28.60, 25.91

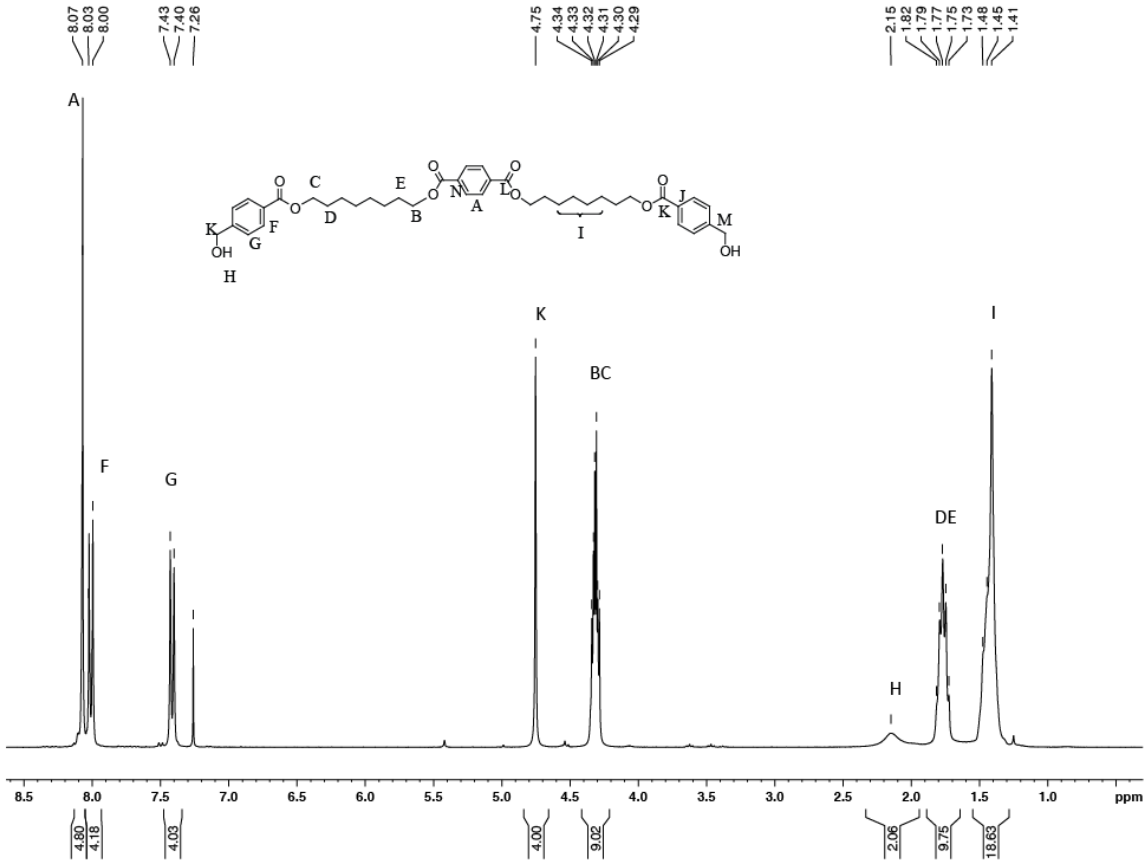

Figure 4-21. ^{1}H 300MHz NMR Spectrum for Compound 17 in $CDCl_3$

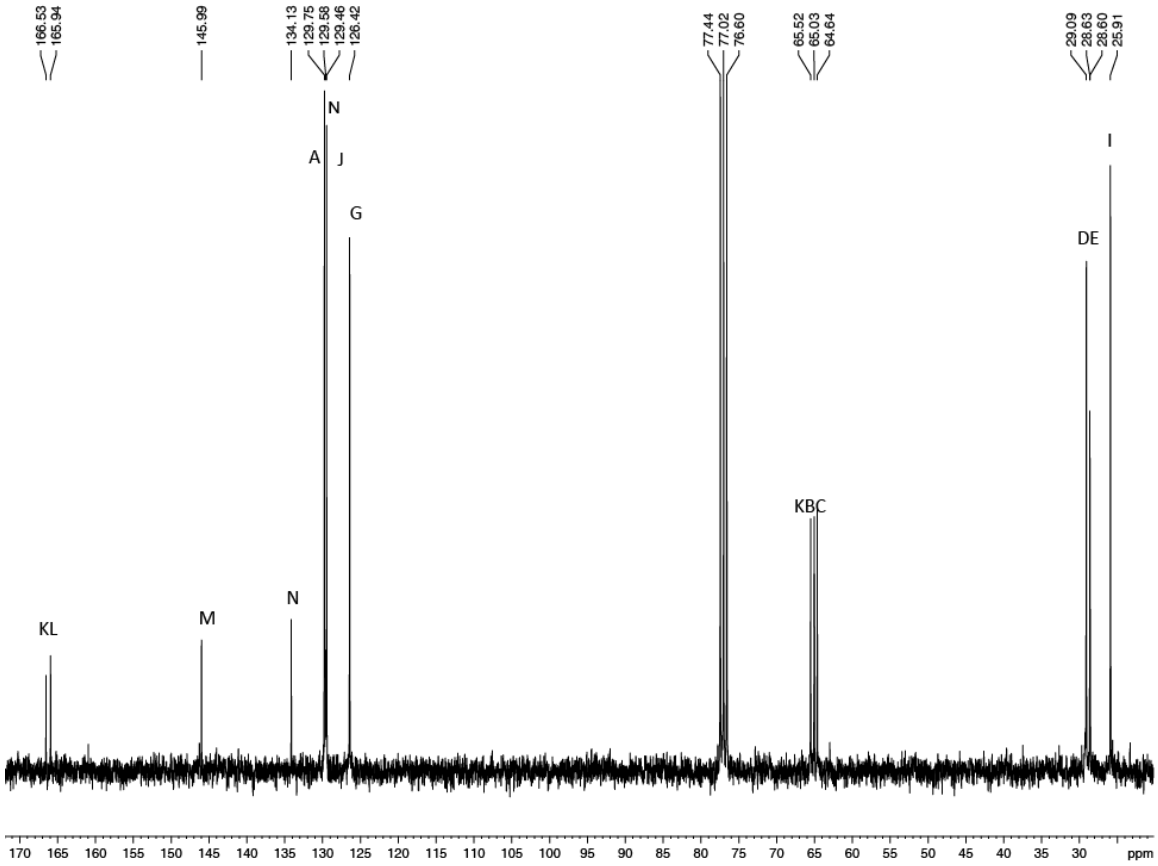

Figure 4-22. ^{13}C 300MHz NMR Spectrum for Compound 17 in $CDCl_3$

4.5.4 Attach TBDMS protected 4-(Hydroxymethyl) Benzoic Acid

4.5.4.1 Protect 4-(Hydroxymethyl) Benzoic Acid with TBDMS

4-hydromethyl benzoic acid (1.00g, 6.57mmol, 1eqv.), imidazole (1.79g, 26.3mmol, 4eqv.) and TBDMS-Cl (2.23g, 14.8mmol, 2eqv.) were dissolved in 50mL DCM. The resulting mixture was stirred 24 hours before 30mL of 2M K_2CO_3 solution, 30mL THF and 80mL methanol were added. The mixture was stirred additional 4 hours before washed with 100mL of 1M HCl once and 100mL water once. The organic layer was dired with Na_2SO_4 and concentrated. The residual solvent was removed under vacuum line. The crude product was purified on column chromatography with Hex:EtOAc = 3:2, yielding 1.11g white crystal (4.17mmol, 63.4%).

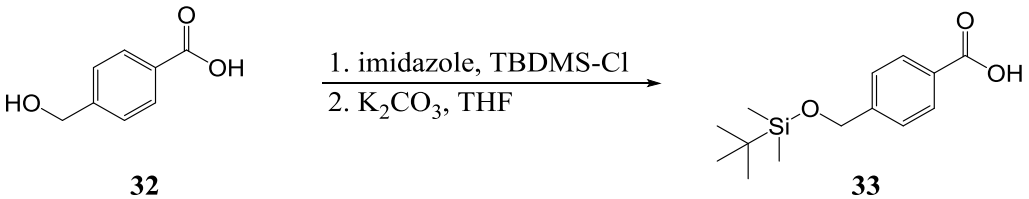

32 **33**

4.5.4.2 Characterization for 33

^{1}H NMR – (300MHz; $CDCl_3$): δ 12.16 (s, br, 1H), 8.10 (d, J=8.8, 2H), 7.45 (d, J=8.8, 2H), 4.83 (s, 2H), 0.97 (s, 9H), 0.13 (s, 6H)

^{13}C NMR – (75MHz; $CDCl_3$): δ172.4, 147.8, 130.3, 127.9, 125.8, 64.5, 25.9, 18.4, 5.3

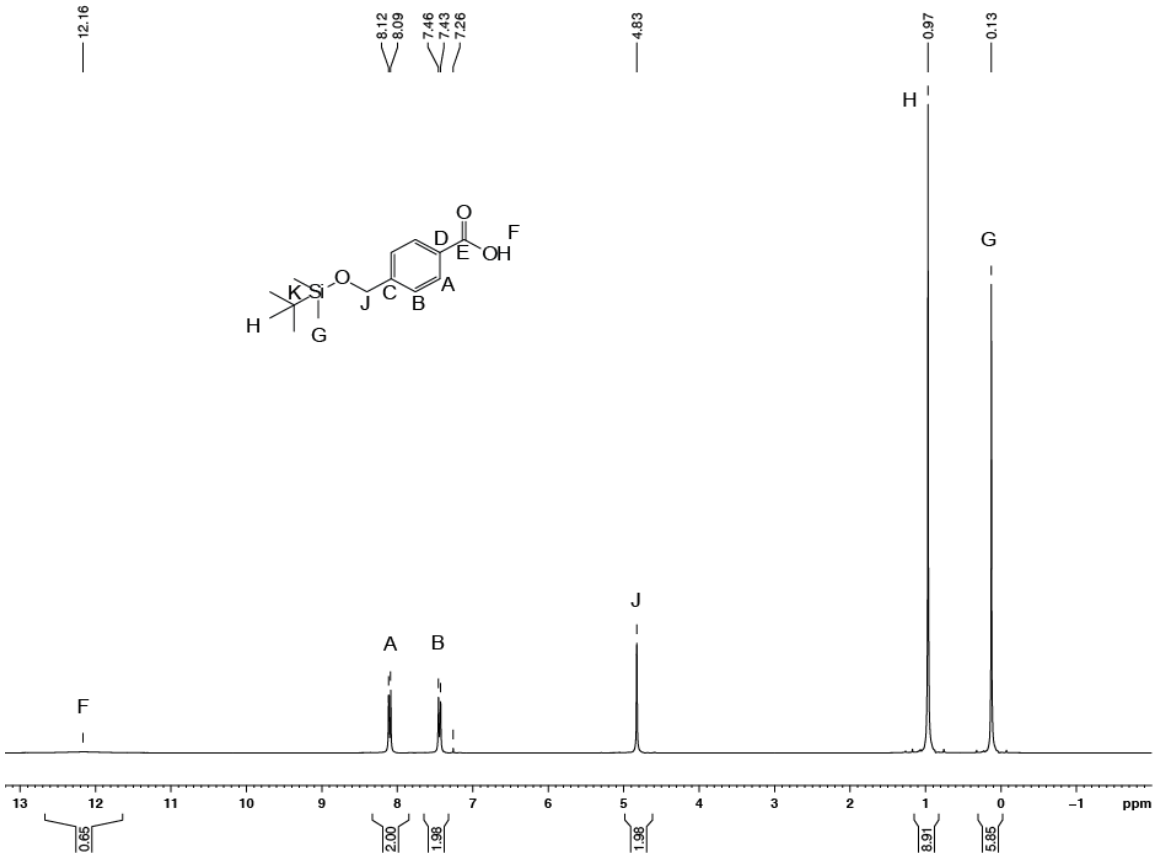

Figure 4-23. ^{1}H 300MHz NMR Spectrum for Compound 33 in $CDCl_3$

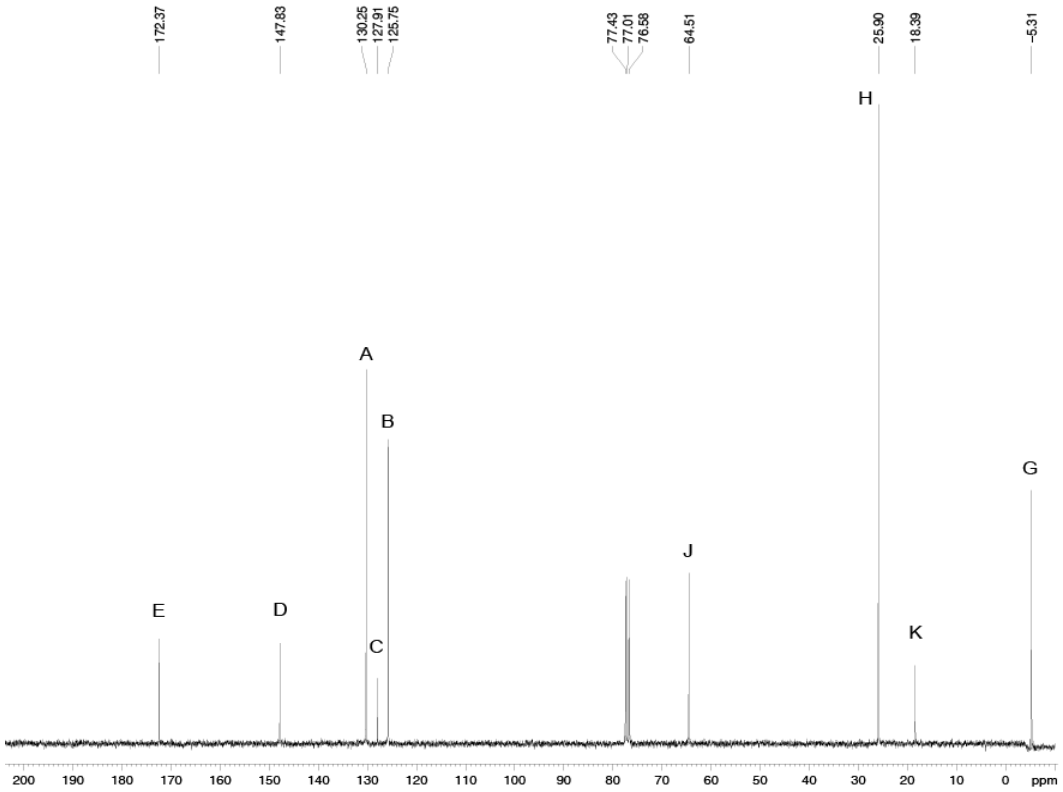

Figure 4-24. ^{13}C 300MHz NMR Spectrum for Compound 33 in $CDCl_3$

4.5.4.3 Attach TBDMS protected 4-(Hydroxymethyl) Benzoic Acid to 25

Dibromide triaromatic core (200mg, 0.254mmol, 1eqv.), 4-hydroxymethyl benzoic acid (150mg, 0.563mmol, 2.2eqv.) and NaI (9mg, 0.06mmol, 0.2eqv.) were dissolved in 20mL DMSO before tetramethyl ammonium hydroxide (101mg, 0.558mmol, 2.2eqv.) were added into the mixture. The reaction was heated to 60^{o}C for 2 hrs and then diluted with 30mL chloroform and washed with brine once. Aqueous layer was backwashed with 40mL chloroform and the organic layers were combined, dried over Na_2SO_4, rotovapped down. Column chromatography with Hex:EtOAc =3:2 as elute then gradually increased to 1:1. The product came out last with 120mg white powder (0.103mmol, 40.6%).

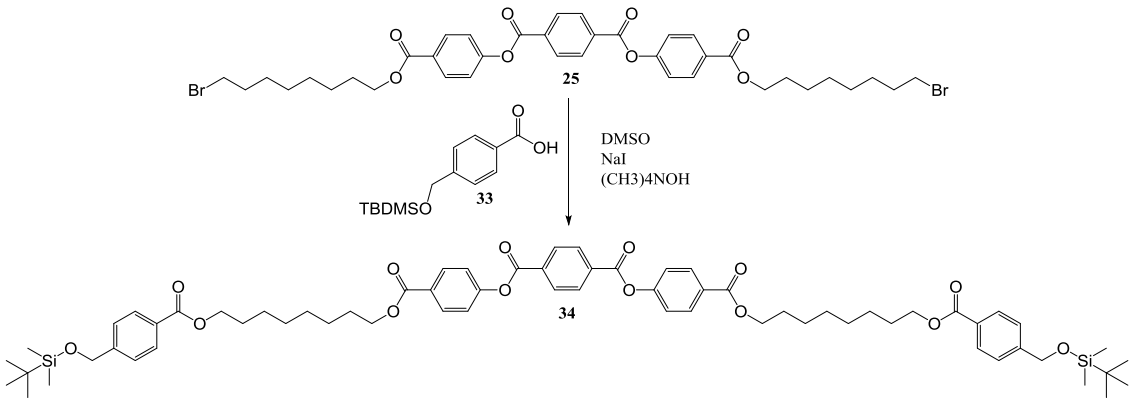

4.5.4.4 Characterization for 34

^{1}H NMR – (300MHz; $CDCl_3$): δ 8.35 (s, 4H), 8.16 (d, J=8.8, 4H), 8.01 (d, J=8.8, 4H), 7.38 (d, J=8.8, 4H) 7.34 (d, J=8.8, 4H), 4.79 (s, 4H), 4.36-4.29 (m, 8H), 1.78 (m, 8H), 1.45 (m, 18H), 0.94 (s, 18H), 0.10 (s, 12H)

^{13}C NMR – (75MHz; $CDCl_3$): δ166.7, 165.8, 163.7, 154.2, 146.7, 133.7, 131.3, 130.4, 129.5, 129.1, 128.5, 125.6, 121.6, 65.3, 64.9, 64.5, 45.1, 29.7, 29.2, 28.7, 26.0, 25.9, 18.4, 5.3

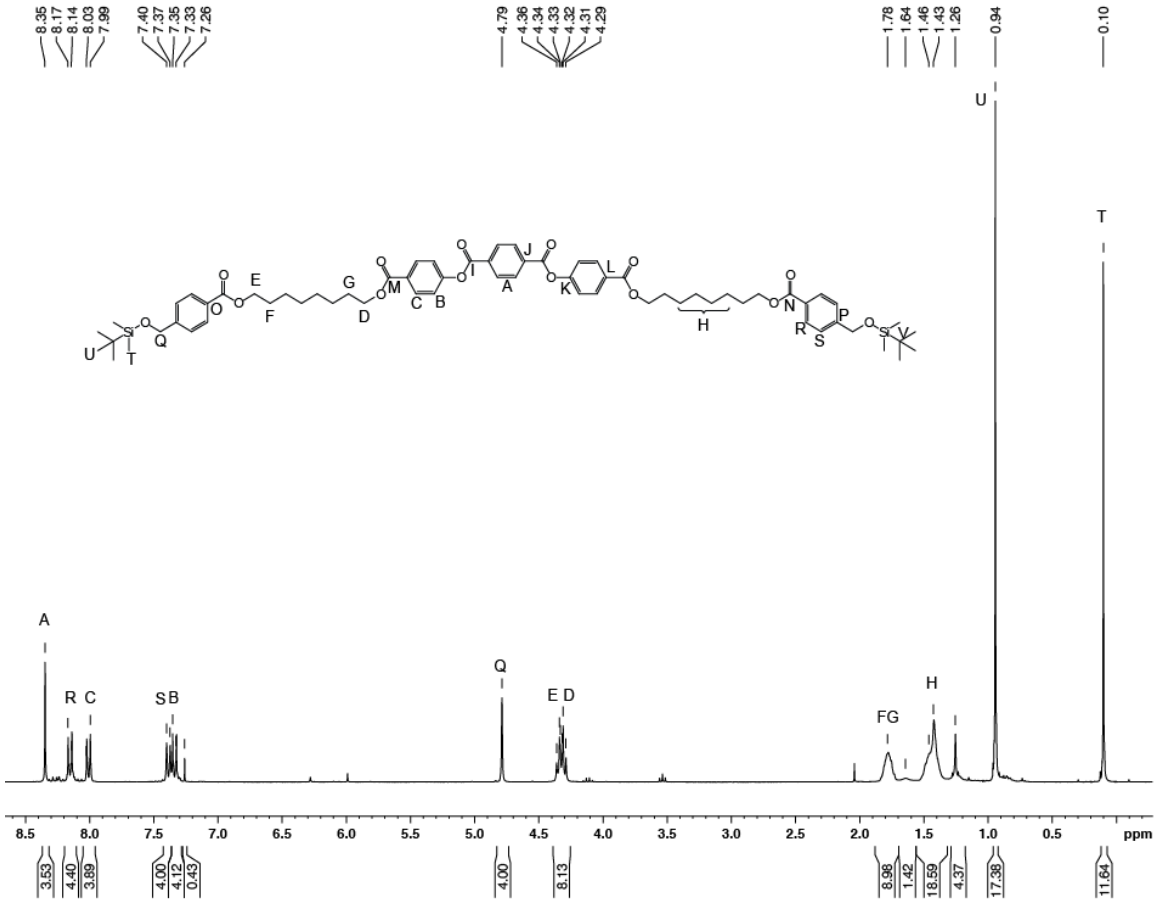

Figure 4-25. ^{1}H 300MHz NMR Spectrum for Compound 34 in $CDCl_3$

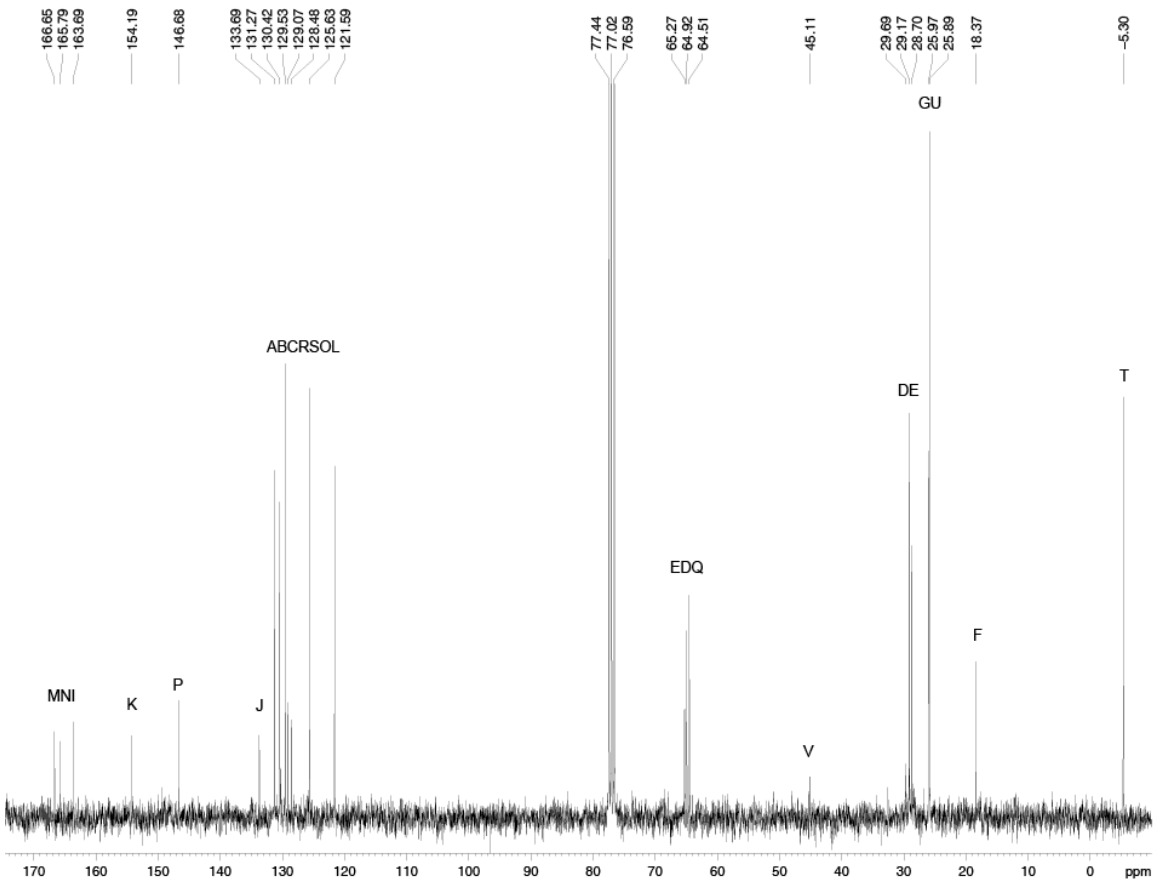

Figure 4-26. ^{13}C 300MHz NMR Spectrum for Compound 34 in $CDCl_3$

4.5.5 Attach BOC protected aniline[1]

4.5.5.1 Attach BOC Protected Aniline to 25

Dibromide triaromatic core (200mg, 0.254mmol, 1eqv.), Boc protected aniline (90mg, 0.559mmol, 2.2eqv.) and NaI (9mg, 0.06mmol, 0.2eqv.) were dissolved in 20mL DMSO before tetramethyl ammonium hydroxide (101mg, 0.558mmol, 2.2eqv.) were added into the mixture. The reaction was heated to 60^{o}C for 2 hrs and then diluted with 30mL chloroform and washed with brine once. Aqueous layer was backwashed with 40mL chloroform and the organic layers were combined, dried over Na_2SO_4, rotovapped down. Column chromatography with Hex:EtOAc =1:1 as elute then gradually increased to 3:7. The product came out last with 120mg white powder (0.174mmol, 68.5%)

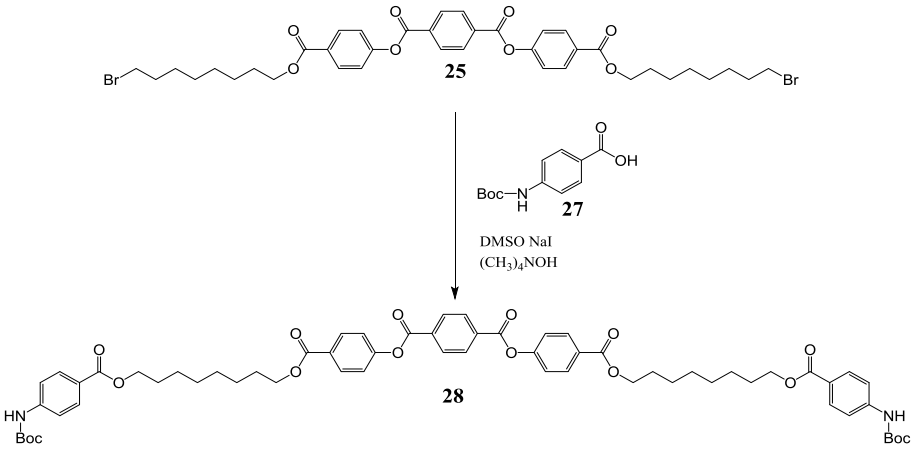

4.5.5.2 Characterization for 28

Reference NMR based on Chui's Thesis

^{1}H NMR – (300MHz; $CDCl_3$): δ 8.28 (s, 4H), 8.08 (d, J=8.8, 4H), 7.89 (d, J=8.8, 4H), 7.35 (d, J=8.8, 4H), 7.26 (d, J=8.8, 4H), 6.70 (s, 2H), 4.30-4.18 (m, 8H), 1.75-1.63 (m, 8H), 1.45 (s, 18H), 1.40-1.34 (m, 16H)

^{13}C NMR – (75MHz; $CDCl_3$): δ166.3, 165.9, 163.8, 154.3, 152.2, 142.7, 133.8, 131.4, 130.9, 130.5, 128.5, 124.6, 121.7, 117.3, 81.3, 65.4, 64.9, 29.2, 28.8, 28.3, 26.1

This sample:

^{1}H NMR – (300MHz; $CDCl_3$): δ 8.35 (s, 4H), 8.15 (d, J=8.8, 4H), 7.96 (d, J=8.8, 4H), 7.35 (d, J=8.8, 4H), 7.26 (d, J=8.8, 4H), 6.70 (s, 2H), 4.30-4.18 (m, 8H), 1.75-1.63 (m, 8H), 1.45 (s, 18H), 1.40-1.34 (m, 16H)

^{13}C NMR – (300MHz; $CDCl_3$): δ166.33, 165.83, 163.74, 154.19, 152.21, 142.58, 133.71, 131.33, 130.81, 130.47, 128.48, 124.72, 121.60, 117.36, 81.17, 65.32, 64.90, 29.15, 28.72, 28.28, 25.97

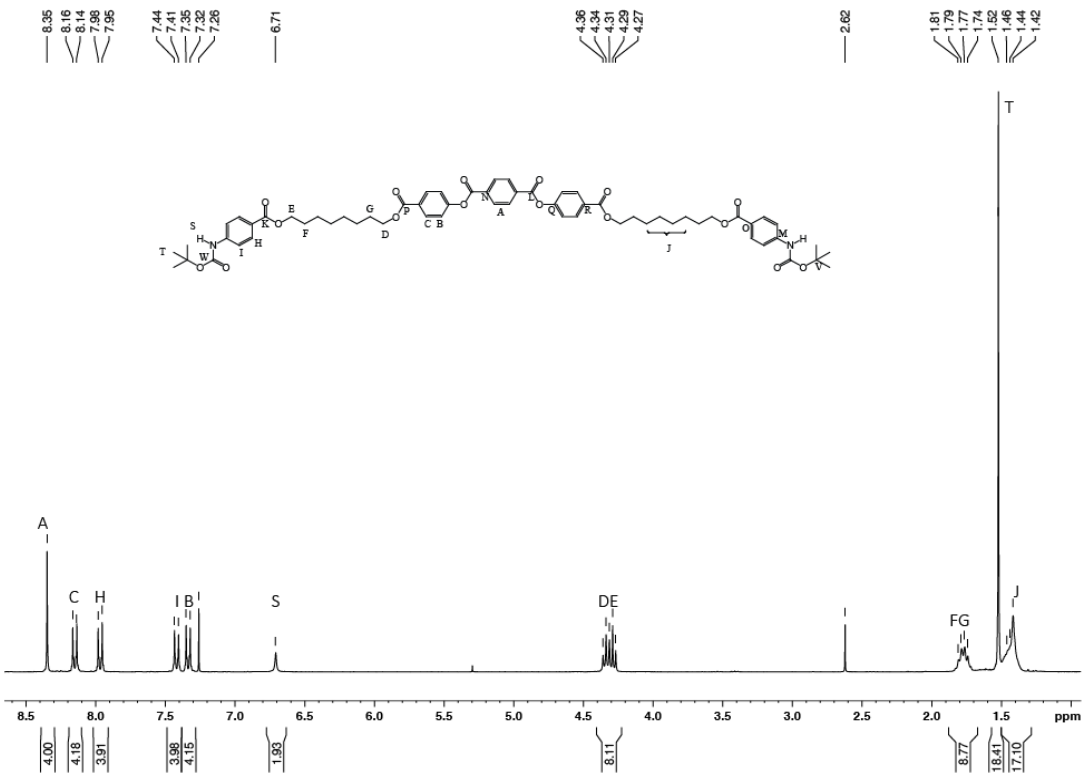

Figure 4-27. ^{1}H 300MHz NMR Spectrum for Compound 28 in $CDCl_3$

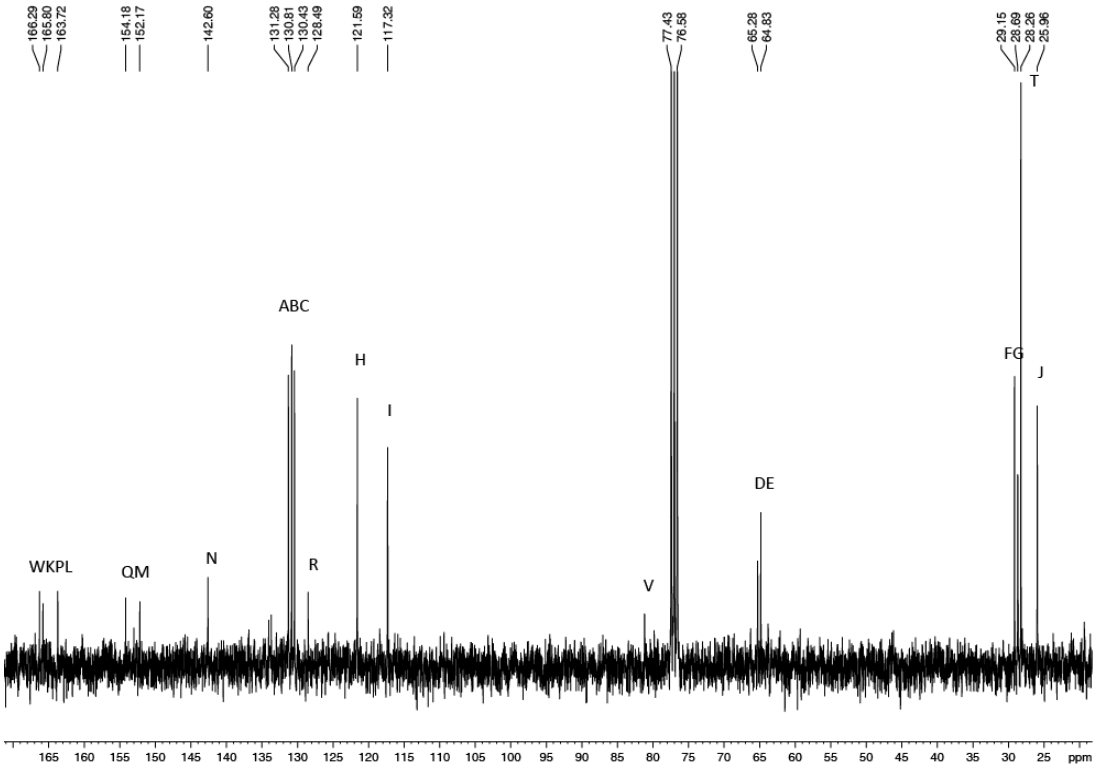

Figure 4-28. ^{13}C 300MHz NMR Spectrum for Compound 28 in $CDCl_3$

4.5.5.3 Attach BOC Protected Aniline to 26

Dibromide monoaromatic core (245mg, 0.446mmol, 1eqv.), Boc protected aniline (149mg, 0.993mmol, 2.2eqv.) and NaI (9mg, 0.06mmol, 0.2eqv.) were dissolved in 20mL DMSO before tetramethyl ammonium hydroxide (178mg, 0.980mmol, 2.2eqv.) were added into the mixture. The reaction was heated to 60^{o}C for 2 hrs and then diluted with 30mL chloroform and washed with brine once. Aqueous layer was backwashed with 40mL chloroform and the organic layers were combined, dried over Na_2SO_4, rotovapped down. Column chromatography with Hex:EtOAc =4:1 as elute then gradually increased EtOAc composition to 1:1. The product came out last with white powder (0.320mmol, 71.7%)

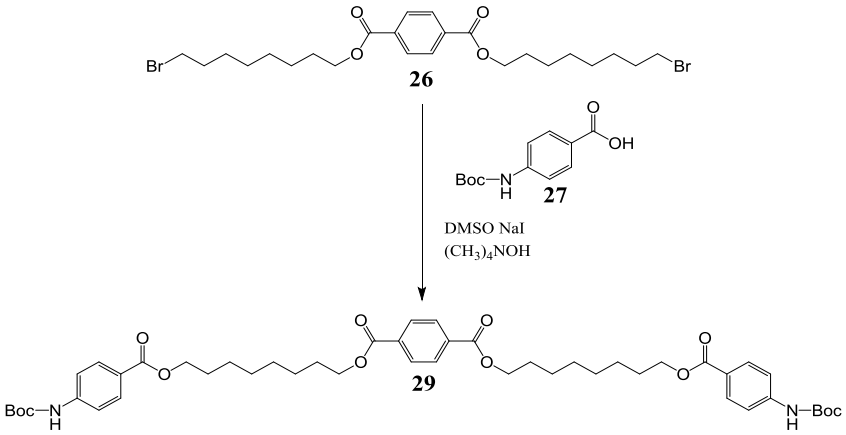

4.5.5.4 Characterization for 29

Reference NMR based on Chui's Thesis

^{1}H NMR – (300MHz; $CDCl_3$): δ 8.08 (s, 4H), 7.89 (d, J=8.8, 4H), 7.36 (d, J=8.8, 4H), 6.71 (s, 2H), 4.26 (t, J=6.7, 4H), 4.21 (t, J=6.7, 4H), 1.73-1.66 (m, 8H), 1.45 (s, 18H), 1.36-1.18 (m, 16H)

^{13}C NMR – (126MHz; $CDCl_3$): δ166.4, 166.0, 152.2 142.7, 134.1, 130.8, 129.5, 124.6, 117.3, 81.2, 65.6, 64.9, 29.2, 28.8, 28.3, 26.1

This sample:

^{1}H NMR – (300MHz; $CDCl_3$): δ 8.09 (s, 4H), 7.96 (d, J=8.8, 4H), 7.43 (d, J=8.8, 4H), 6.67 (s, 2H), 4.36-4.26 (m, 8H), 1.81-1.71 (m, 8H), 1.52 (s, 18H), 1.45-1.41(m, 16H)

^{13}C NMR – (300MHz; $CDCl_3$): δ 166.28, 165.88, 152.17, 142.64, 134.18, 130.79, 129.46, 124.71, 117.34, 81.13, 65.48, 64.80, 29.13, 28.70, 28.62, 28.25, 25.93

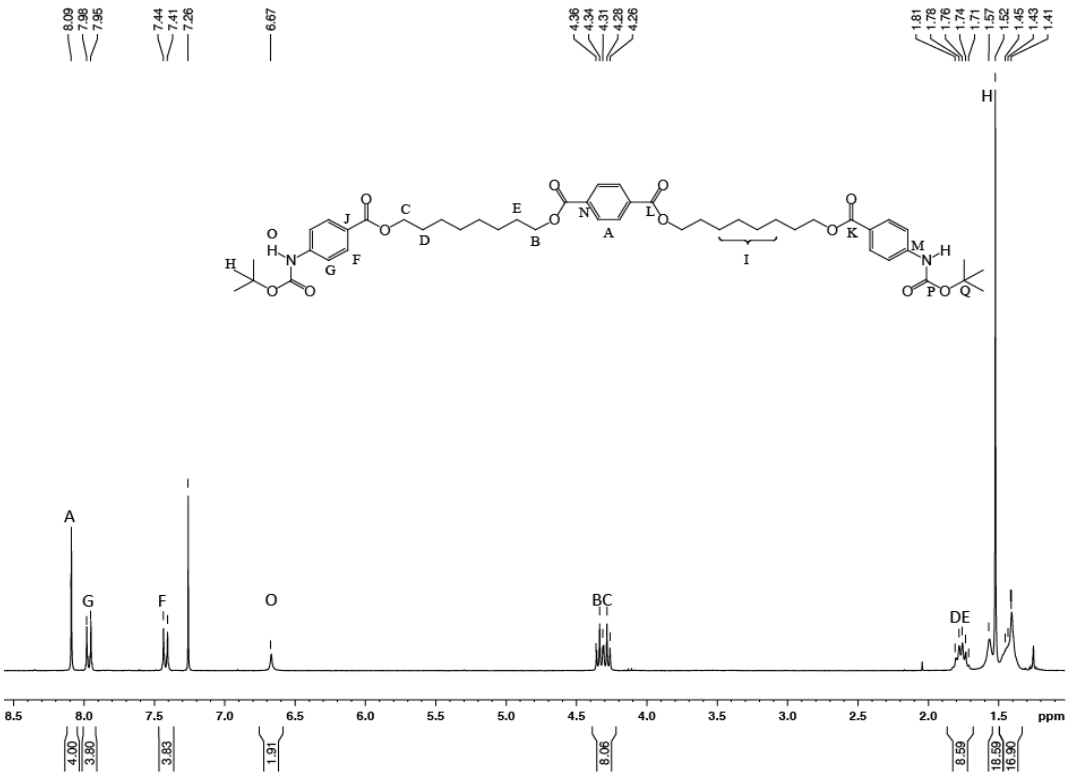

Figure 4-29. ^{1}H 300MHz NMR Spectrum for Compound 29 in $CDCl_3$

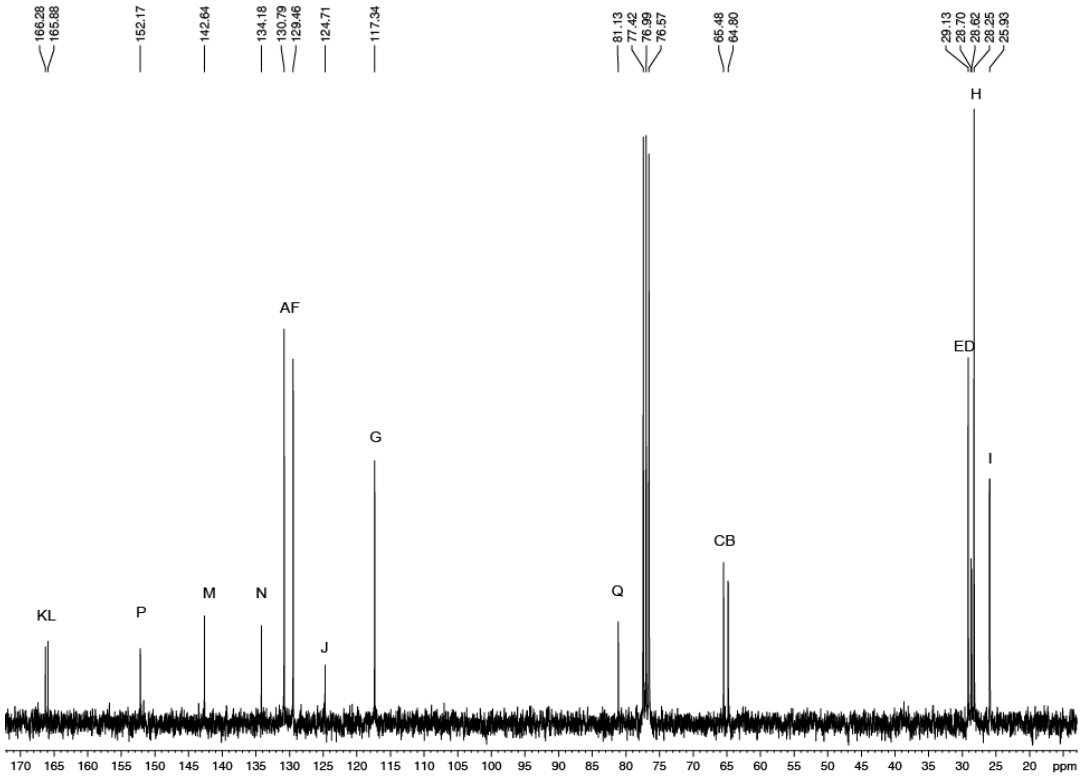

Figure 4-30. ^{13}C 300MHz NMR Spectrum for Compound 29 in $CDCl_3$

4.6 tBOC Deprotection[1]

4.6.1 Deprotect tBOC from Triaromatic Compound

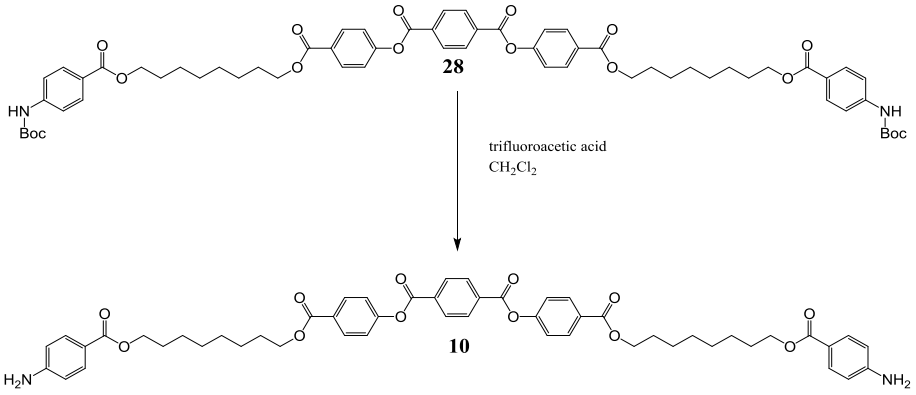

To prepare tBOC cleavage reagent, trimethylsilyl chloride (1.09g, 10mmol) was weighed into a 10mL graduated cylinder and diluted to the 5mL mark with CH_2Cl_2. Phenol (2.82g, 30mmol) was added as a solid, and the solution diluted to the 10mL mark. In a flame dried 5mL round-bottom-flask equipped with a stir-bar, tBOC protected aniline (100mg, 0.089mmol) was added. To this solid 2.5mL of the cleavage reagent was added. The flask was then capped, sealed with Teflon tape, and allowed to stir over 14 hours. The reaction slowly turns cloudy over time. The reaction was quenched with an aqueous solution of saturated K_2CO_3; pH of the solution should be 12. Repeat extractions with chloroform, followed by drying organic layer with Na_2SO_4, filtering, and drying gives a white solid. The solid was recrystallized from MeOH-CH_2Cl_2 to give 39mg white powder (0.044mmol, 50%)

4.6.2 Characterization for 10

Reference NMR based on Chui's thesis

^{1}H NMR – (300MHz; $CDCl_3$): δ 8.33 (s, 4H), 8.13 (d, J=8.9, 4H), 7.83 (d, J=8.8, 4H), 7.32 (d, J=8.8, 4H), 6.61 (br, s, 2H), 4.32 (t, J=6.7, 4H), 4.24 (t, J=6.7, 4H), 4.00 (s, br, 4H), 1.77-1.70 (m, 8H), 1.43-1.23 (m, 16H)

^{13}C NMR – (126MHz; $CDCl_3$): δ131.8, 131.5, 130.7, 121.8, 114.0, 65.6, 64.7, 29.4, 29.04, 28.95, 26.27, 26.22. insufficient sample to observe quaternary carbons

This sample:

^{1}H NMR – (300MHz; $CDCl_3$): δ 8.36 (s, 4H), 8.16 (d, J=8.9, 4H), 7.85 (d, J=8.8, 4H), 7.34 (d, J=8.8, 4H), 6.64 (s, 2H), 4.34 (t, J=6.7, 4H), 4.26 (t, J=6.7, 4H), 4.04 (s, br, 4H), 1.81-1.70 (m, 8H), 1.49-1.43 (m, 16H)

^{13}C NMR – (126MHz; $CDCl_3$): insufficient sample to generate decent carbon NMR

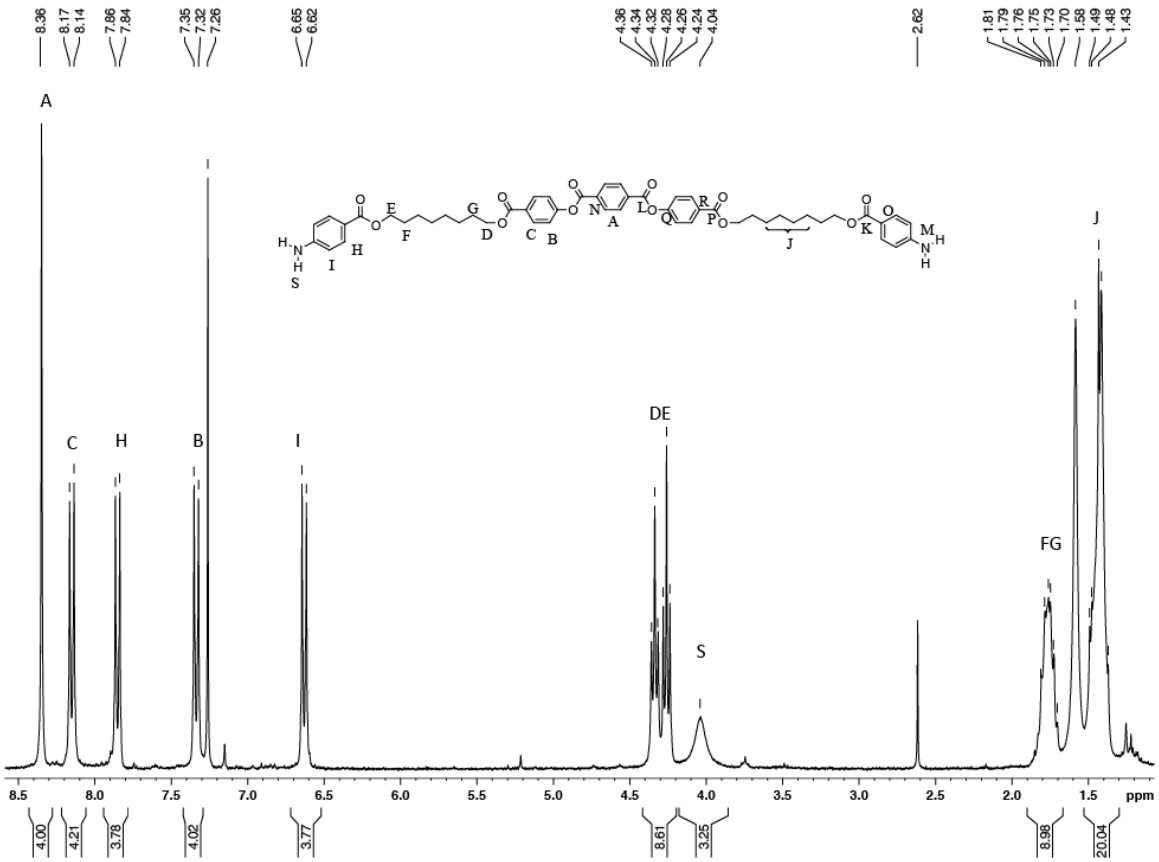

Figure 4-31. ^{1}H 300MHz NMR Spectrum for Compound 10 in $CDCl_3$

4.6.3 Deprotect tBOC from Monoaromatic Compound

To prepare tBOC cleavage reagent, trimethylsilyl chloride (1.09g, 10mmol) was weighed into a 10mL graduated cylinder and diluted to the 5mL mark with CH_2Cl_2. Phenol (2.82g, 30mmol) was added as a solid, and the solution diluted to the 10mL mark. In a flame dried 5mL round-bottom-flask equipped with a stir-bar, tBOC protected aniline (100mg, 0.089mmol) was added. To this solid 2.5mL of the cleavage reagent was added. The flask was then capped, sealed with Teflon tape, and allowed to stir over 14 hours. The reaction slowly turns cloudy over time. The reaction was quenched with an aqueous solution of saturated K_2CO_3; pH of the solution should be 12. Repeat extractions with chloroform, followed by drying organic layer with Na_2SO_4, filtering, and drying gives a white solid. The solid was recrystallized from MeOH-CH_2Cl_2 to give 39mg white powder (0.044mmol, 50%)

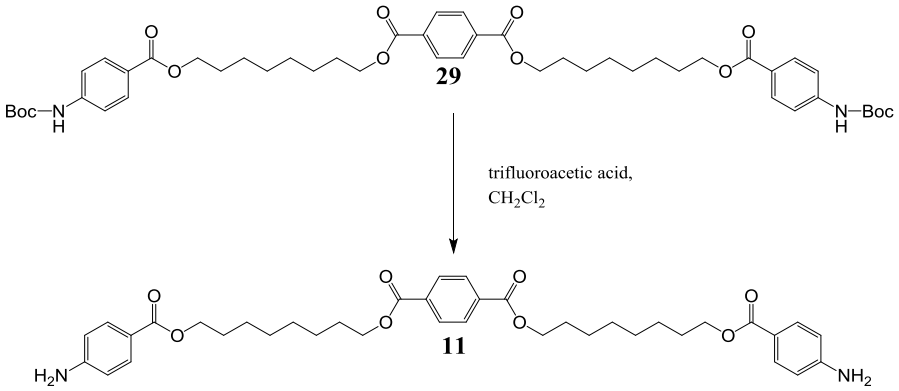

4.6.4 Characterization for 11

Reference NMR based on Chui's thesis

^{1}H NMR – (300MHz; $CDCl_3$): δ 8.02 (s, 4H), 7.77 (d, J=8.9, 4H), 6.56 (d, J=8.9, 4H), 4.26 (t, J=6.6, 4H), 4.18 (t, J=6.6, 4H), 3.97 (s, br, 4H), 1.71-1.67 (m, 8H), 1.39-1.33 (m, 16H)

^{13}C NMR – (126MHz; $CDCl_3$): δ167.0, 165.5, 150.0, 134.7, 131.5, 129.4, 119.7, 113.7, 66.2, 64.4, 29.3, 28.1, 26.4

This sample:

^{1}H NMR – (300MHz; $CDCl_3$): δ 8.09 (s, 4H), 7.84 (d, J=8.9, 4H), 6.64 (d, J=8.9, 4H), 4.36 (t, J=6.7, 4H), 4.25 (t, J=6.7, 4H), 4.03 (s, br, 4H), 1.80-1.70 (m, 8H), 1.45-1.40 (m, 16H)

^{13}C NMR – (300MHz; $CDCl_3$): 166.76, 165.91, 150.81, 134.16, 131.53, 129.47, 119.97, 113.75, 65.52, 64.39, 29.68, 29.15, 28.77, 28.62, 25.98, 25.93

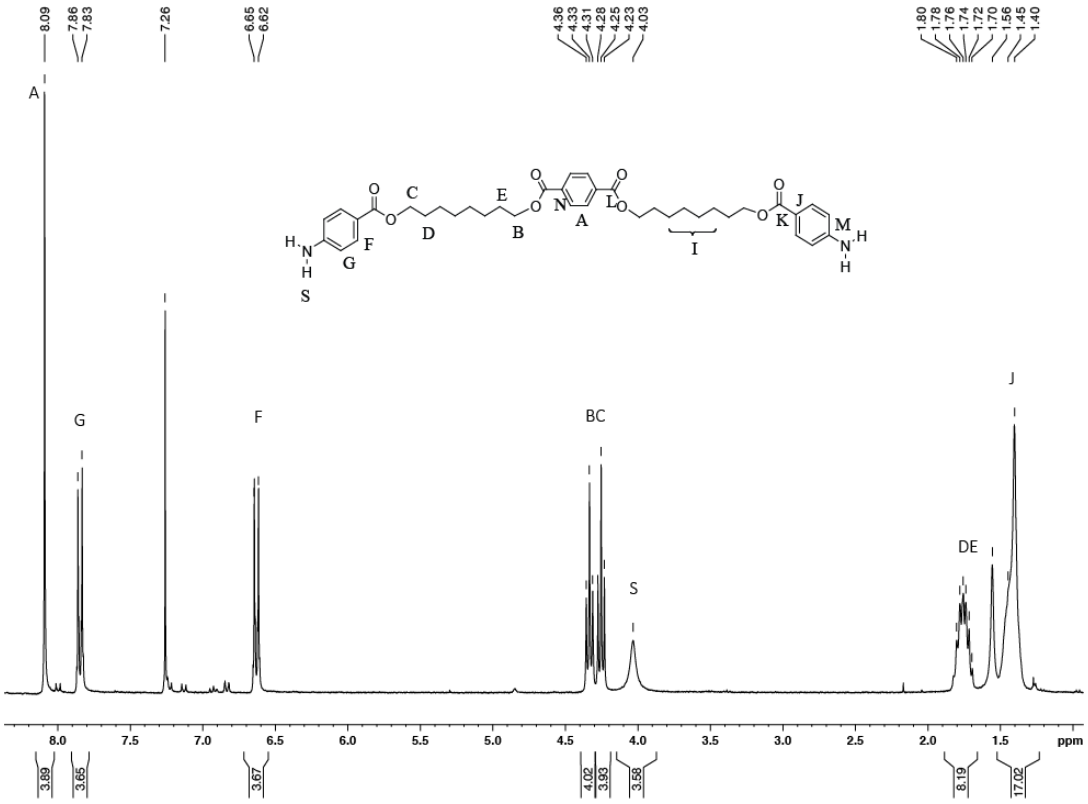

Figure 4-32. ^{1}H 300MHz NMR Spectrum for Compound 11 in $CDCl_3$

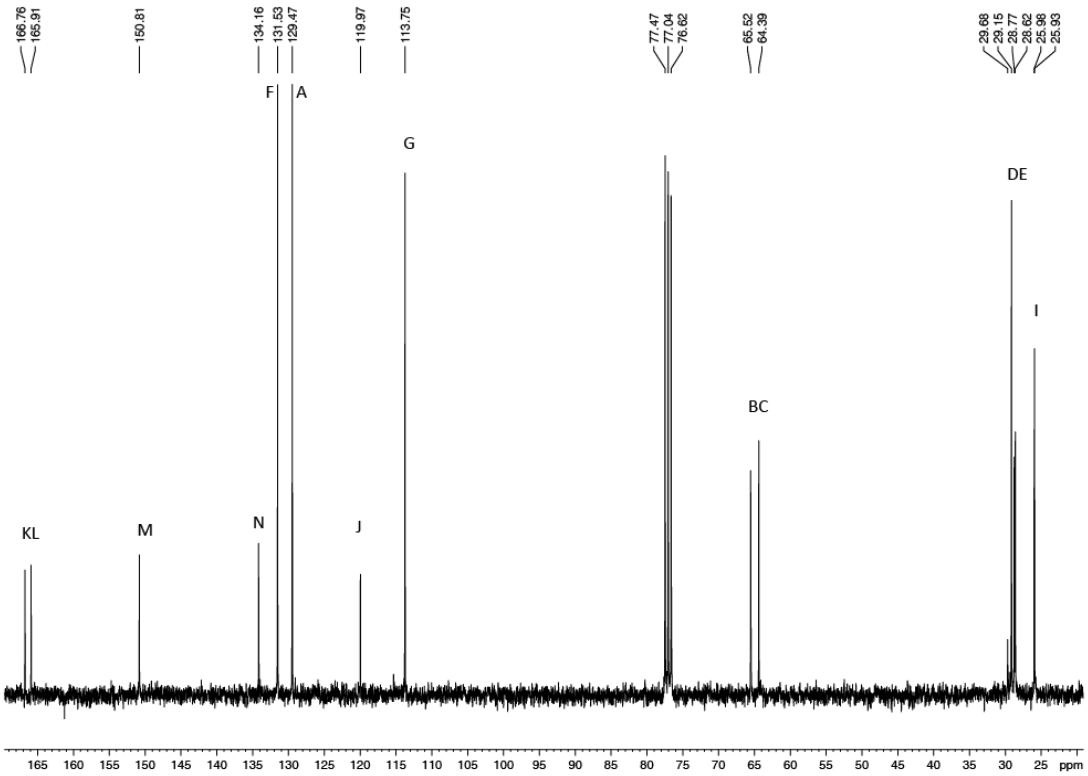

Figure 4-33. ^{1}H 300MHz NMR Spectrum for Compound 11 in $CDCl_3$

4.7 Making Trimethylamino Monoaromatic Compounds

4.7.1 Making 4-Trimethylamino Benzoic Acid

4-dimethylamino benzoic acid (3.00g, 18mmol) was dissolved in 40mL MeOH and 30mL MeI was then added to the solution. The reaction mixture was refluxed 16-24 hours to give orange pink solution and the solvent was rotovap down to give brown powder. 50mL water was added, and most solid was dissolved with some residual solid remaining. The residual solid was filtered out. The remaining aqueous solution was rotovaped down to give 2.60g brown crystals (14mmol, 77.8%).

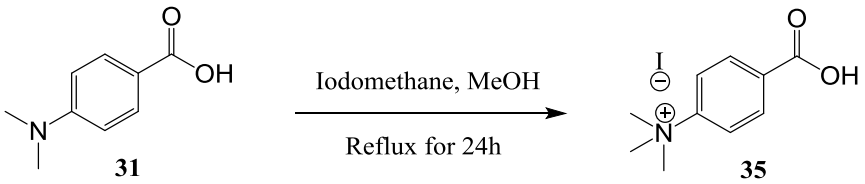

4.7.2 Characterization of 4-Trimethylamino Benzoic Acid

^{1}H NMR – (300MHz; MeOD): δ 8.13 (d, J=8.8, 2H), 7.91 (d, J=8.9, 2H), 3.71 (s, 9H)

^{13}C NMR – (300MHz; MeOD): δ 167.54, 151.60, 134.20, 132.83, 121.75, 57.82

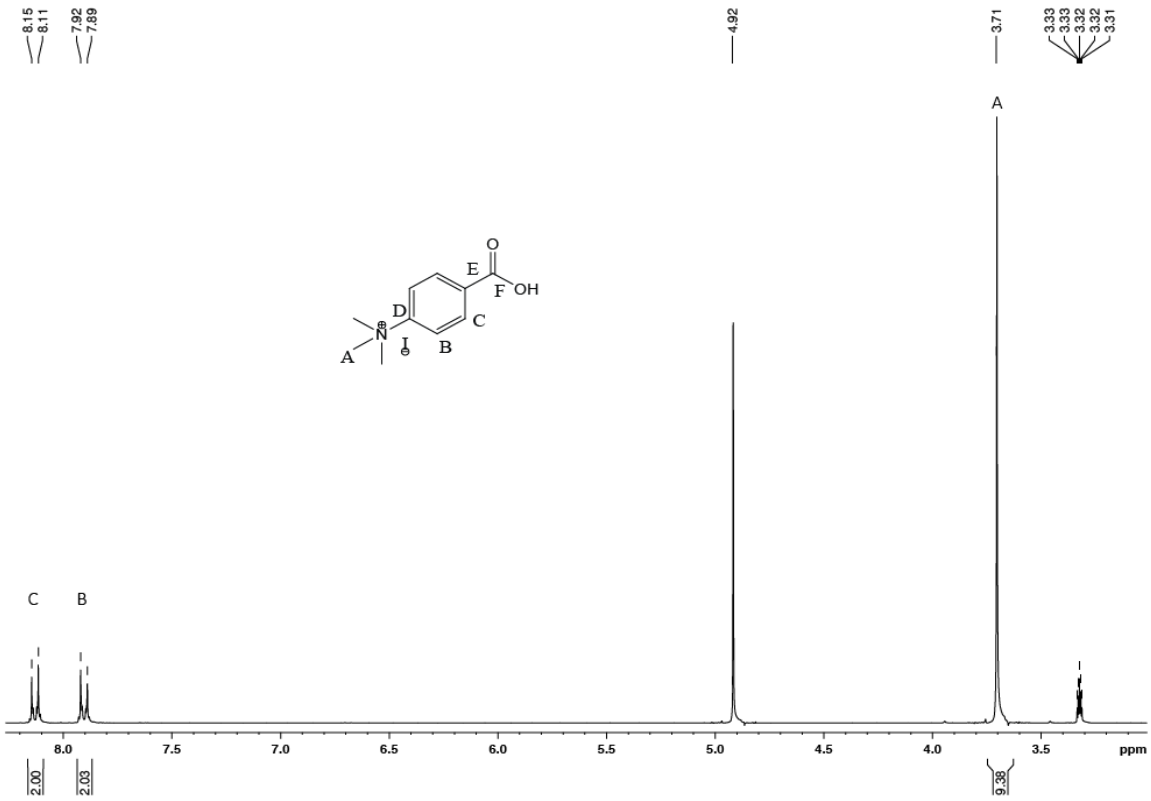

Figure 4-34. ^{1}H 300MHz NMR Spectrum for Compound 35 in MeOD

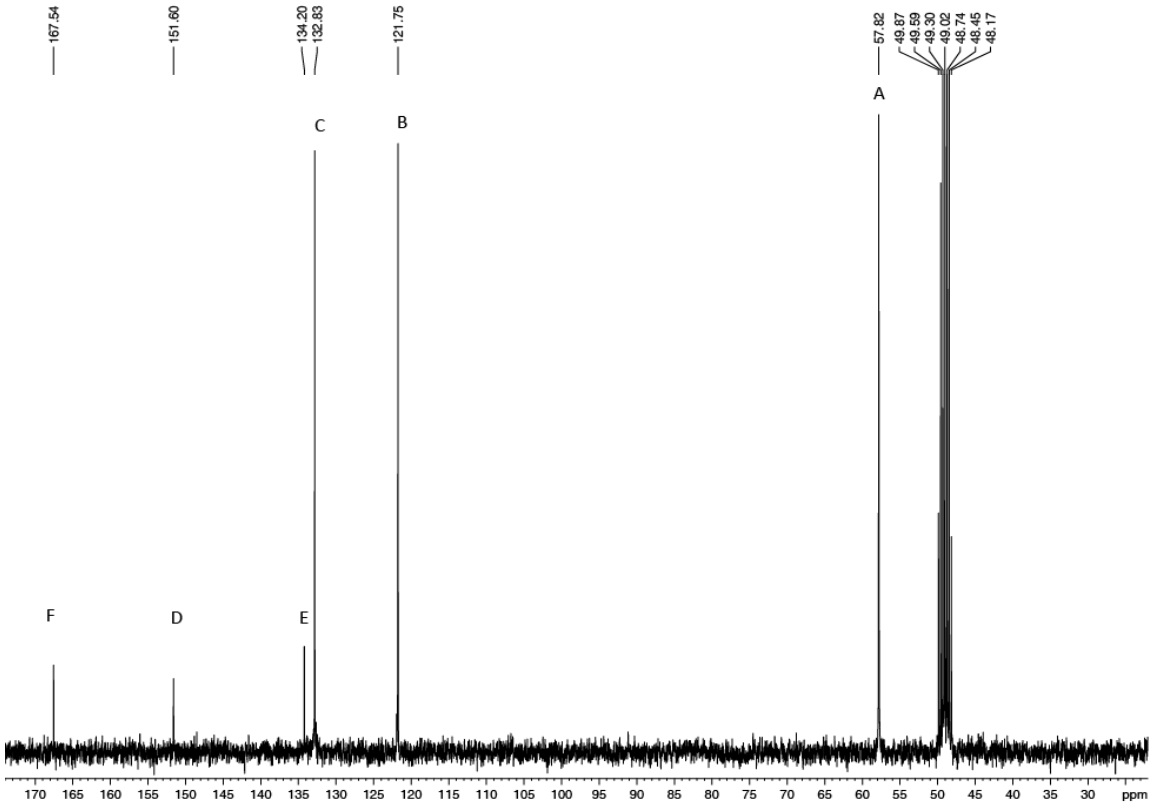

Figure 4-35. ^{13}C 300MHz NMR Spectrum for Compound 35 in MeOD

4.7.3 Attach 4-Trimethylamino Benzoic Acid To Monoaromatic Core

Dibromo-monoaromatic core (200mg, 0.364mmol, 1eqv.) and 4-trimethylamino benzoic acid (155mg, 0.861mmol, 2.4eqv.) and NaI (9mg, 0.06mmol, 0.2eqv.) were dissolved in 20mL DMSO before tetramethyl ammonium hydroxide (178mg, 0.980mmol, 2.2eqv.) was added into the mixture. The reaction was heated to 60^{o}C for 2 hrs and then diluted with 30mL chloroform and washed with brine once. Aqueous layer was backwashed with 40mL chloroform and the organic layers were combined, dried over Na_2SO_4, fitered and concentrated. However, the resulting solid was mixture of trimethyl amino and dimethyl amino head groups and they were difficult to separate (Figure 4-29).

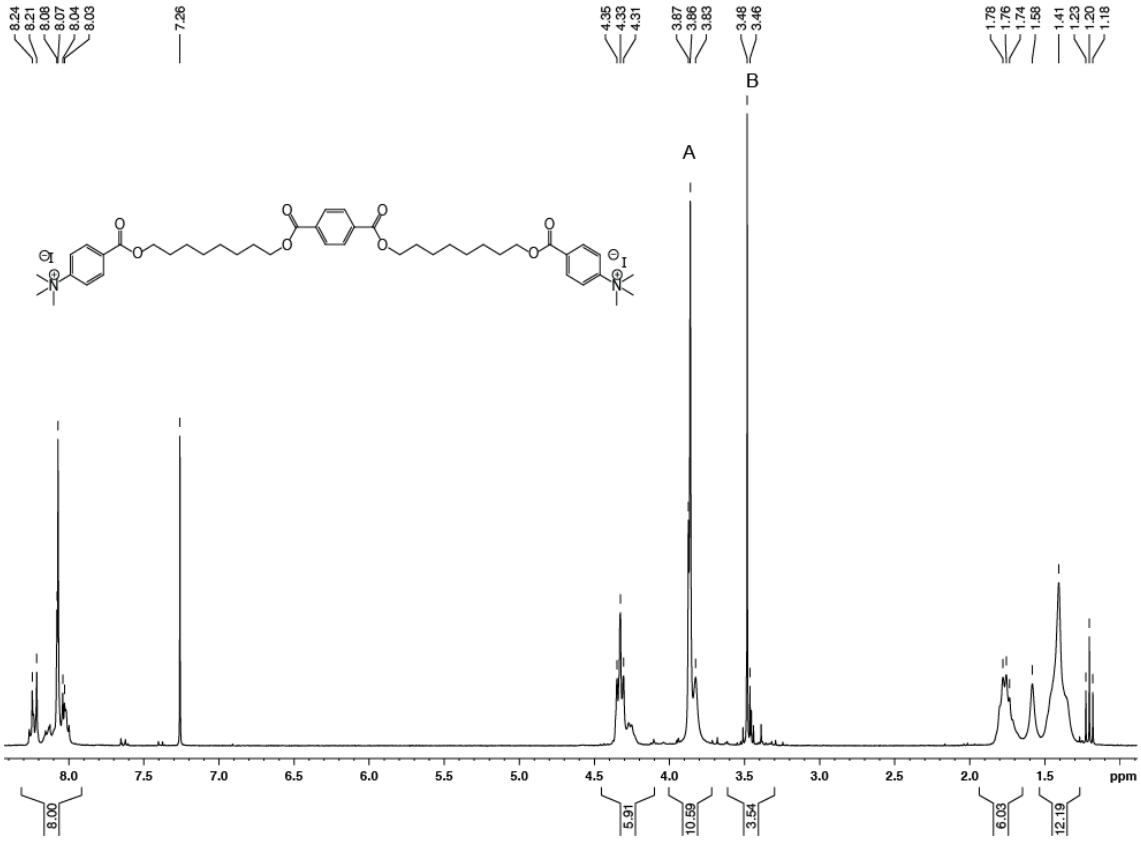

Figure 4-36. ^{1}H 300MHz NMR Spectrum for Compound 18 in $CDCl_3$

4.7.4 Methylate Dimethyl Amino Monoaromatic Compound

Dimethyl amino monoaromatic compound (200mg, 0.279mmol) was dissolved in 10mL MeI and refluxed overnight giving mixture dimetyl amino and trimethyl amino head groups. To push equilibrium to the product side, iodide was removed from the reaction using $AgNO_3$-Celite. The reaction generate better result, however there are still contamination from dimethyl amino head groups which were difficult to remove (Figure 4-30). The plan of making triamino monoaromatic compound was given up.

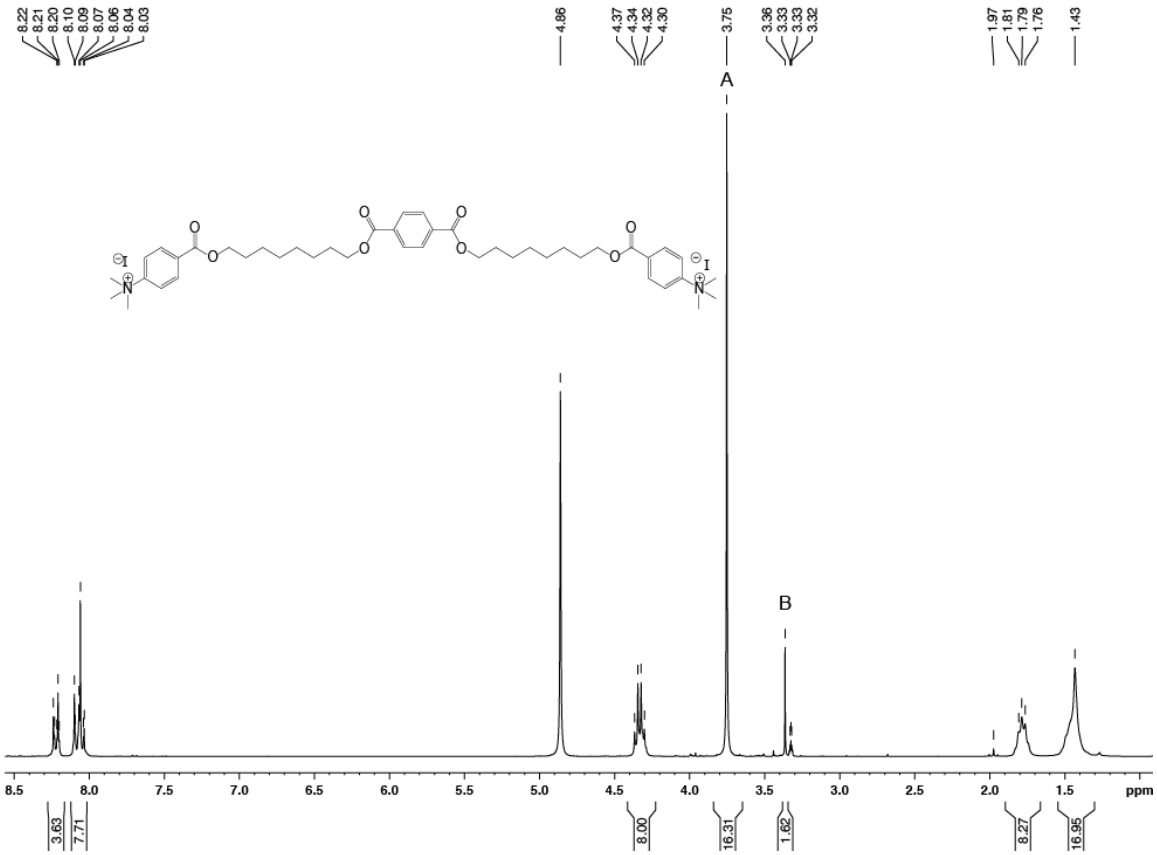

Figure 4-37. ^{1}H 300MHz NMR Spectrum for Compound 18 in $CDCl_3$

4.8 Voltage-Clamp Experiment

The experiment setup consists of a BC-525A bilayer clamp (Warner Instrument Corp.), an Axon Digidata 1440A digitizer (Molecular Devices), a LPF-8 filter (Warner Instrument Corp.), a bilayer clamp probe, electrolyte-filled holding cells, polystyrene cups, Ag/AgCl electrodes and KCl/Agar salt bridges. The cups used in the experiment had 250um diameter apertures (Warner Instrument Corp.). The lipid used in the experiments was diphytanoyl phosphatidylcholine (diPhyPC) (Avanti Polar Lipid). The electrolyte used was a solution of 1M CsCl, 10mM HEPES and 10mM TRIS. To start, 200uL of a stock solution of 25mg/mL lipid in CHCl3 was dried under argon and then resuspended in 200uL decane. For compounds that required pre-mixing into the lipid, 1 mol% compound in THF was added to the 200uL lipid, dried down under argon and then resuspended in 200uL decane. The aperture was painted with 0.5-1.0uL of decane/lipid. Excess decane was blown away with argon. The cup was then placed in the holding cells and filled with 3mL electrolyte solution. The outside of the cup within the holding cell was filled with 5mL electrolyte solution. The electrolytes inside and outside of the cup were respectively connected to two reference KCl electrolytes through two KCl/Agar salt bridges. The reference electrolytes were connected to the bilayer clamp probe through Ag/AgCl electrodes. The lipid bilayer membrane was formed either right after the electrolyte was filled in or by lift/dip motion (lifting the cup out of the electrolyte and then re-dipping the cup into the electrolyte). In some cases, bilayer membrane was formed by re-painting 0.5-1uL of the decane/lipid over the aperture. The stability of the bilayer membrane formed was tested by applying positive and negative potentials on both sides of the membrane over a period of 10-20minutes, and capacitance was checked repeatedly. Test compounds were added by injecting 2-10uL of 1mM compound solution on both sides of the membrane near the aperture. Data was acquired via the data acquisition software, Clampex V10.2 and filtered through LPF-8 filter 1kHz with acquisition rate 2kHz. Data was surveyed in various positive and negative potentials. This allowed the activity to be explored under operator control to ensure the activity was as expected and reliable. Once current activity was observed, the following instrumental controlled mode was applied: 1.150mV~-150mV 16 sweeps, 20mV decrease per sweep, 110 seconds per sweep; 2. -150mV~150mV 16 sweeps, 20mV increase per sweep, 110 seconds per sweep; 3. 75mV~ -75mV 16 sweeps, 10mV decrease per sweep, 110 seconds per sweep; 4. -75mV~75mV 16 sweeps, 10mV increase per sweep, 110 seconds per sweep; 5. 150mV~-150mV 16 sweeps, 20mV decrease per sweep, 11 seconds per sweep; 6. -150mV~150mV 16 sweeps, 20mV decrease per sweep, 11 seconds per sweep; Under these conditions the acquisition is automated and no operator intervention aor perturbation is possible. If there was no activity observed, inject 2uL compound solution near the aperture outside the cup, and brush over the aperture once. Brushing usually resulted membrane breakage which would require lift/dip to reform the membrane and the capacitance is rechecked.

Bibliography

1. Chui, J. K. W. A New Paradigm for Voltage-Clamp Studies of Synthetic Ion Channels. Doctoral Dissertation, University of Victoria, 2011.
2. Fyles, T. M., Synthetic Ion Channels in Bilayer Membranes. *Chemical Society reviews* **2007,** *36* (2), 335-47.
3. Eggers, P. K.; Fyles, T. M.; Mitchell, K. D. D.; Sutherland, T., Ion Channels from Linear and Branched Bola-Amphiphiles. *J. Org. Chem.* **2002,** *2003* (68), 1050-1058.
4. Chui, J. K.; Fyles, T. M., Ionic Conductance of Synthetic Channels: Analysis, Lessons, and Recommendations. *Chemical Society reviews* **2012,** *41* (1), 148-75.
5. Fox, R. O., Jr.; Richards, F. M., A Voltage-Gated Ion Channel Model Inferred from The Crystal Structure of Alamethicin at 1.5-A Resolution. *Nature* **1982,** *300* (5890), 325-30.
6. Fyles, T. M.; Loock, D.; Zhou, X., A Voltage-Gated Ion Channel Based on a Bis-Macrocyclic Bolaamphiphile. *Journal of the American Chemical Society* **1998,** *120* (13), 2997-3003.
7. Genge, K.; Moszynski, J. M.; Thompson, M.; Fyles, T. M., Membrane Activity of 3-Hydroxyglutarate Diesters. *Supramolecular Chemistry* **2012,** *24* (1), 29-39.
8. Hjorringgaard, C. U.; Vad, B. S.; Matchkov, V. V.; Nielsen, S. B.; Vosegaard, T.; Nielsen, N. C.; Otzen, D. E.; Skrydstrup, T., Cyclodextrin-Scaffolded Alamethicin with Remarkably Efficient Membrane Permeabilizing Properties and Membrane Current Conductance. *The journal of physical chemistry. B* **2012,** *116* (26), 7652-9.
9. Kobuke, Y.; Ueda, K.; Sokabe, M., Totally Synthetic Voltage Dependent Ion Channel. *Chem. Lett* **1995**, 435-436.
10. Reiss, P.; Al-Momani, L.; Koert, U., A Voltage-Responding Ion Channel Derived by C-Terminal Modification of Gramicidin A. *ChemBioChem* **2008,** *9*, 377-379.
11. Sakai, N.; Ni, C.; Bezrukov, S.; Matile, S., Voltage-Dependent Ion Channel Formation by Rigid Rod-Shaped Polyols in Planar Lipid Bilayers. *Bioorg. Med. Chem. Lett.* **1998,** *8* (19), 2743-2749.
12. Schlesinger, P. H.; Ferdani, R.; Liu, J.; Pajewska, J.; Pajewski, R.; Saito, M.; Shabany, H.; Gokel, G. W., SCMTR: A Chloride-Selective, Membrane-Anchored Peptide Channel that Exhibits Voltage Gating. In *American Chemical Society*, 2002; Vol. 124, pp 1848-1849.
13. Jog, P. V.; Gin, M. S., A Light-Gated Synthetic Ion Channel. *Org. Lett.* **2008,** *10* (17), 3693–3696.
14. Litvinchuk, S.; Tanaka, H.; Miyatake, T.; Pasini, D.; Tanaka, T.; Bollot, G.; Mareda, J.; Matile, S., Synthetic Pores with Reactive Signal Amplifiers as Artificial Tongues. *Nat. Mater* **2007,** (6), 576–580.
15. Long, S. B.; Tao, X.; Campbell, E. B.; MacKinnon, R., Atomic Structure of a Voltage-Dependent K+Channel in a Lipid Membrane-Like Environment. *Nature* **2007,** *450*, 376–382.
16. Yang, N.; Horn, R., Evidence for voltage-dependent S4 movement in sodium channels. *Neuron* **1995,** *15* (1), 213-8.
17. Kubo, Y.; Adelman, J. P.; Clapham, D. E.; Jan, L. Y.; Karschin, A.; Kurachi, Y.; Lazdunski, M.; Nichols, C. G.; Seino, S., Nomenclature and Molecular Relationships of Kir Channels. *Pharmacol Rev* **2005,** *57*, 509–526.
18. Gokel, G. W.; Carasel, I. A., Biologically Active, Synthetic Ion Transporters. *Chemical Society reviews* **2007,** *36* (2), 378-89.

19. Gokel, G. W.; Daschbach, M. M., Coordination and Transport of Alkali Metal Cations Through Phospholipid Bilayer Membranes by Hydraphile Channels. *Coordination Chemistry Reviews* **2008,** *252* (8-9), 886-902.
20. Gokel, G. W.; Negin, S., Synthetic Membrane Active Amphiphiles. *Adv Drug Deliv Rev* **2012,** *64* (9), 784-96.
21. Matile, S.; Sakai, N., The characterization of synthetic ion channels and pores. In *In Analytical Methods in Supramolecular Chemistry*, Wiley -VCH: Weinheim: Schalley, C. A., Ed, 2007; pp 381-418.
22. Matile, S.; Som, A.; Sorde, N., Recent Synthetic Ion Channels and Pores. *Tetrahedron* **2004,** *60*, 6405-6435.
23. Matile, S.; Vargas Jentzsch, A.; Montenegro, J.; Fin, A., Recent Synthetic Transport Systems. *Chemical Society reviews* **2011,** *40* (5), 2453-74.
24. Sisson, A. L.; Shah, M. R.; Bhosale, S.; Matile, S., Synthetic Ion Channels and Pores (2004-2005). *Chem. Soc. Rev.* **2006,** *35*, 1269-1286.
25. Fyles, T. M., How Do Amphiphiles Form Ion-Conducting Channels in Membranes? Lessons from Linear Oligoesters. *Accounts of Chemical Research* **2013**.
26. Gokel, G. W.; Negin, S., Synthetic Ion Channels: From Pores to Biological Applications. *Accounts of Chemical Research* **2013**.
27. Guo, W.; Tian, Y.; Jiang, J., Asymmetric Ion Transport Through Ion-Channel-Mimetic Solid-State Nanopores. *Accounts of Chemical Research* **2013**.
28. Jentzsch, A. V.; Hennig, A.; Mareda, J.; Matile, S., Synthetic Ion Transporters that Work with Anion π Interactions, Halogen Bonds, and Anion Macrodipole Interactions

Accounts of Chemical Research **2013**.
29. Montenegro, J.; Ghadiri, M. R.; Granja, J. R., Ion Channel Models Based on Self-Assembling Cyclic Peptide Nanotubes. *Accounts of Chemical Research* **2013**.
30. Mosgaard, L. D.; Heimburg, T., Lipid Ion Channels and the Role of Proteins. *Accounts of Chemical Research* **2013**.
31. Otis, F.-O.; Auger, M. L.; Voyer, N., Exploiting Peptide Nanostructures To Construct Functional Artificial Ion Channels. *Accounts of Chemical Research* **2013**.
32. Reib, P.; Koert, U., Ion-Channels: Goals for Function-Oriented Synthesis. *Accounts of Chemical Research* **2013**.
33. Riccardis, F. D.; Izzo, I.; Montesarchio, D.; Tecilla, P., Ion Transport through Lipid Bilayers by Synthetic Ionophores: Modulation of Activity and Selectivity. *Accounts of Chemical Research* **2013**.
34. Sakai, N.; Houdebert, D.; Matile, S., Voltage-Dependent Formation of Anion Channels by Synthetic Rigid-Rod Push-Pull Beta-Barrels. *Chem. Eur. J.* **2003,** *9* (1), 223-232.
35. Goto, C.; Yamamura, M.; Satake, A.; Kobuke, Y., Aritificial Ion Channels Showing Rectified Current Behavior. *J. Am. Chem. Soc* **2001,** *123*, 12152-12159.
36. Cameron, L. M.; Fyles, T. M.; Hu, C.-w., Synthesis and Membrane Activity of a Bis(metacyclophane)bolaamphiphile. *J. Org. Chem.* **2002,** *67*, 1548-1553.
37. Fyles, T. M.; Luong, H., Structure-Activity Relationships In Linear Oligoester Ion-Channels. *Organic & biomolecular chemistry* **2009,** *7* (4), 733-8.
38. Fyles, T. M.; Luong, H., Solid-Phase Synthesis of A Library Of Linear Oligoester Ion-Channels. *Organic & biomolecular chemistry* **2009,** *7* (4), 725-32.
39. Moszynski, J. M.; Fyles, T. M., Synthesis, Transport Activity, Membrane Localization, and Dynamics Of Oligoester Ion Channels Containing Diphenylacetylene Units. *Organic & biomolecular chemistry* **2010,** *8* (22), 5139-49.

40. Moszynski, J. M.; Fyles, T. M., Synthesis and Ion Transport Activity of Oligoesters Containing An Environment-Sensitive Fluorophore. *Organic & biomolecular chemistry* **2011,** *9* (21), 7468-75.
41. Moszynski, J. M.; Fyles, T. M., Mechanism of Ion Transport by Fluorescent Oligoester Channels. *Journal of the American Chemical Society* **2012,** *134* (38), 15937-45.
42. Moszynski, J. M. The synthesis and characterization of diphenylacetylene containing ion channels. Doctoral Thesis, University of Victoria, 2011.
43. Dambenieks, A. K. Explorations in synthetic ion channel research: metal-ligand self-assembly and dissipative assembly. Doctoral Thesis, University of Victoria, 2013.
44. Riddell, F. G.; Hayer, M. K., The Monensin-Mediated Transport of Sodium Ions Through Phospholipid Bilayers Studied by 23Na-NMR Spectroscopy. *Biochimica et Biophysica Acta* **1985,** *817*, 313-317.
45. Katsu, T. N., H.; Kanamori, T.; Kamo, N.; Tsuchiya, T., Ion-Selective Electrode For Transmembrane pH Difference Measurements. *Analytical Chemistry* **2001,** *73*, 1849-1854.
46. Pajewski, R. F., R.; Pajewska, J.; Djedovic, N.; Schlesinger, P. H.; Gokel, G. W., Evidence for Dimer Formation by An Amphiphilic Heptapeptide That Mediates Chloride and Carboxyfluorescein Release From Liposomes. *Organic and Biomolecular Chemistry* **2005,** *3*, 619-625.

Appendix 1 - Voltage-Clamp Data

Compound 10 Activities

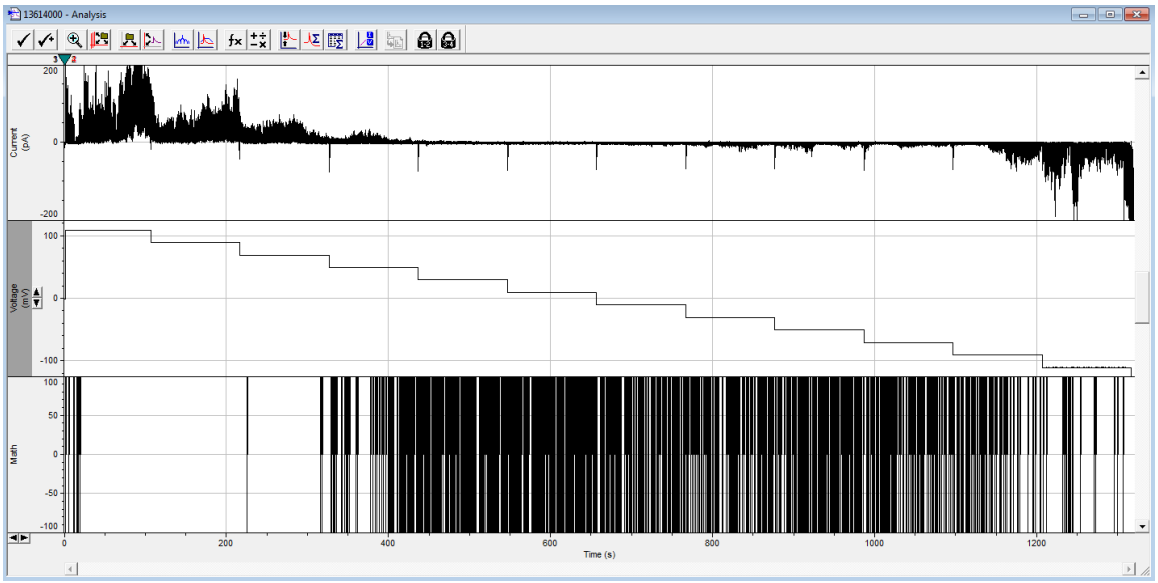

4nmole of **10**, 110mV to -110mV, 1M CsCl, 110s per potential level.

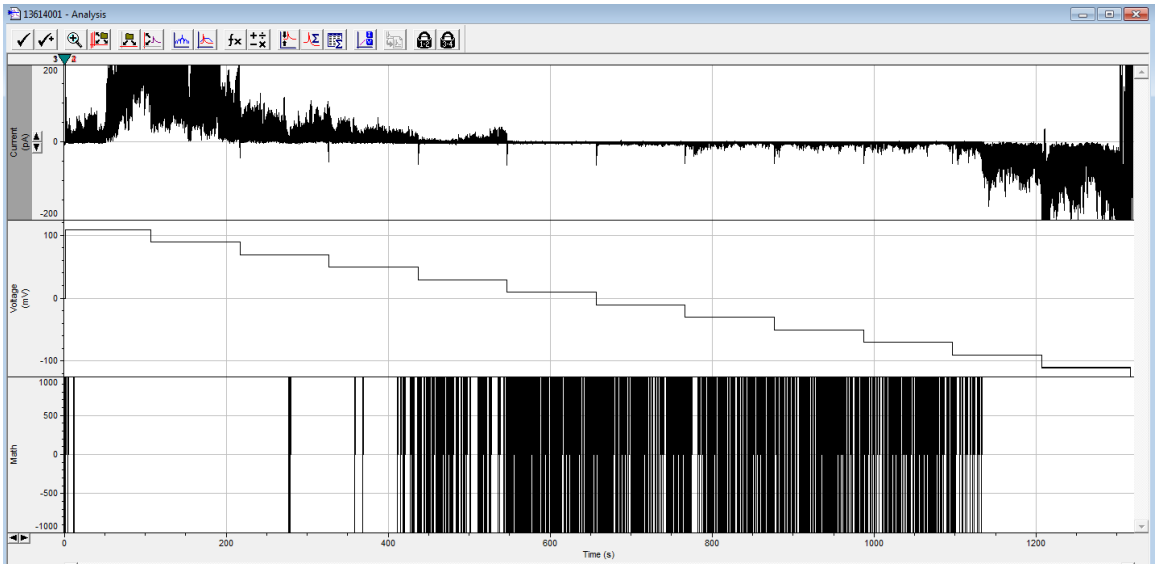

4nmole of **10**, 110mV to -110mV, 1M CsCl, 110s per potential level.

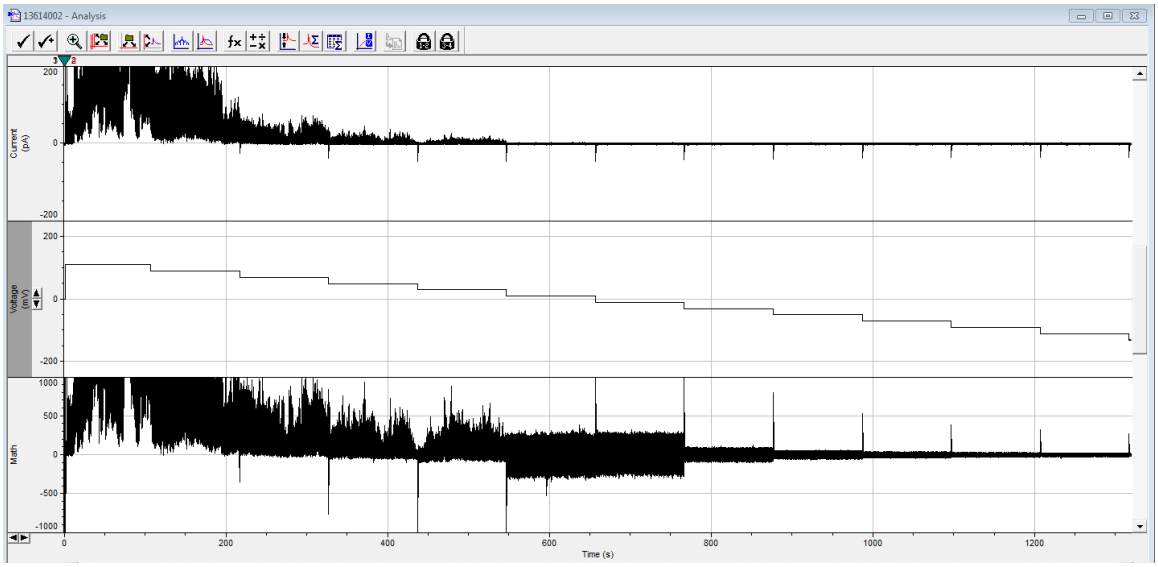

4nmole of **10**, 110mV to -110mV, 1M CsCl, 110s per potential level.

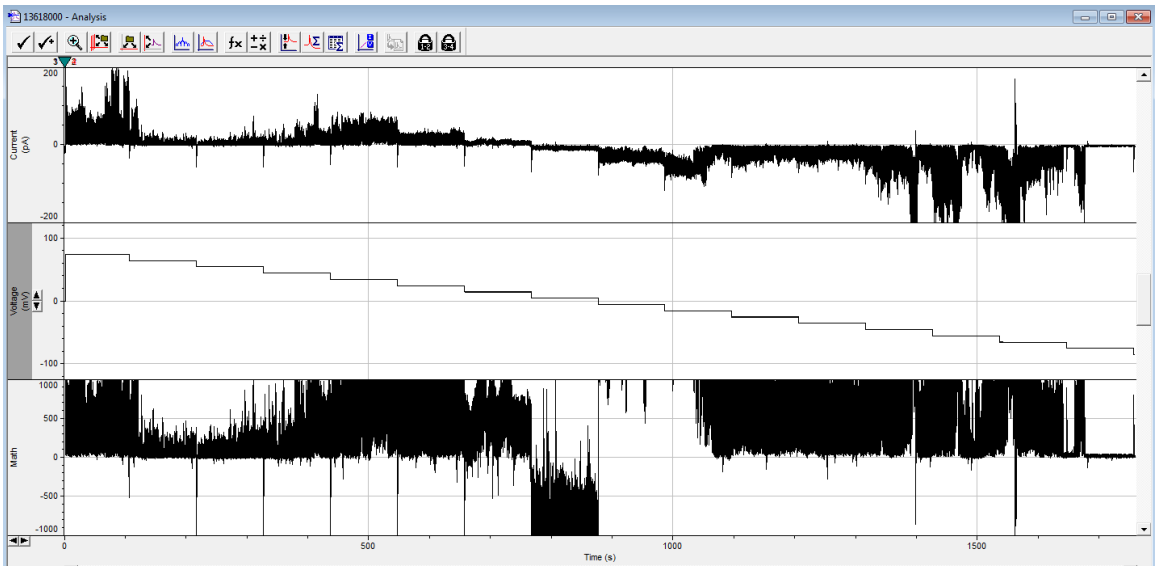

12nmole of **10** with brush, 75mV to -75mV, 1M CsCl, 110s per potential level

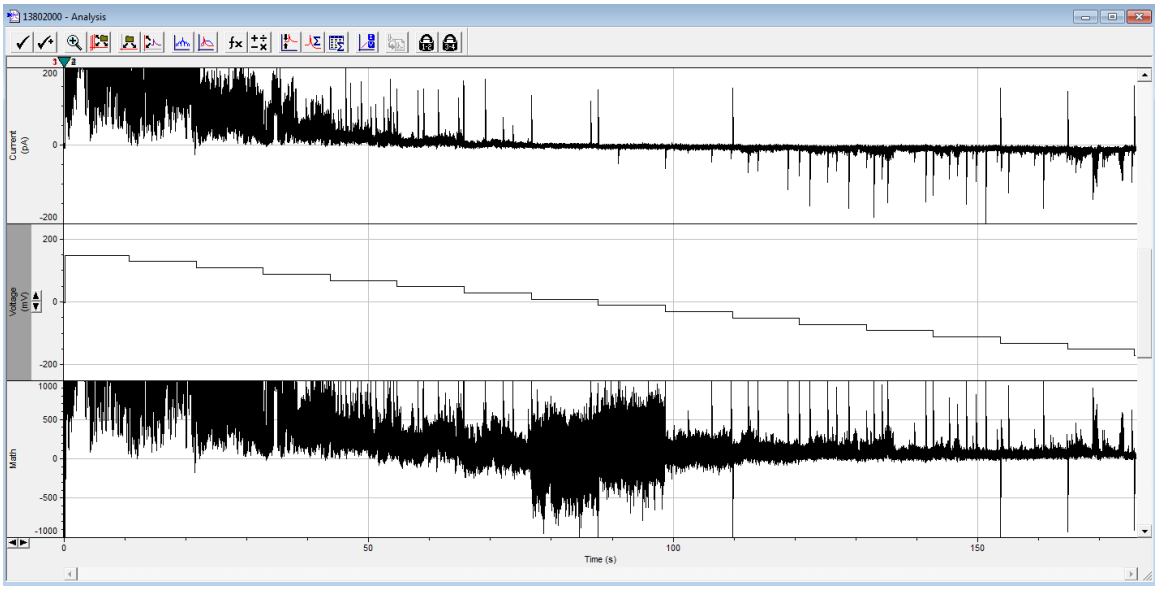

1mole% of **10** premixed with the lipid and then added 12nmole of **10**, 150mV to -150mV, 1M CsCl, 11s per potential level.

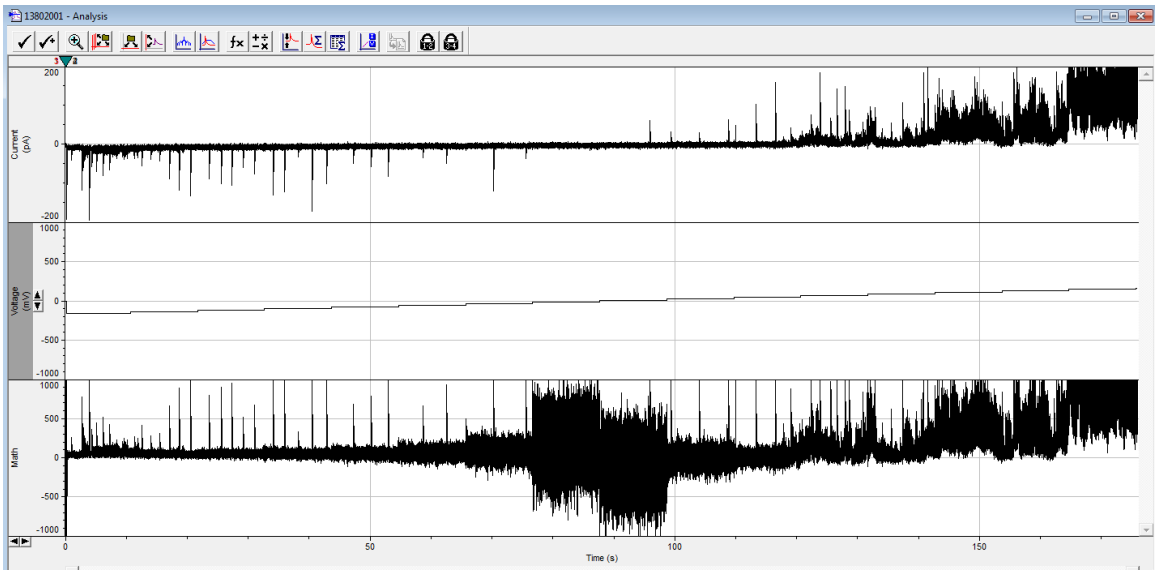

1mole% of **10** premixed with the lipid and then added 12nmole of **10**, 150mV to -150mV, 1M CsCl, 11s per potential level.

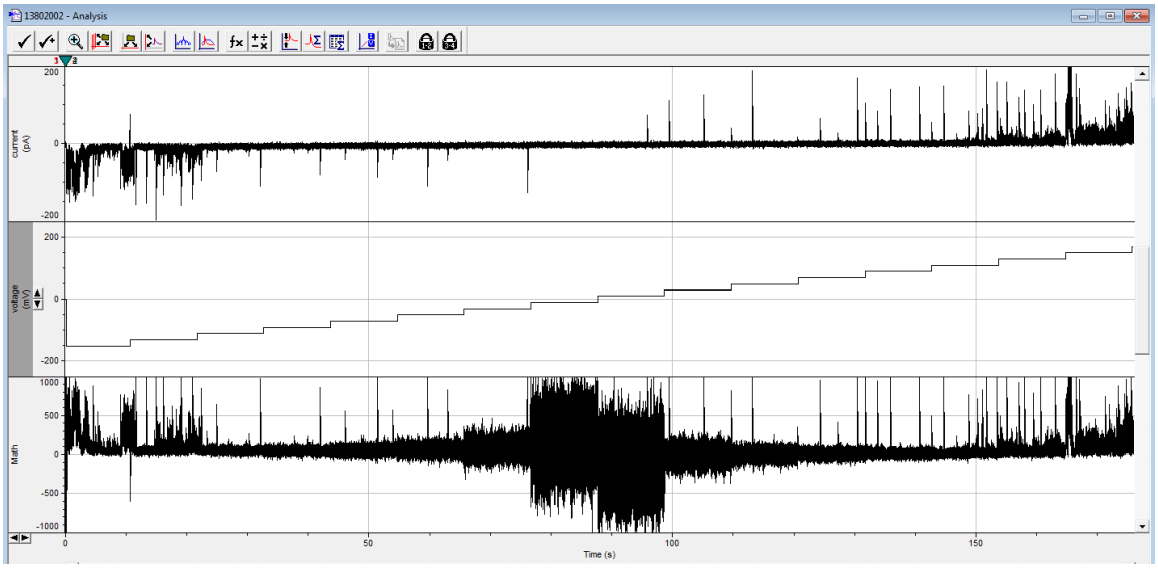

1mole% of **10** premixed with the lipid and then added 12nmole of **10**, 150mV to -150mV, 1M CsCl, 11s per potential level.

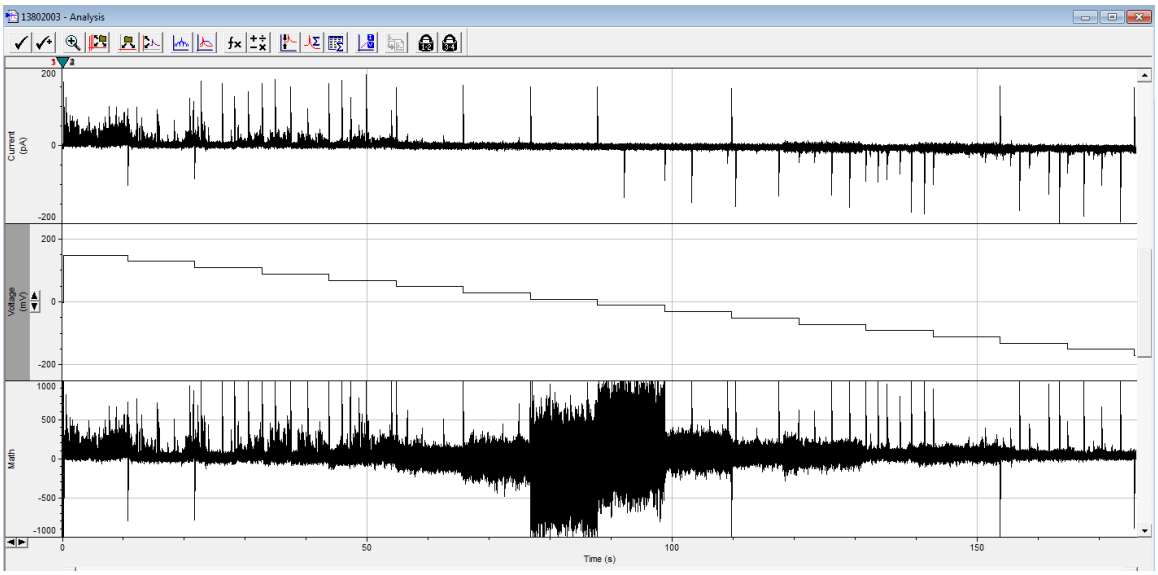

1mole% of **10** premixed with the lipid and then added 12nmole of **10**, 150mV to -150mV, 1M CsCl, 11s per potential level.

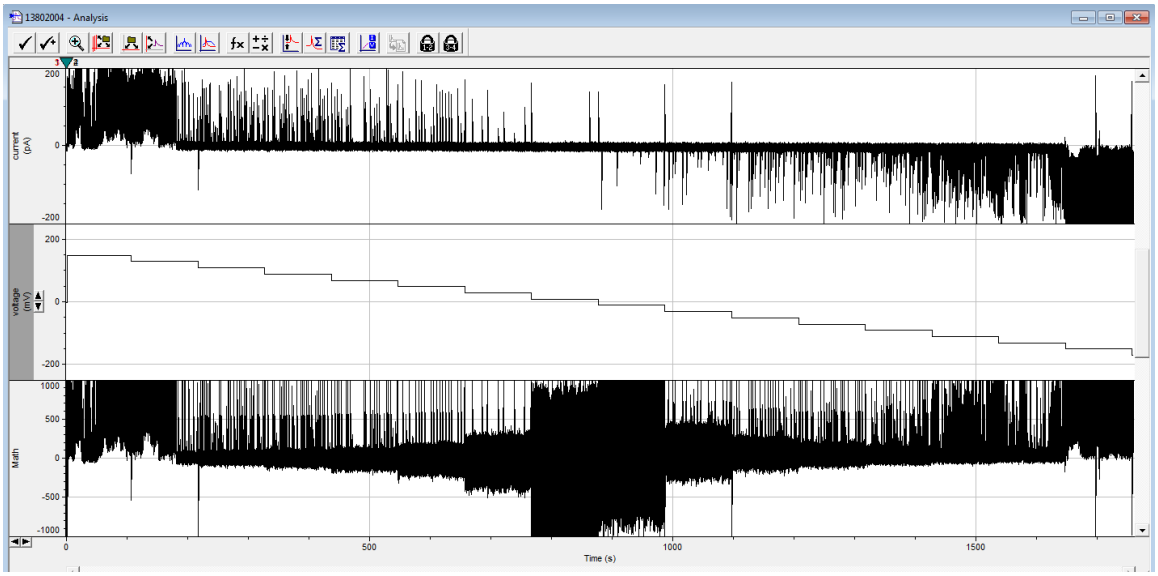

1mole% of **10** premixed with the lipid and then added 12nmole of **10**, 150mV to -150mV, 1M CsCl, 110s per potential level.

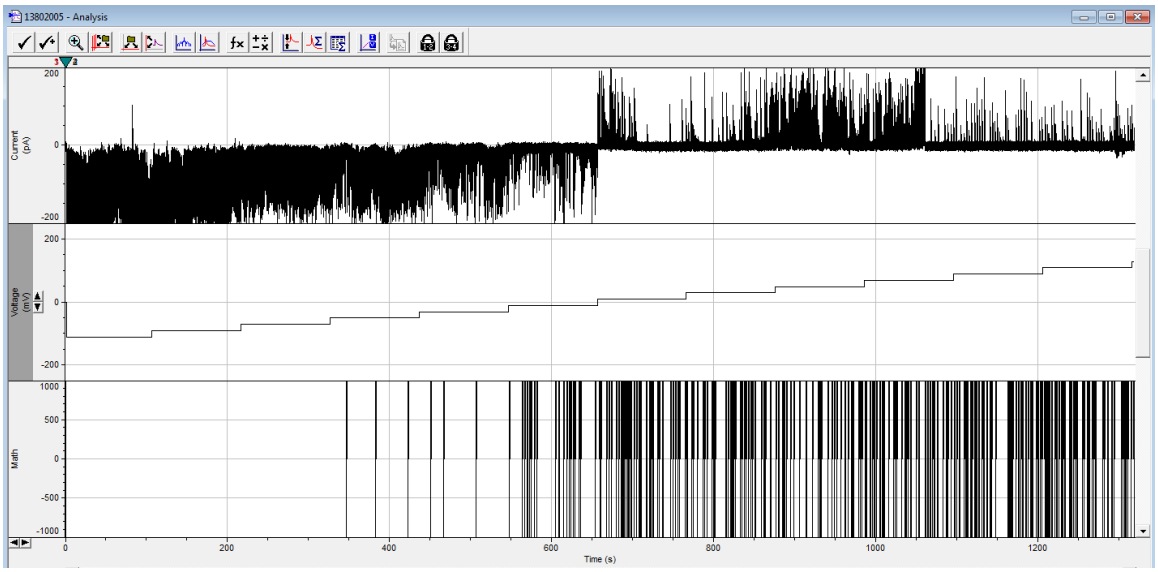

1mole% of **10** premixed with the lipid and then added 12nmole of **10**, -110mV to 110mV, 1M CsCl, 110s per potential level.

Compound 11 Activities

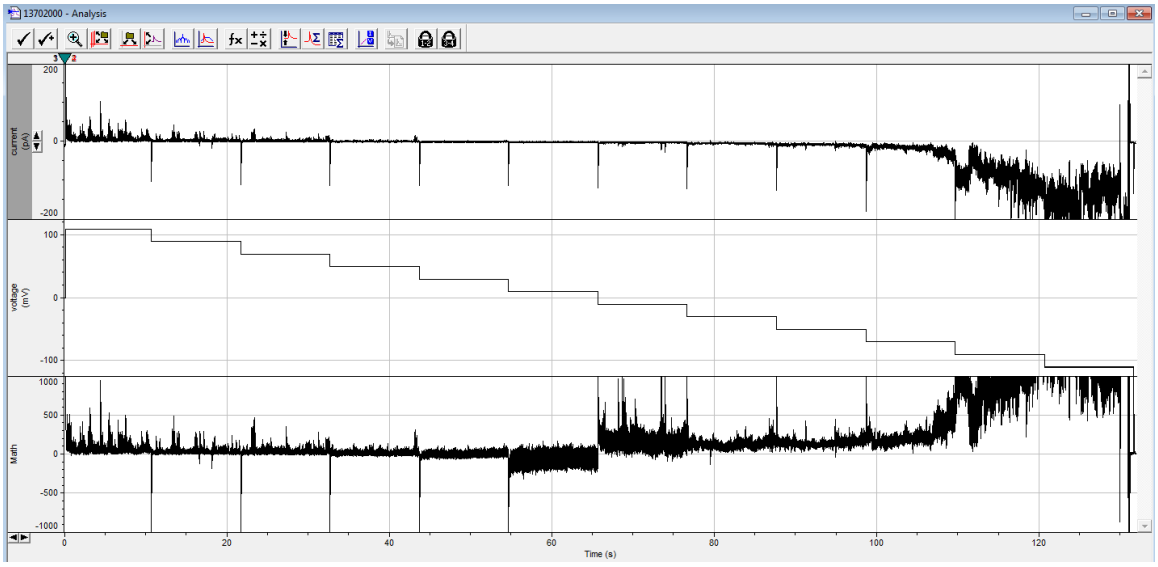

1mole% of **11** premixed with the lipid and then 12nmole of **11** added, 110mV to -110mV 1M CsCl, 11s per potential level

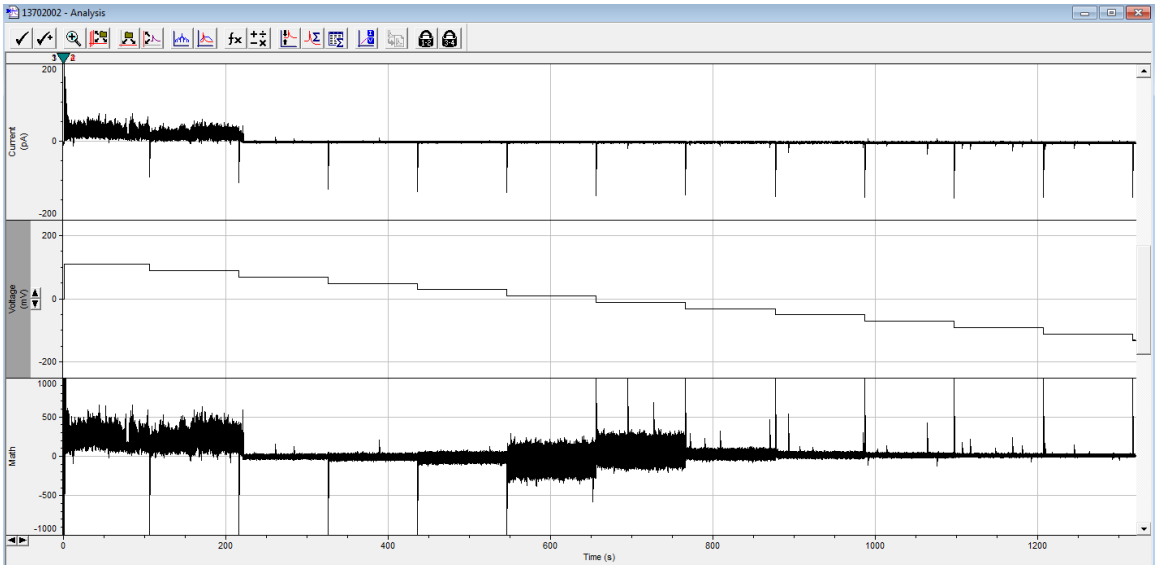

1mole% of **11** premixed with the lipid and then 12nmole of **11** added, 110mV to -110mV 1M CsCl, 110s per potential level

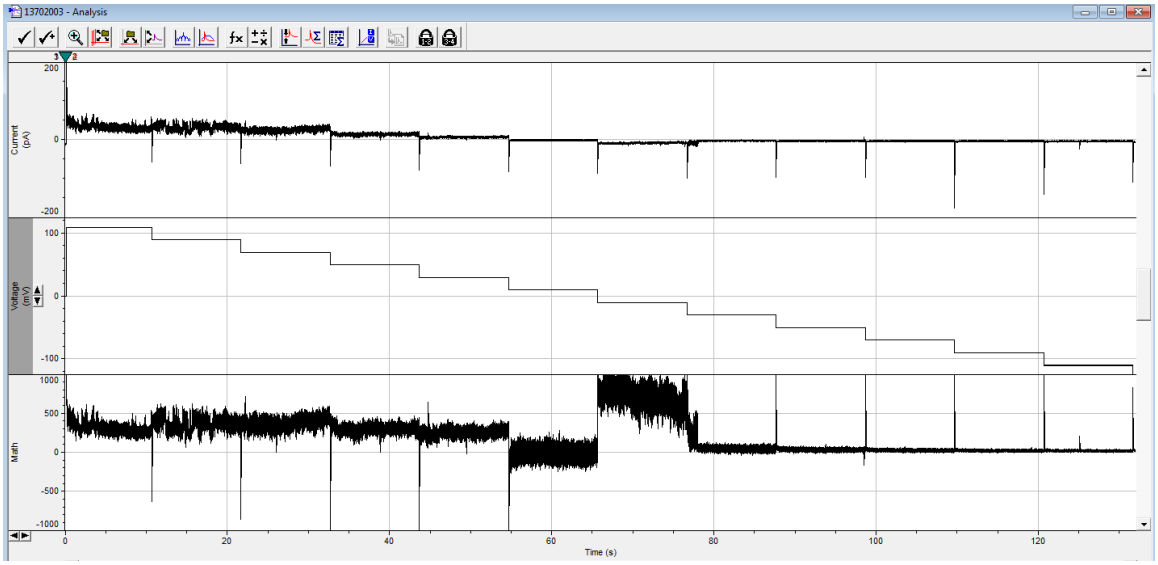

1mole% of **11** premixed with the lipid and then 12nmole of **11** added, 110mV to -110mV 1M CsCl, 11s per potential level

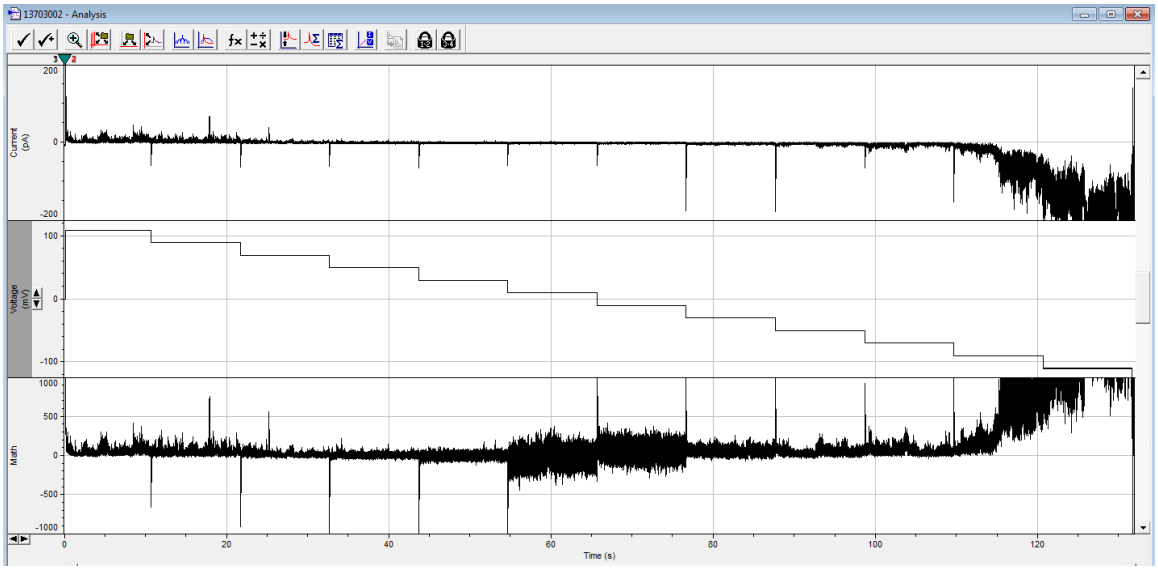

1mole% of **11** premixed with the lipid and then 4nmole of **11** added, 110mV to -110mV 1M CsCl, 11s per potential level

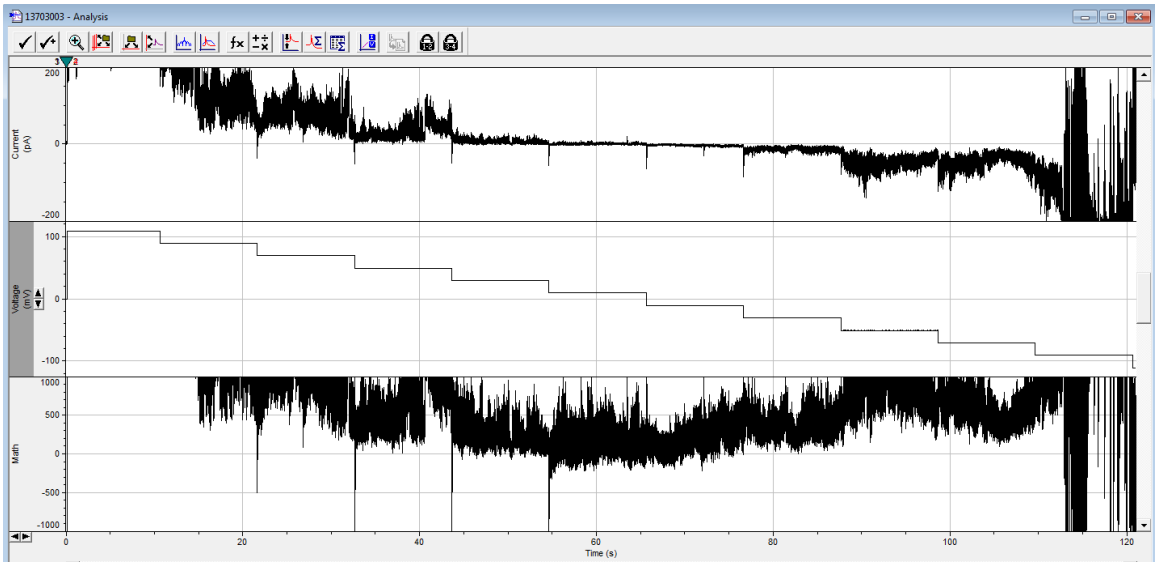

1mole% of **11** premixed with the lipid and then 4nmole of **11** added, 110mV to -110mV 1M CsCl, 11s per potential level

Compound 12 Activities

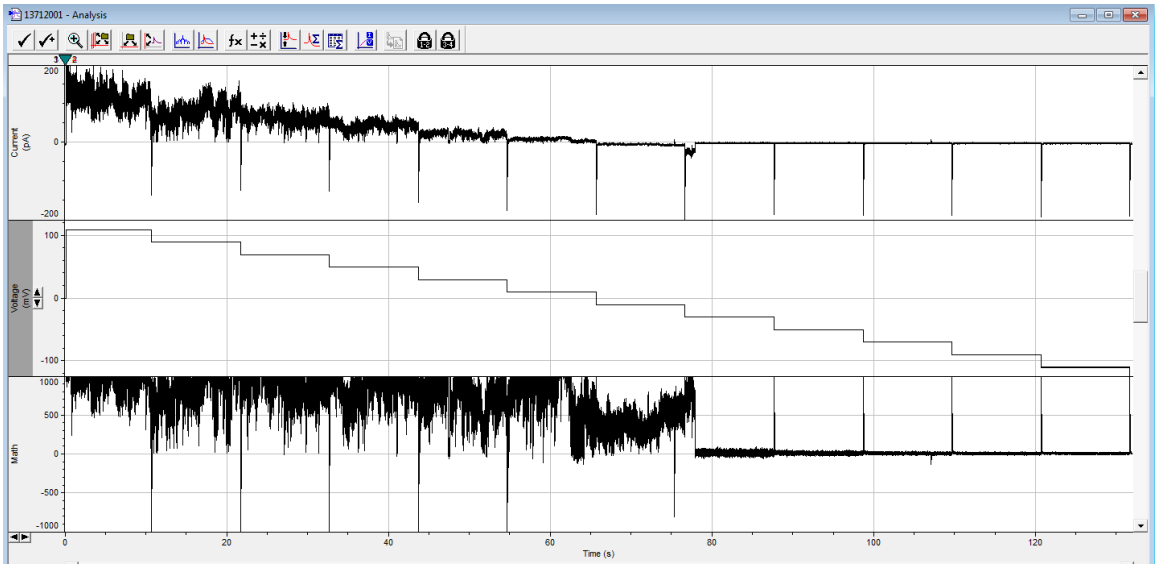

16nmole of **12** with brush, 110mV to -110mV, 1M CsCl, 11s per potential level

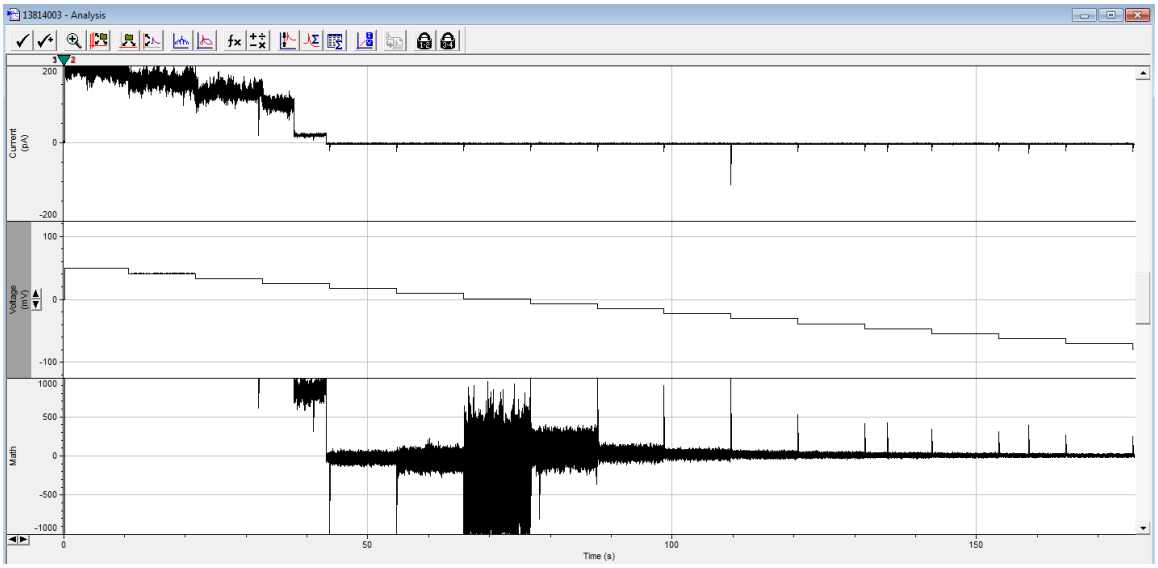

12nmole of **12,** 50mV to -50mV, 1M CsCl, 11s per potential level

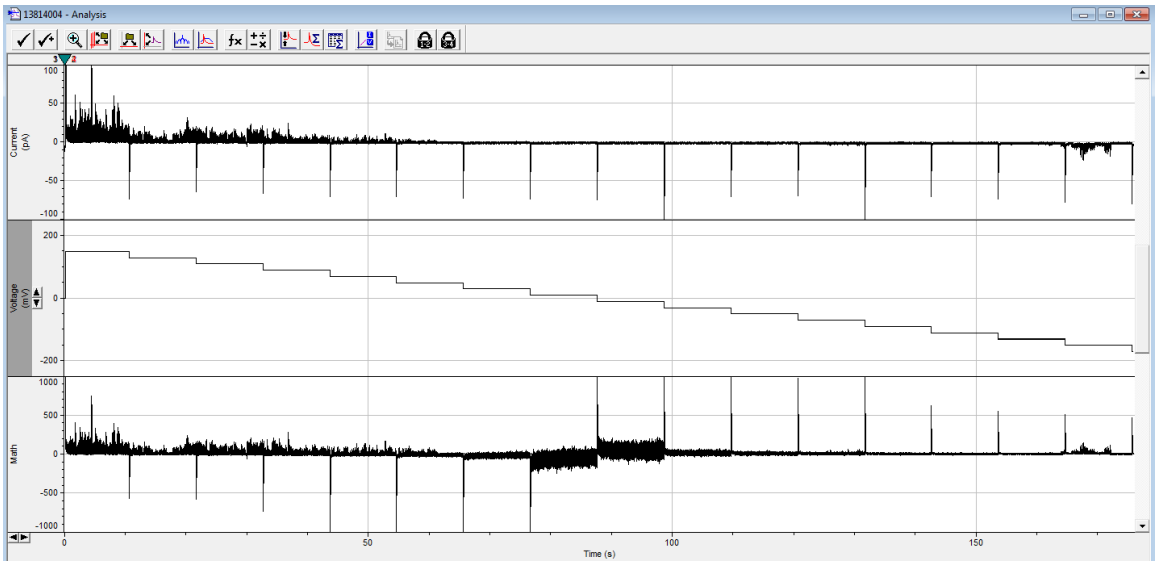

4nmole of **12,** 150mV to -150mV, 1M CsCl, 11s per potential level

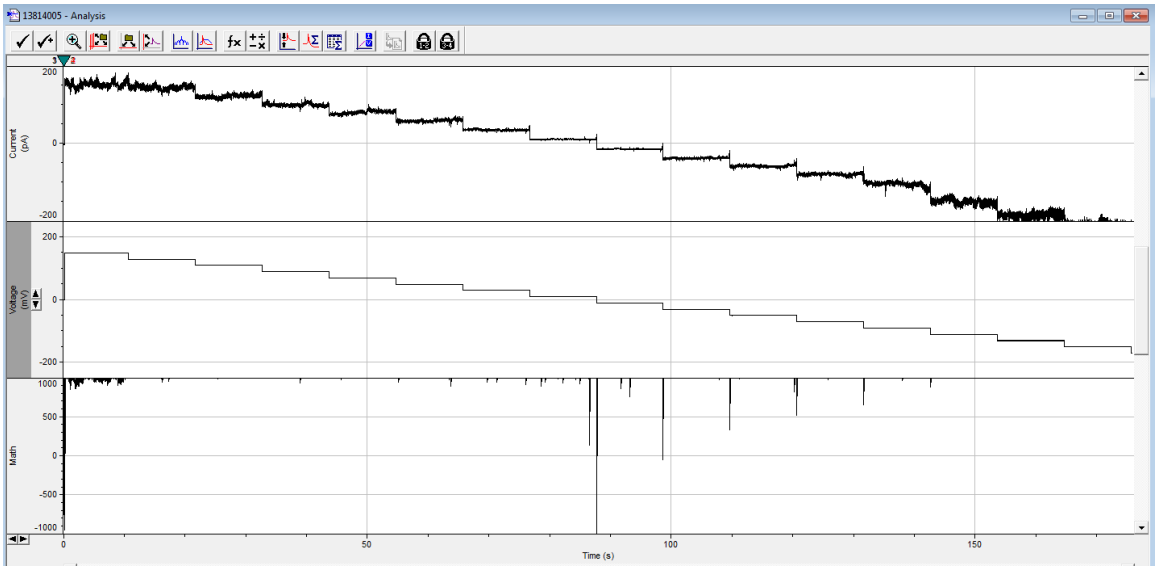

20nmole of **12,** 150mV to -150mV, 1M CsCl, 11s per potential level

Compound 13 Activities

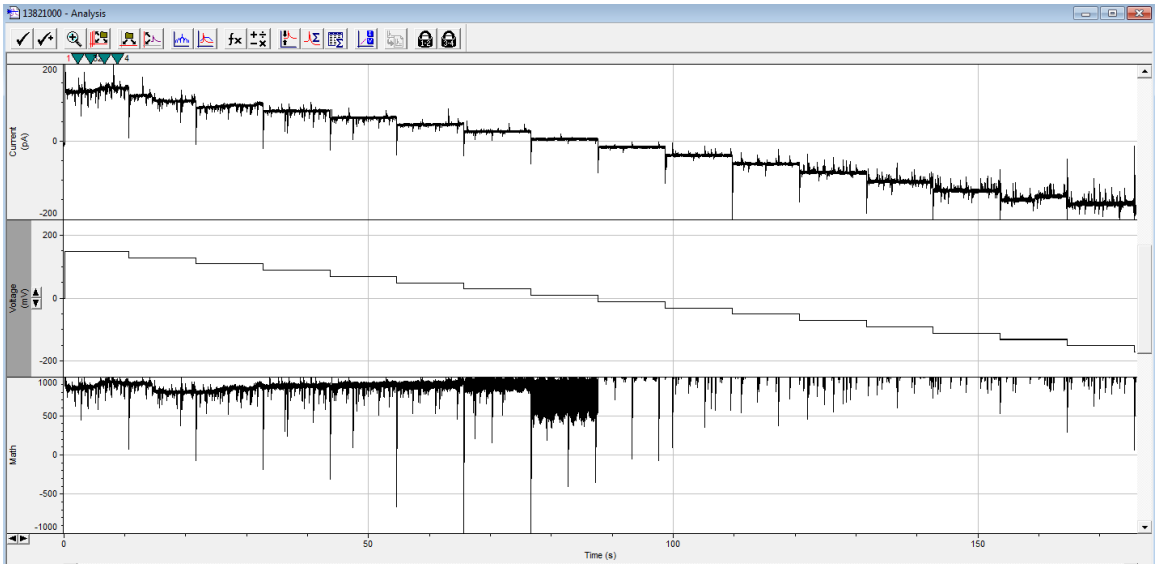

90nmole of **13,** 150mV to -150mV, 1M CsCl, 11s per potential level

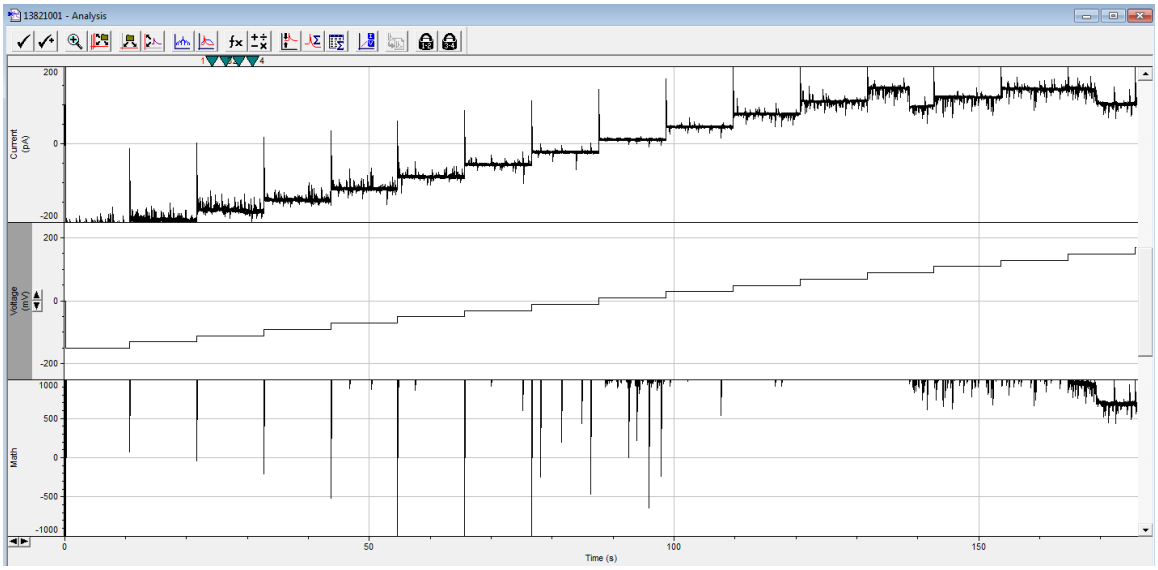

90nmole of **13,** -150mV to 150mV, 1M CsCl, 11s per potential level

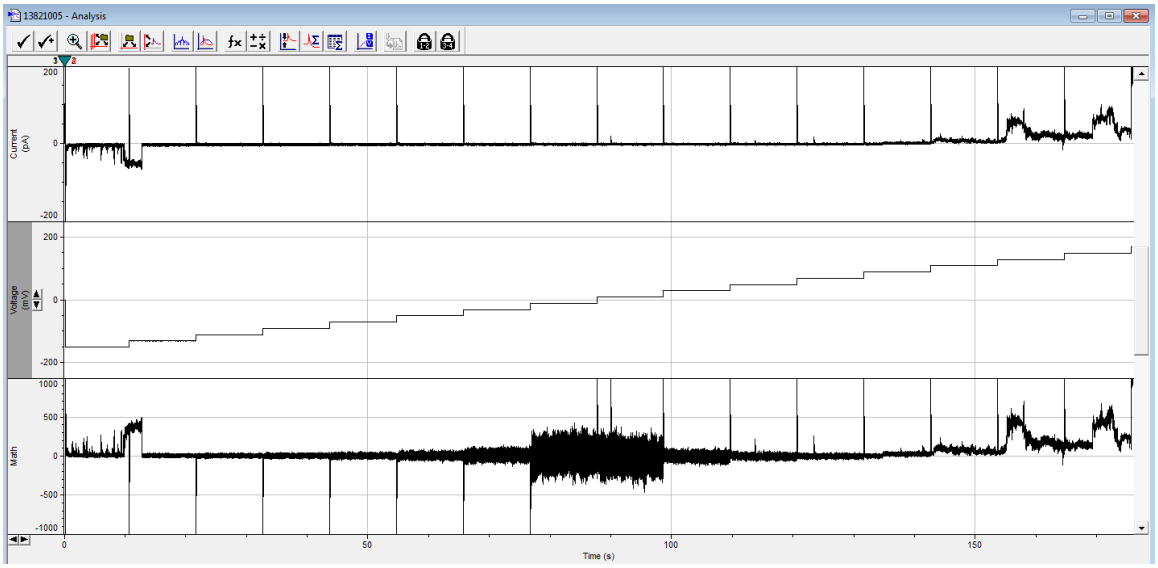

60nmole of **13,** 150mV to -150mV, 1M CsCl, 11s per potential level

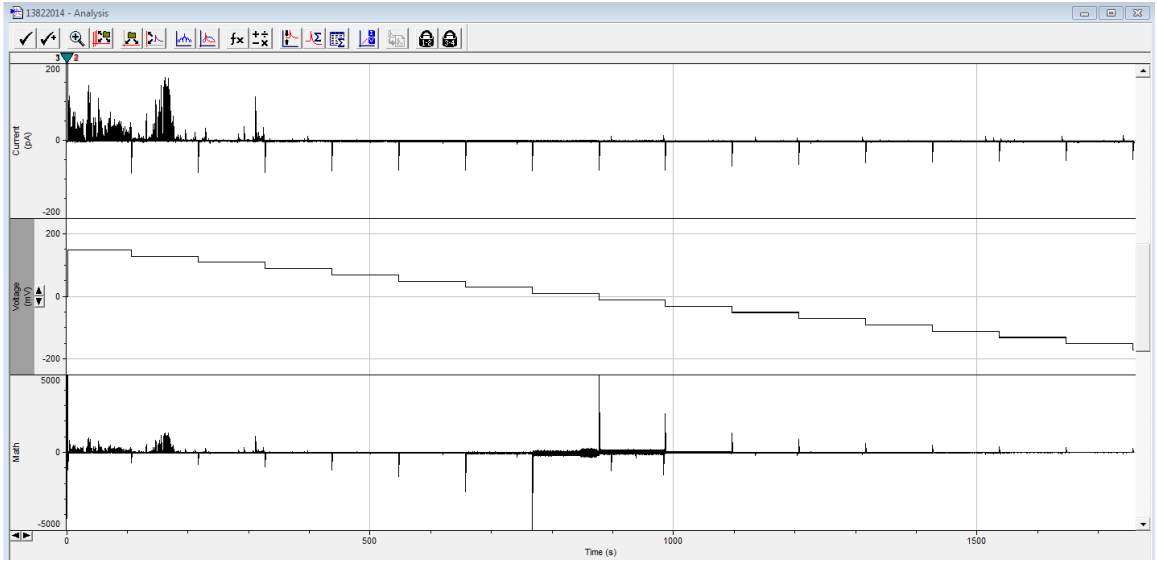

4nmole of **13,** 150mV to -150mV, 1M CsCl, 110s per potential level

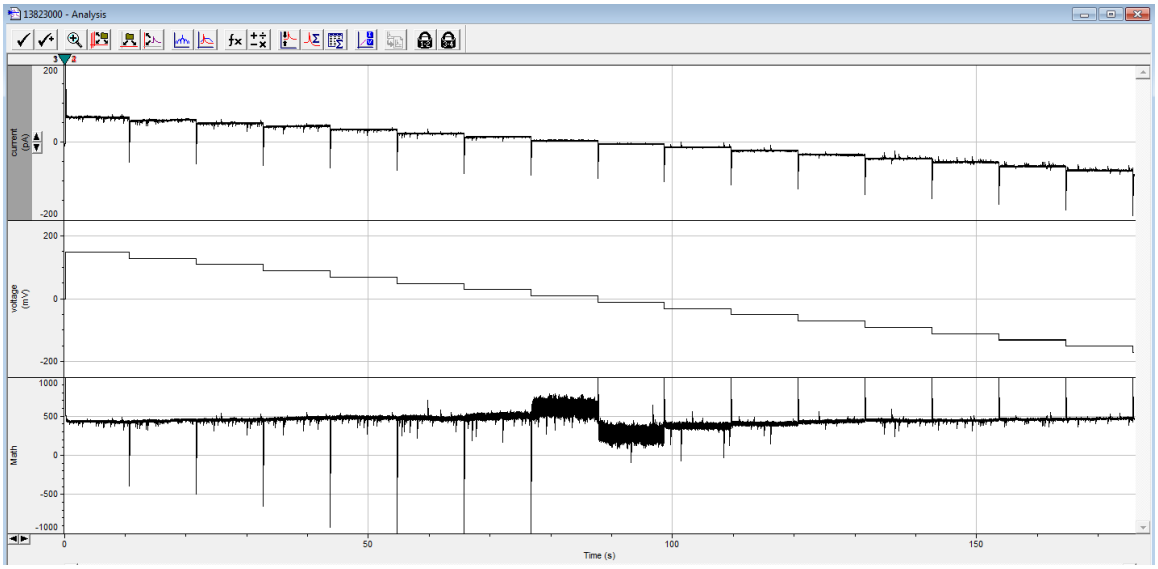

16nmole of **13,** 150mV to -150mV, 1M CsCl, 11s per potential level

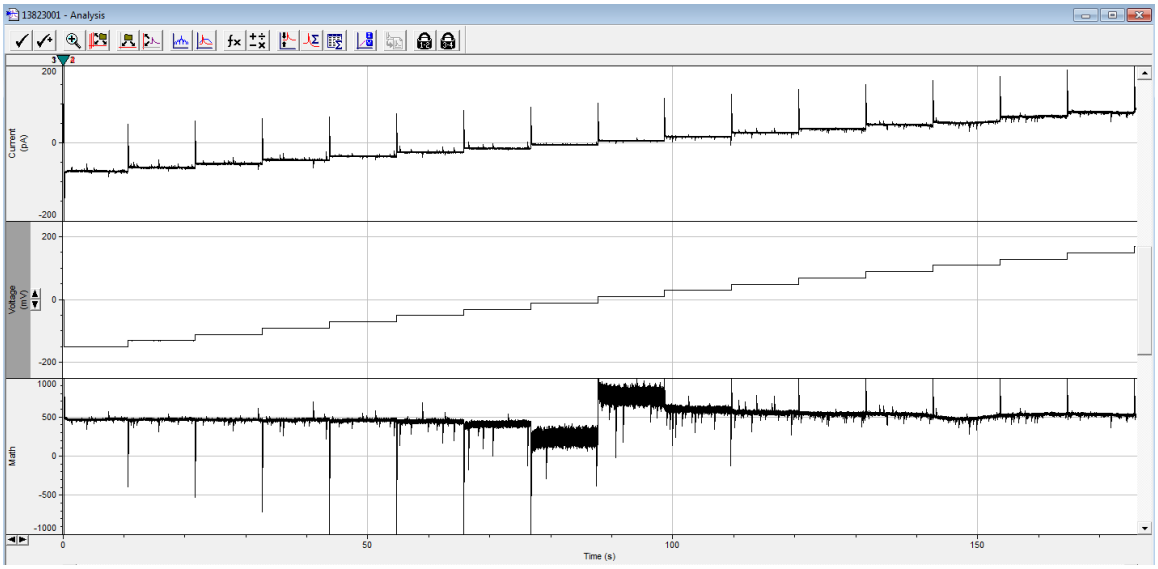

16nmole of **13,** -150mV to 150mV, 1M CsCl, 11s per potential level

Compound 15 Activities

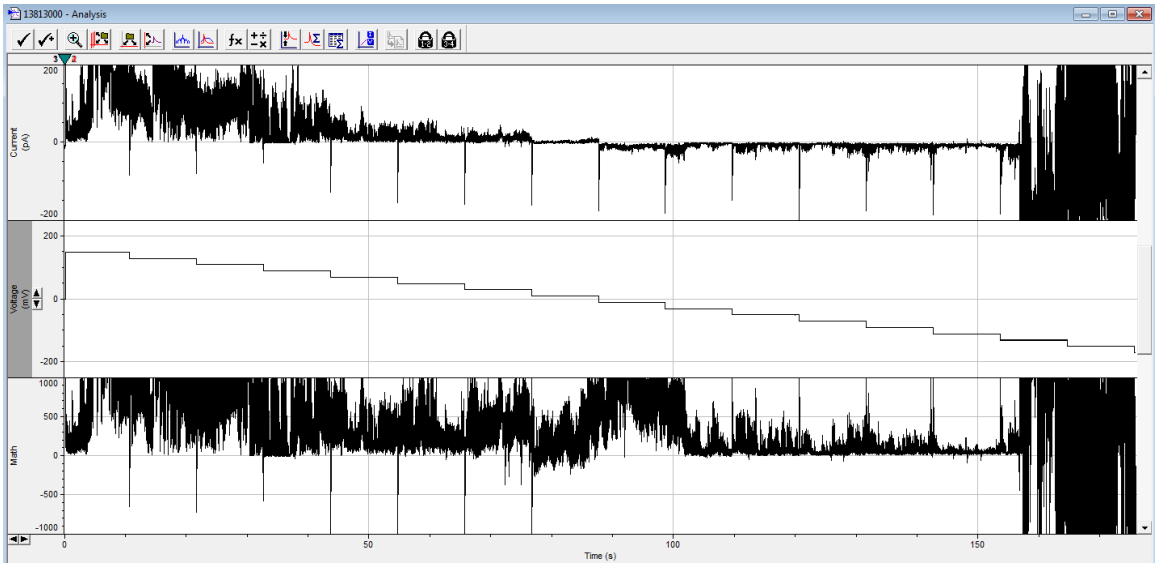

1mole% of **15** premixed with the lipid and then 12nmole of **15** added, 150mV to -150mV 1M CsCl, 11s per potential level

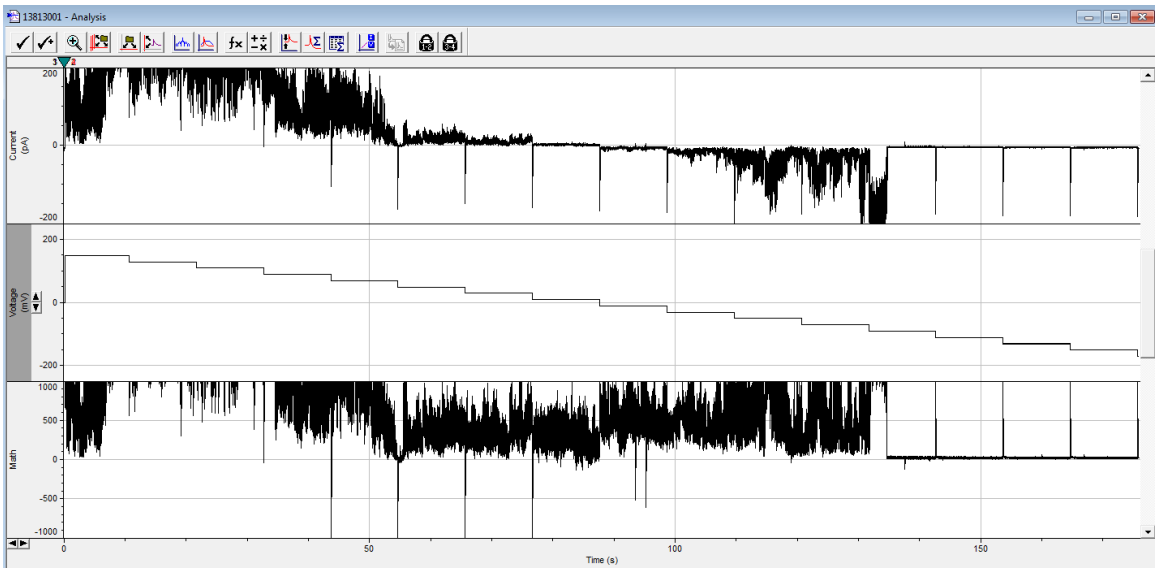

1mole% of **15** premixed with the lipid and then 12nmole of **15** added, 150mV to -150mV 1M CsCl, 11s per potential level

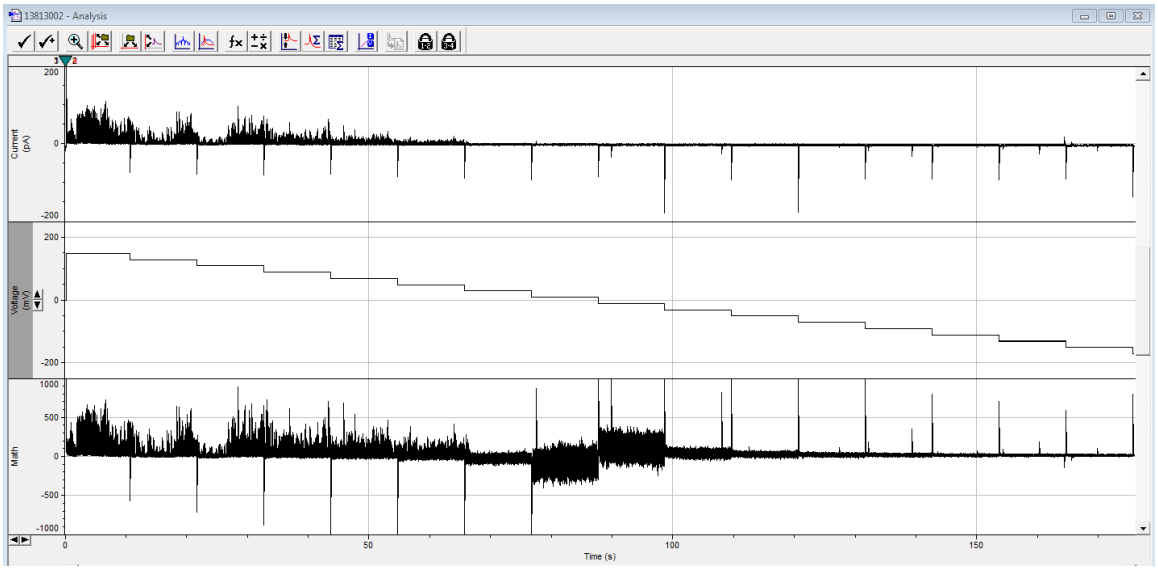

1mole% of **15** premixed with the lipid and then 12nmole of **15** added, 150mV to -150mV 1M CsCl, 11s per potential level

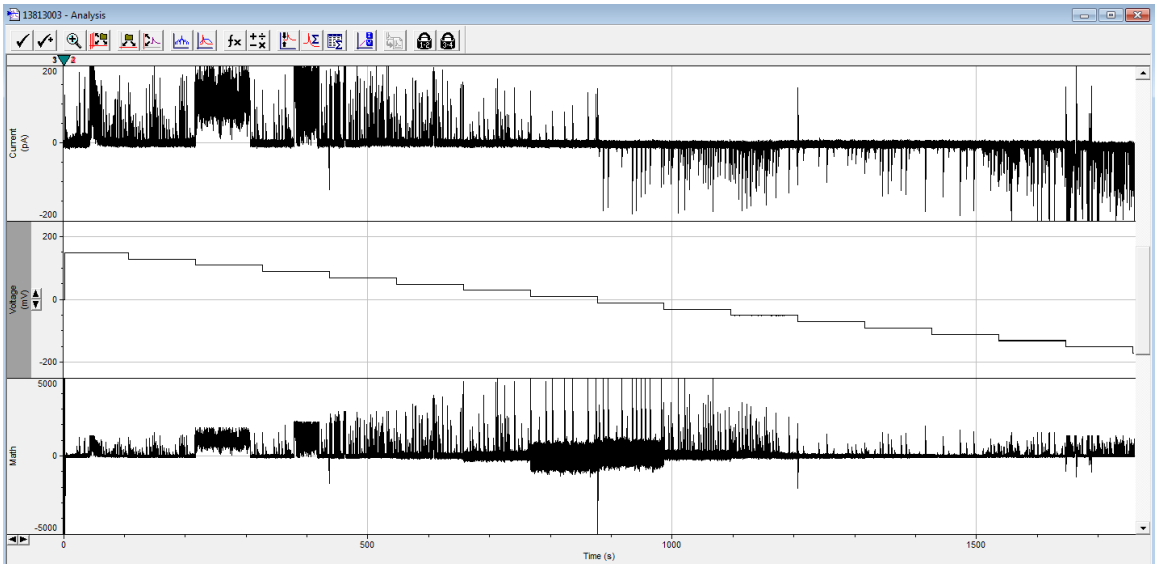

1mole% of **15** premixed with the lipid and then 12nmole of **15** added, 150mV to -150mV 1M CsCl, 11s per potential level

Compound 16 Activities

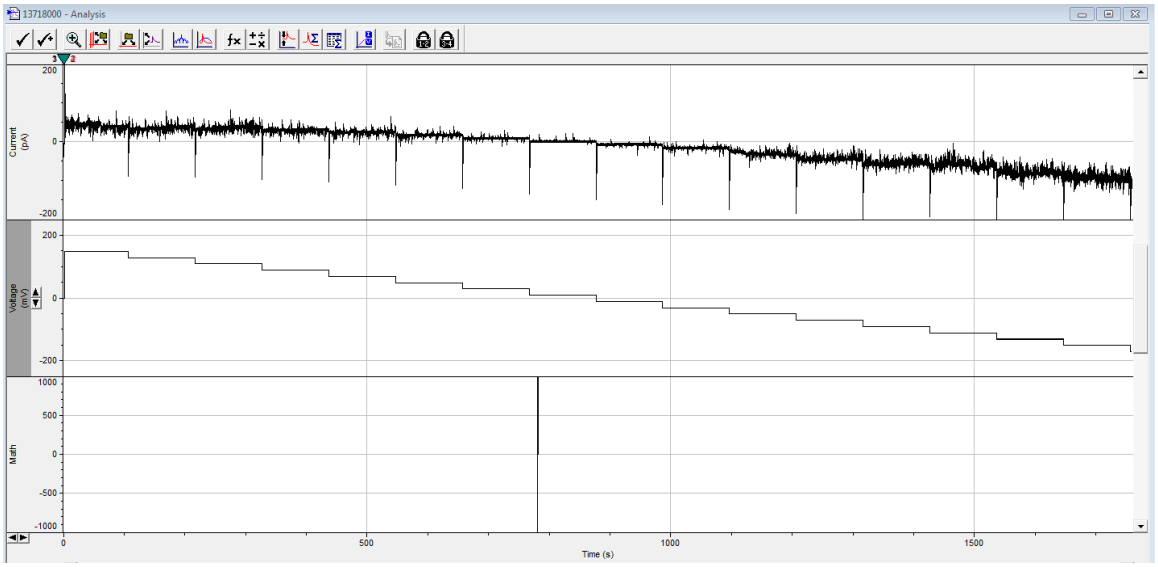

1mole% of **16** premixed with the lipid, 150mV to -150mV 1M CsCl, 110s per potential level

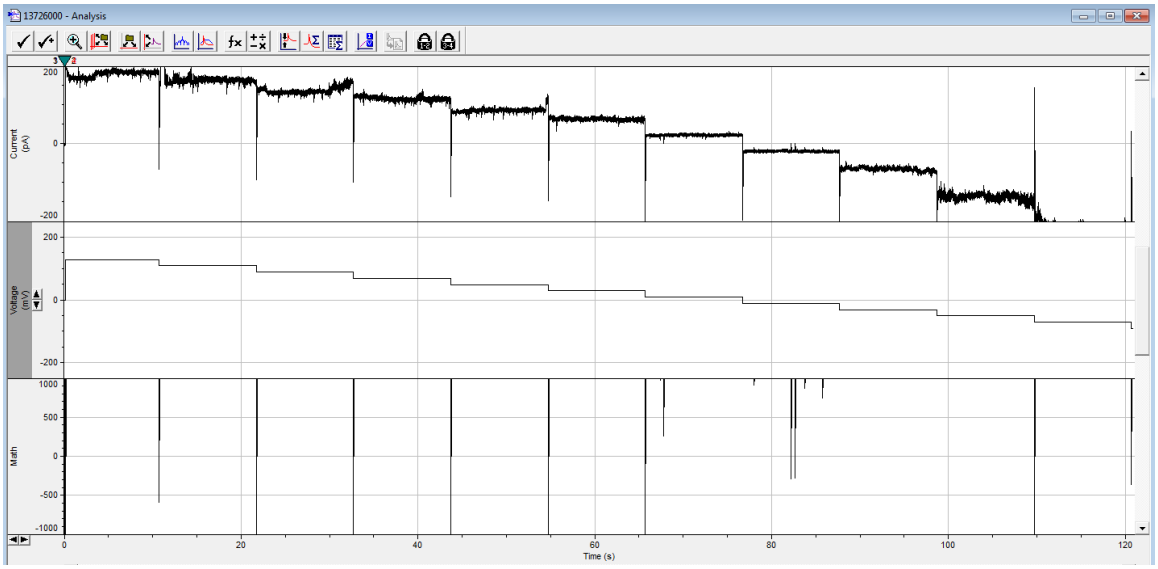

1mole% of **16** premixed with the lipid and then 4nmole of **16** added 150mV to -150mV 1M CsCl, 11s per potential level

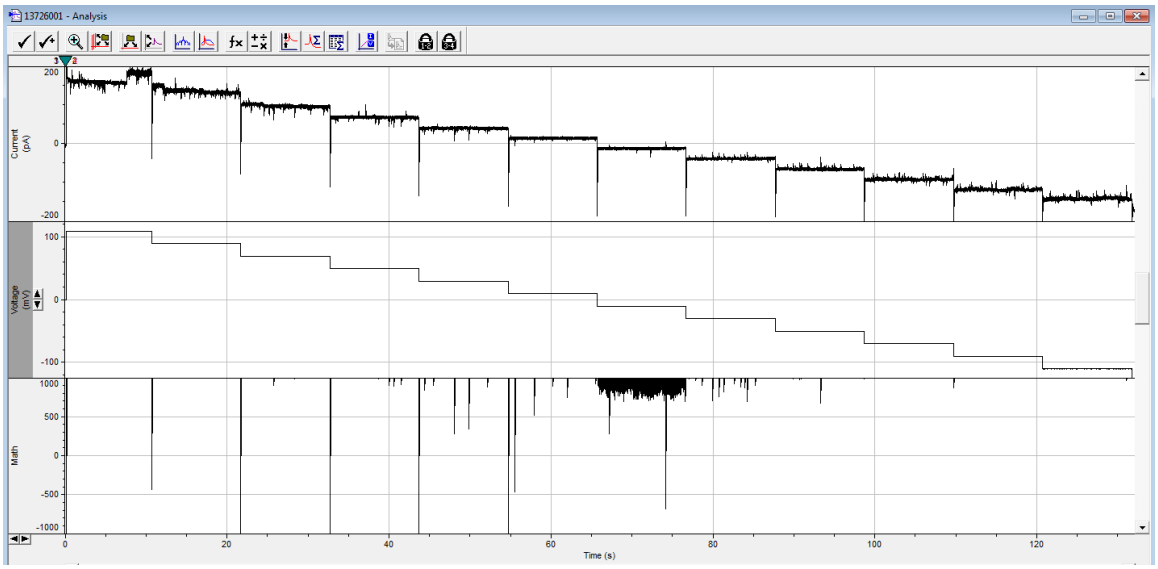

1mole% of **16** premixed with the lipid and then 4nmole of **16** added 110mV to -110mV 1M CsCl, 11s per potential level

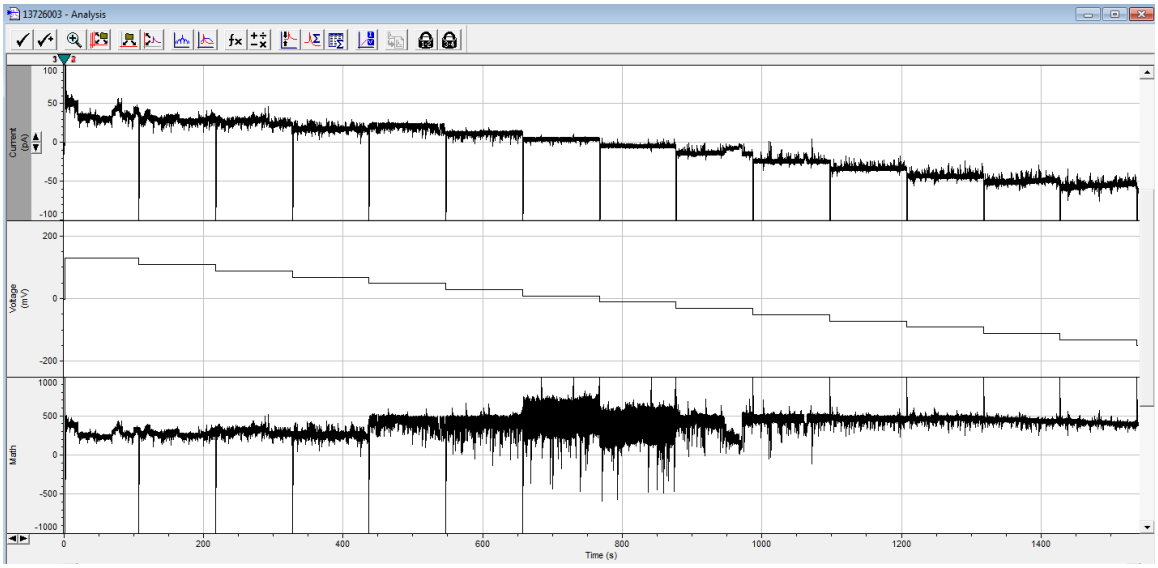

1mole% of **16** premixed with the lipid and then 4nmole of **16** added 150mV to -150mV 1M CsCl, 110s per potential level

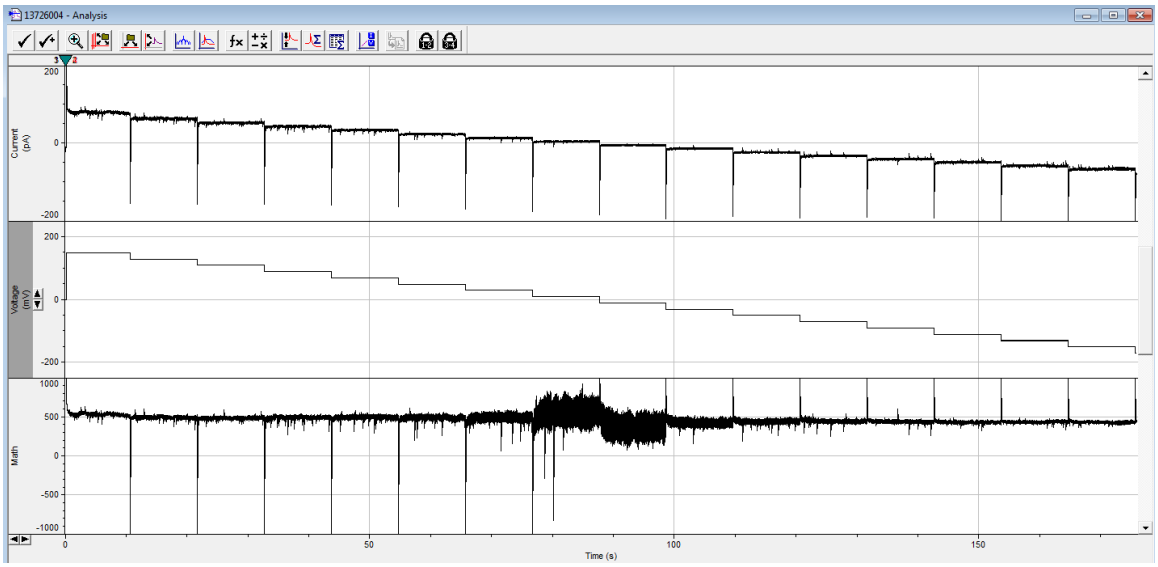

1mole% of **16** premixed with the lipid and then 4nmole of **16** added 150mV to -150mV 1M CsCl, 11s per potential level

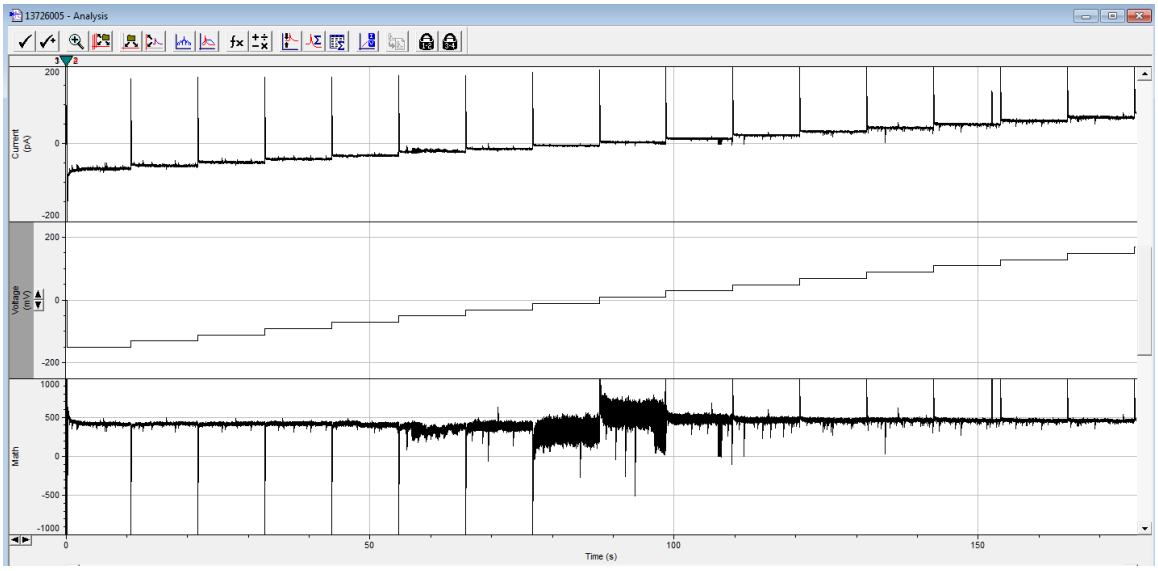

1mole% of **16** premixed with the lipid and then 4nmole of **16** added -150mV to 150mV 1M CsCl, 11s per potential level

Compound 17 Activities

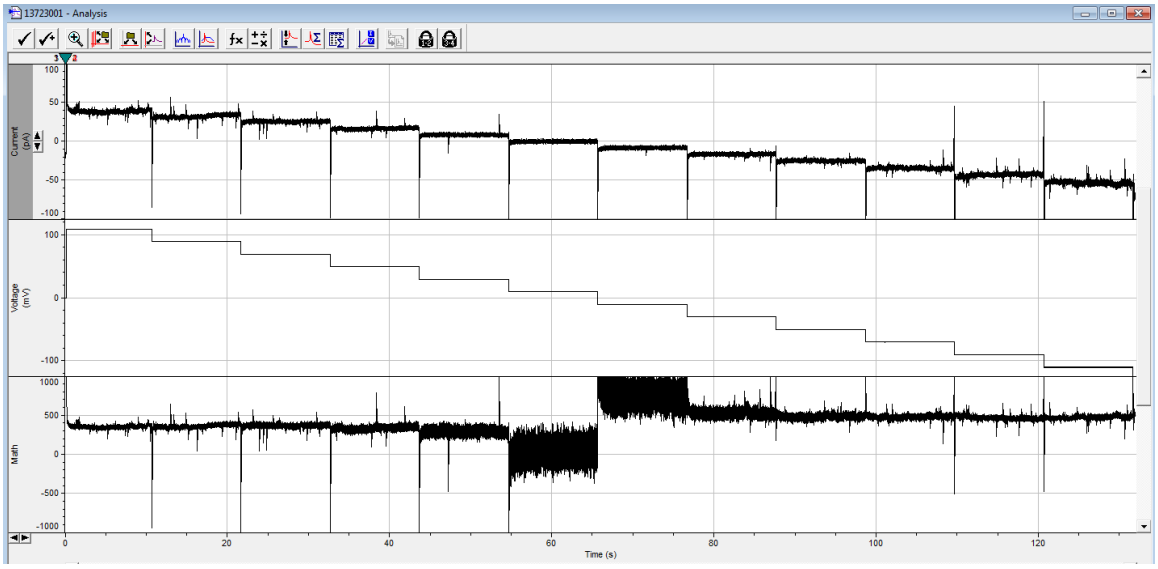

1mole% of **17** premixed with the lipid and then 20nmole of **17** added 110mV to -110mV 1M CsCl, 11s per potential level

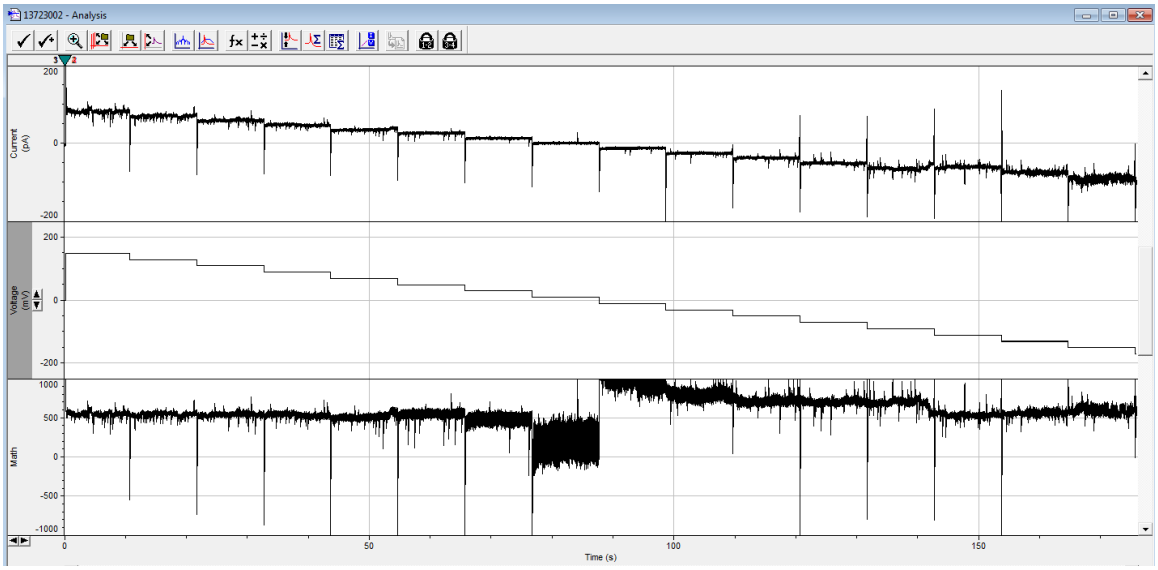

1mole% of **17** premixed with the lipid and then 20nmole of **17** added 110mV to -110mV 1M CsCl, 11s per potential level

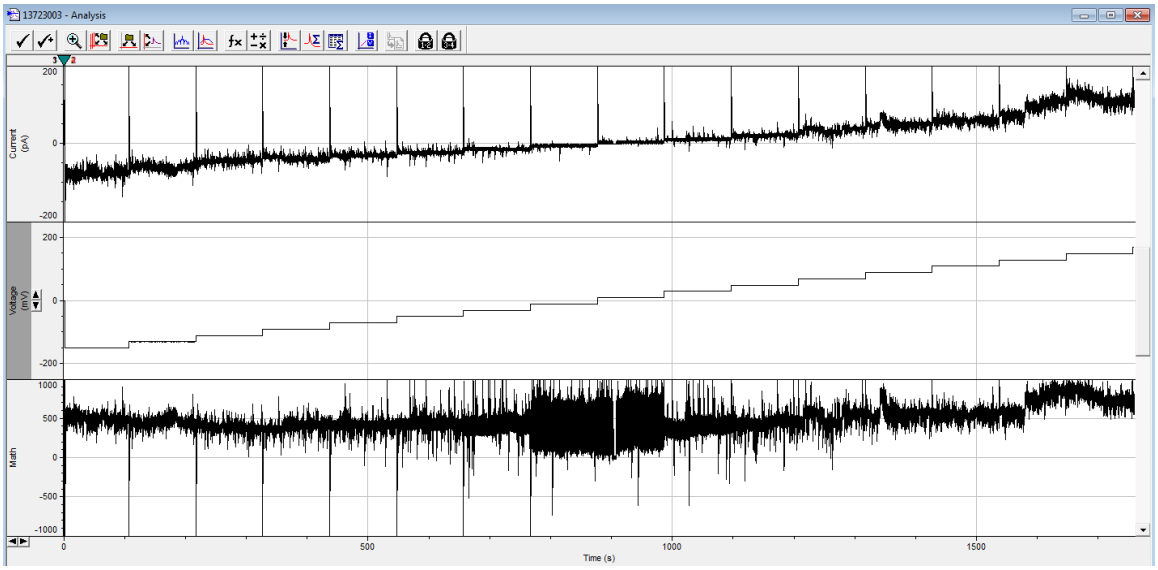

1mole% of **17** premixed with the lipid and then 20nmole of **17** added 110mV to -110mV 1M CsCl, 11s per potential level

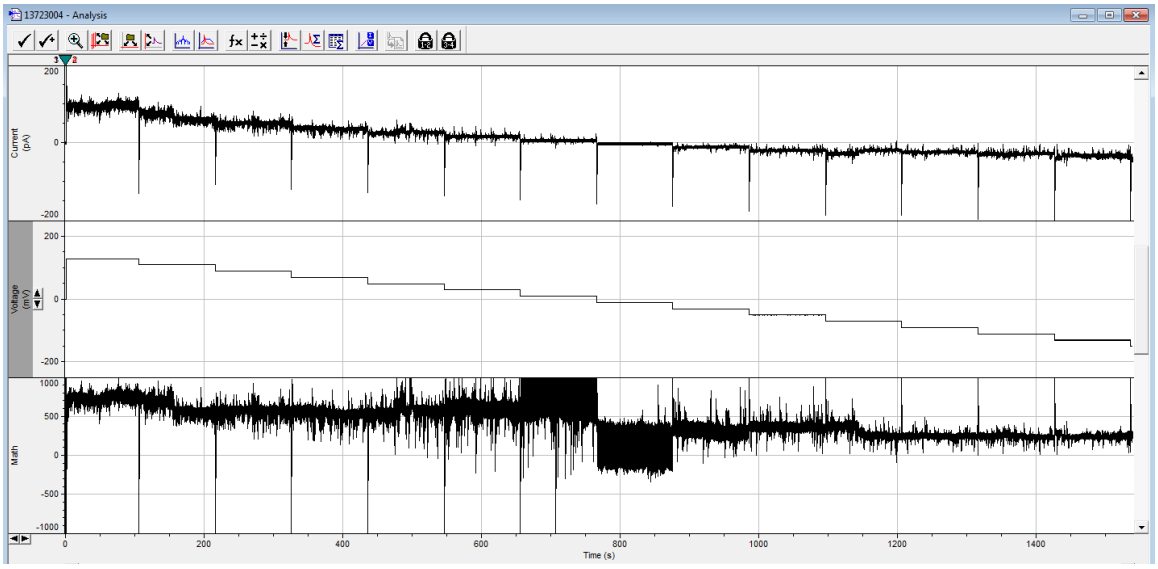

1mole% of **17** premixed with the lipid and then 20nmole of **17** added 110mV to -110mV 1M CsCl, 11s per potential level

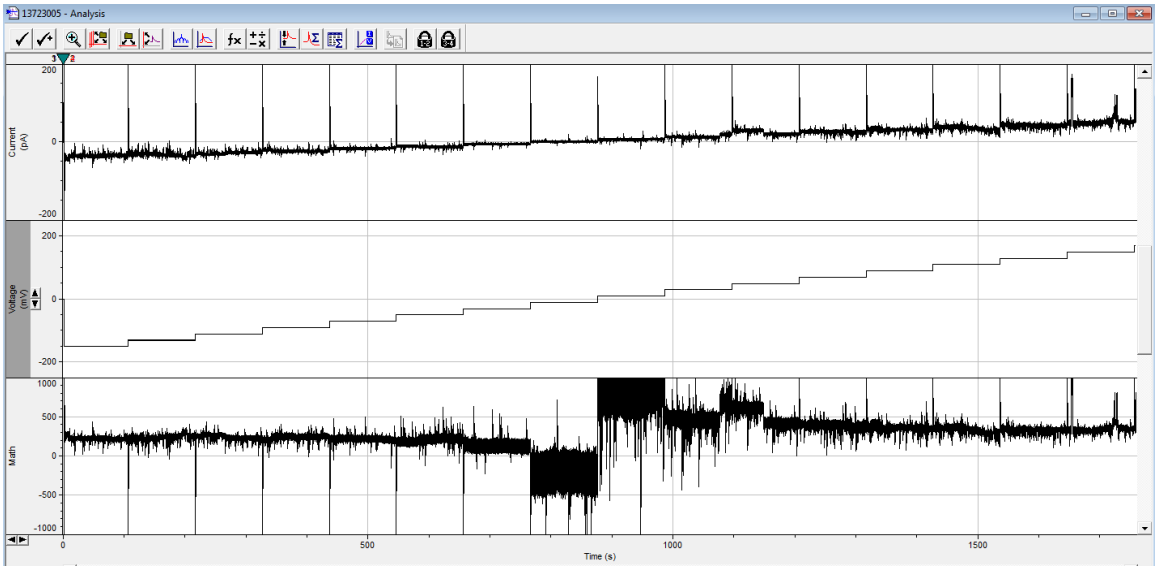

1mole% of **17** premixed with the lipid and then 20nmole of **17** added 110mV to -110mV 1M CsCl, 11s per potential level